

Die approbierte Originalversion dieser  
Dissertation ist in der Hauptbibliothek der  
Technischen Universität Wien aufgestellt und  
zugänglich.

<http://www.ub.tuwien.ac.at>



The approved original version of this thesis is  
available at the main library of the Vienna  
University of Technology.

<http://www.ub.tuwien.ac.at/eng>



TECHNISCHE  
UNIVERSITÄT  
WIEN

DISSERTATION

# Operando PM-IRAS and SFG Spectroscopy of Cu, Pt and Pd Model Catalysts Prepared in Ultra-High Vacuum

ausgeführt zum Zwecke der Erlangung des akademischen Grades  
eines Doktors der Naturwissenschaften unter der Leitung von

**Univ.Prof. Mag.rer.nat. Dr.rer.nat. Günther Rupprechter**

und

**Dr.rer.nat Christoph Rameshan**

Institut für Materialchemie E 165

Eingereicht an der Technischen Universität Wien  
Fakultät für Technische Chemie

von

**MSc. Matteo Roiaz**

Matrikelnummer 1429716

Via Donato Bramante 4, 34143 Trieste, Italien

Trieste, Mai 2018



## KURZFASSUNG

---

Hauptziel der vorliegenden Arbeit war die Präparation und Charakterisierung wohldefinierter Modellkatalysatoren, die technologisch relevanten Materialien nahekommen. Weiterführendes zweites Ziel war die Überbrückung des „pressure gap“ zwischen der technischen Katalyse und der klassischen Oberflächenanalytik (Surface Science) im Ultra-hoch-Vakuum (UHV). Sum frequency generation (SFG) Spektroskopie und polarization-modulation infrared reflection absorption (PM-IRAS) Spektroskopie wurden als vorrangige Untersuchungsmethoden eingesetzt, da beide sowohl im UHV als auch unter Atmosphärendruck angewandt werden können. Beide Methoden sind oberflächensensitiv und ermöglichen die Untersuchung von Schwingungseigenschaften von Molekülen, die an der Oberfläche des Modellkatalysators absorbiert sind. Die SFG und PM-IRAS Untersuchungen wurden durch Standardmethoden zur Präparation und Charakterisierung von Proben im UHV ergänzt, wie z.B. der Röntgen-Photoelektronen Spektroskopie (XPS), der Beugung niederenergetischer Elektronen (LEED), und der Temperatur-programmierter Desorption (TPD).

Betreffend SFG, widmete sich ein Großteil der Arbeiten dem Design, dem Aufbau und der Inbetriebnahme einer UHV-Kammer mit angebundener SFG Spektroskopiezelle für katalytische Aktivitätsmessungen. Diese besondere Ankoppelung ermöglicht die Präparation und Charakterisierung einer Probe unter genau definierten Bedingungen im UHV, gefolgt vom UHV-Transfer des Modellkatalysators in die SFG Spektroskopiezelle. In der Zelle erfolgen dann *gleichzeitig* in situ SFG Messungen und Massenspektrometrie (MS) Messungen der katalytischen Aktivität in einem weiten Druck- und Temperaturbereich. Um die neue Apparatur zu testen, wurden gut-bekannte Systeme erneut untersucht, wie beispielweise die Kohlenstoffmonoxid Adsorption auf Platin und Palladium Einkristallen. Auf der Pt-(111) Oberfläche wurden druck- und polarisationsabhängige Untersuchungen durchgeführt. Das CO/Pd (111) System wurde dabei

entweder im UHV bei flüssiger Stickstoff Temperatur untersucht (wodurch die bekannte (2x2)-3CO Struktur entstand), oder bei mbar Gasdruck und Raumtemperatur. Weiters wurde die Oxidation von Kohlenmonoxid zu Kohlendioxid auf einem Modellkatalysator aus Pt Nanopartikeln auf einem dünnen Zirkoniumoxid Film untersucht, wieder verfolgt durch simultane SFG und MS Messungen unter Atmosphärendruck.

Der zweite Teil der Arbeit widmete sich der Untersuchung der Interaktion zwischen Kohlenstoffmonoxid und der Kupfer (100) Einkristalloberfläche mittels PM-IRAS, XPS, LEED, und TPD. Diese Modellstudie beschäftigt sich mit der wichtigen Frage nach der Rolle des katalytisch-aktiven Kupfers in Prozessen wie der Methanol-Synthese. Zunächst wurde dazu die Adsorption bei niedriger Temperatur untersucht: CO absorbiert reversibel in einer regelmäßigen c(2x2) Struktur, mit einer typische C-O Schwingungswellenzahl von 2082 cm<sup>-1</sup>, einer Desorptionsenergie von 0.46 eV und charakteristische XPS Spektren wurden ebenfalls beobachtet. Im Gegensatz dazu verursachte die Raumtemperatur CO Exposition von Cu(100) im mbar Druckbereich irreversible Änderungen der Oberfläche. Die C-O Wellenzahl verschob sich nach oben (2093-2103 cm<sup>-1</sup>); was auf die Adsorption auf niedrig-kordinierten Kupferatomen hinweist. Nach der CO-Exposition wurden mittels XPS zusätzlich atomarer Sauerstoff und Kohlenstoff beobachtet, was eine Oberflächenaktivität für CO-Dissoziation nahelegt. Die Ergebnisse bzw. Die Interpretation der Schwingungsspektroskopie wurden mittels density functional theory (DFT) bestätigt (Kooperation mit dem KAUST Catalysis Center). Sie lassen auf einen Reaktionsmechanismus schließen, bei dem die Kupferoberfläche unter mbar CO Druck stark aufräut, v.a. durch die Mobilisierung von Cu Atomen aus Stufen, gefolgt von der Bildung von Cu<sub>1</sub> und Cu<sub>5</sub> Clustern. Dieses Modell ist mit den Resultaten aus high-pressure scanning tunneling spectroscopy (HP-STM) gut vereinbar, welche vor Kurzem von der Forschungsgruppe rund um M. Salmeron am Lawrence Berkeley National Laboratory veröffentlicht wurden.

Der dritte Teil der Arbeit wurde in Kooperation mit der Universität Trieste durchgeführt. Eine 2D metalorganische-Schicht aus carbonyliertem Eisen-Phthalocyanin auf einer Graphenschicht auf Iridium (111) wurde mittels PM-IRAS und SFG untersucht. Vier unterschiedliche C-O Schwingungen konnten mit SFG beobachtet werden, während nur eine einzige Bande in unseren PM-IRAS Spektren sichtbar war. Dies bestätigt, dass die in SFG Spektren beobachtete vierfache-Aufspaltung der C-O Streckschwingung elektronischen Ursprungs war; verursacht durch eine low spin/high spin Anregung durch den sichtbaren (grünen) Strahl der SFG Spektroskopie. Andere mögliche Ursachen der Aufspaltung, wie z.B. Koadsorption oder Dipol-Dipol Wechselwirkungen, konnten somit ausgeschlossen werden.



## ABSTRACT

---

The aim of this thesis was the preparation and characterization of well-defined model catalysts with structure and catalytic activity close to those of industrially used ones. Furthermore, bridging the “pressure gap” between technical catalysis and classical ultra-high vacuum (UHV) surface science studies was a second goal. Sum frequency generation spectroscopy (SFG) and polarization-modulation infrared reflection absorption spectroscopy (PM-IRAS) have been employed as main spectroscopic techniques to accomplish the task because of their capability to operate from UHV to ambient pressure. Both techniques are surface specific, and probe the vibrational properties of molecular species adsorbed on the surface of model catalysts. Investigations by SFG and PM-IRAS have been complemented by standard techniques for the characterization and preparation of the samples in UHV, such as X-ray photoelectron spectroscopy (XPS), low energy electron diffraction (LEED), and temperature programmed desorption (TPD).

Concerning SFG, a major part of the thesis work has been devoted to the design, assembling, and commissioning of an UHV experimental chamber coupled to an atmospheric pressure compatible SFG spectroscopic cell for catalytic measurements. This special combination allows controlled sample preparation and characterization in UHV, followed by UHV-transfer of the model catalyst to the spectroscopic cell. In the cell in-situ SFG measurements combined with simultaneous catalytic activity measurements by mass spectroscopy (MS) are performed in a wide pressure and temperature window. To test the capability of the new setup some well-known systems have been revisited, such as the adsorption of carbon monoxide on platinum and palladium single crystals. A pressure- and polarization-dependent study has been performed on Pt(111), while the CO/Pd(111) system was addressed either in UHV at liquid N<sub>2</sub> temperature (reproducing the (2×2)-3CO structure), or at room temperature and mbar pressure. Furthermore,

the simultaneous measurements by SFG and MS were employed to study the oxidation of carbon monoxide to carbon dioxide at near-atmospheric pressure by a model catalysts of Pt nanoparticles supported on zirconia thin films.

In the second part of the thesis the interaction of carbon monoxide with the copper (100) single crystal surface was investigated by PM-IRAS, XPS, LEED, and TPD. This model study addresses the important question of the role of catalytically active copper in processes like the methanol synthesis. First, the adsorption at low temperature was revisited: CO adsorbs reversibly as an ordered  $c(2\times 2)$  overlayer characterized by a C-O stretching vibrational fingerprint at  $2082\text{ cm}^{-1}$ , a calculated desorption activation energy of  $0.46\text{ eV}$  per molecule, and characteristic XPS features in the C1s and O1s binding energy regions. In contrast, the exposure of Cu(100) to CO at mbar pressure and room temperature induced non-reversible modifications of the surface. The C-O stretching vibrational fingerprint was detected at higher wavenumber ( $2093\text{--}2103\text{ cm}^{-1}$ ), corresponding to adsorption at low-coordinated Cu sites. Additionally, XPS detected atomic oxygen and carbon after exposure, suggesting activity of such sites for CO dissociation. The vibrational results were in good agreement with density functional theory (DFT) calculations performed by collaboration partners at KAUST Catalysis Center, and allowed to propose a mechanism by which the elevated pressure exposure to CO leads to a roughening of the Cu surface. This conclusion is consistent with high-pressure scanning tunneling spectroscopy (HP-STM) results recently published by the research group of M. Salmeron, Lawrence Berkeley National Laboratory.

In the third part of the thesis, results obtained in the framework of a joint project with the University of Trieste, Italy, are discussed. A 2D metalorganic layer of carbonylated iron phthalocyanines supported on a graphene sheet grown on Ir(111) was investigated both by PM-IRAS and SFG. Four distinct C-O stretching vibrational fingerprints were observed by SFG, while



only a single one was detected by PM-IRAS. This results allowed to confirm that the four-fold splitting observed in SFG was of electronic origin, induced by the impinging visible laser radiation field, and not due to cooperative adsorption, adsorption on non-equivalent sites, or dipole-dipole interaction.



## ACKNOWLEDGEMENTS

---

Several words of Gratitude go to Prof. Günther Rupprechter. He gave me the opportunity to join his research group, and the three years I spent at the IMC are among the most rewarding throughout my life as a student. He has been not only the fundamental figure for a critical analysis and guide of my work, but also a continuous source of inspiration.

Many thanks go to Dr. Christoph Rameshan, the experience I could gain under his supervision is invaluable, and he was always within reach and available even in probably one of the busiest times of his life.

I want to express my thankfulness for having been given the opportunity of attending the Doctorate School Solids4Fun. The discussions with the professors and student colleagues during lectures, seminars, and summer schools led to unforgettable learning occasions. Furthermore, the funding involved therein (FWF W1243) made this work possible. Among the people involved in Solids4Fun, a special thank goes to André Vogel for his unlimited and friendly help in organizing and office issues.

This work benefitted from the positive working atmosphere set at the TU Wien and, in particular, at the IMC. I am grateful to Verena Pramhaas and Xia Li, for much I could learn in discussing and during the hours spent together in the lab. Thanks to Hao Li for patiently introducing to me the experimental details of the PM-IRAS setup and to Kresimir Anic for his help and the great time spent together. Many thanks go to Rainald Rosner, Johannes Frank, and Rupert Kleinl for the technical support in building the SFG apparatus, and to Ulrike Prohaska and Melanie Schärer for administrative issues. I should acknowledge Nevzat Yigit for several reasons, among others for keeping me awake by continuously rearranging the office desks disposition. Thanks to Klaus Dobrezberger, Andreas Nagl, Abdul Motin, Thomas Haunold, Liliana Lukahsuk, Ivan Bespalov, Andrey Bukhtiyarov, and all the people from the groups of Prof. Yuri Suchorski, Prof.

Hinrich Grothe, Prof. Karin Föttinger, and Dr. Noelia Barrabés. Many thanks to Prof. Erik Vesselli from University of Trieste for having introduced me to the fascinating world of surface science and spectroscopy and for his passionate attitude towards the shared projects we worked at. Thanks to Manuel Corva for the great lab time we shared in Vienna and Trieste.

Finally, I would like to thank my family: Michele, Maria, Timoteo and Frida, and Fiorenza, for their love and support, and to Valeria: the hours we spent together during the last three years were worth every countless km we had to travel by flibus, blablacar, or railjet. For our love is worth any obstacle.

# TABLE OF CONTENTS

---

<b>Kurzfassung .....</b>	<b>iii</b>
<b>Abstract.....</b>	<b>vii</b>
<b>Acknowledgements.....</b>	<b>xi</b>
<b>1 Introduction .....</b>	<b>1</b>
<b>2 Spectroscopic Techniques and Experimental Setup.....</b>	<b>9</b>
2.1 Ultra-high vacuum technology.....	9
2.2 Polarization-modulation infrared reflection absorption spectroscopy .....	14
2.3 Sum frequency generation spectroscopy .....	19
2.4 X-Ray photoelectron spectroscopy.....	22
2.5 Low energy electron diffraction.....	24
2.6 Temperature programmed desorption .....	28
<b>3 Atmospheric Pressure Reaction Cell for Operando Sum Frequency Generation Spectroscopy of Ultrahigh Vacuum Grown Model Catalysts.....</b>	<b>33</b>
3.1 Introduction .....	34
3.2 Equipment design .....	35
3.2.1 General layout.....	37
3.2.2 Sample holder and xyz $\phi$ manipulator.....	37
3.2.3 UHV preparation/analysis chamber and load lock .....	40
3.2.4 SFG spectroscopy cell and gas supply .....	41
3.2.5 Laser and optical detection system .....	45
3.3 Applications of the UHV-setup and SFG spectroscopic cell.....	46
3.3.1 CO adsorption on single crystalline Pt(111) and Pd(111) .....	47
3.3.2 CO oxidation on an ALD-grown Pt-ZrO <sub>2</sub> nanoparticle model catalyst .....	50
3.4 Conclusions .....	53
<b>4 CO-Induced Surface Roughening of Copper (100) at Elevated Pressure: Cu Cluster Formation and CO Dissociation.....</b>	<b>63</b>
4.1 Introduction .....	63
4.2 Experimental details .....	65
4.3 Results and discussion .....	67
4.3.1 CO adsorption on Cu(100) under UHV conditions .....	67
4.3.2 CO adsorption on Cu(100) at mbar pressure .....	73

4.4	Conclusions .....	78
<b>5</b>	<b>Vibronic Properties of Carbonylated Iron Phthalocyanines.....</b>	<b>87</b>
5.1	Introduction .....	87
5.2	Experimental details .....	88
5.3	Results and discussion .....	91
5.4	Conclusions .....	99
<b>6</b>	<b>Conclusions .....</b>	<b>103</b>
	<b>Publication List .....</b>	<b>107</b>
	Journal articles .....	107
	Oral and poster presentations as first author .....	107
	<b>Curriculum Vitae .....</b>	<b>111</b>

# 1 INTRODUCTION

---

Surface science and model catalysis have been recognized for long as powerful tools to gain fundamental, atomistic, insight into the processes and phenomena of heterogeneous catalysis [1-4].

The basic idea of such investigations is to unravel the working principles of heterogeneous systems by addressing their complexity stepwise and by working under well-controlled conditions [5]. The latter refers to both the solid sample (surface), characterized by defined atomic composition, purity, and crystallographic orientation; and to the environment in which the model catalyst is placed. This is in many cases an ultra-high vacuum (UHV) vessel, in which the samples are exposed to the desired reaction gases. Real catalysts are typically highly dispersed powders consisting of metal nanoparticles deposited on high surface area metal-oxide supports, sometimes including smaller amounts of promoting agents. Several variables contribute to the performance of such catalysts, from the electronic and morphological structure of the nanoparticles, to their interaction with the oxide support, and the presence of promoters. A fundamental understanding can be obtained only by investigating the effect of such parameters one by one, in a stepwise approach. One may address this “material gap” by starting to analyze the interaction of the reactants with an ordered single crystalline metal surface or with the more complex metal-oxide surface. It is possible to further increase complexity by introducing morphological defects such as steps and adatoms, or finally investigate the behavior of deposited nanoparticles on a support, or that of metal-oxide nanoclusters (islands) on a metallic support (“inverse” catalysts) [6].

The key techniques in traditional surface studies are often based on the detection of electrons (photoelectron spectroscopies, electron energy loss spectroscopies, electron

## 1. Introduction

diffraction), which limits their applicability to the (ultra-)high vacuum regime. Conversely, most processes in real (industrial) heterogeneous catalysis take place at much higher pressure (>1 bar), this difference constituting the *pressure gap*. Results obtained in UHV cannot always be straightforwardly applied to a real catalytic environment [5, 7, 8]. Therefore, in the last decades several efforts have been made to extend the working range of surface science techniques towards higher pressure regimes [9] by developing tools such as near-ambient pressure X-ray photoelectron spectroscopy (NAP-XPS) [10-13], high pressure scanning tunneling microscopy (HP-STM) [14], or the photon-based sum frequency generation spectroscopy (SFG) [15-18] and polarization-modulation IR reflection absorption spectroscopy (PM-IRAS) [19, 20].

Indeed, higher gas pressure have in some cases dramatic effects on model catalyst systems, for example leading to formation of new adsorbate structures [5, 21], sintering (i.e. growth) of the nanoparticles [22-24], and adsorbate-induced restructuring of nanoparticles [25-27] or surfaces [28-31].

The aim of this thesis was to carry out spectroscopic investigations of model catalysts by SFG and PM-IRAS, particularly characterizing the properties of species adsorbing and reacting from a gas phase at mbar pressure.

The fundamentals of SFG and PM-IRAS, along with those of the other main techniques employed for this work such as XPS, low energy electron diffraction (LEED), and temperature programmed desorption (TPD), are discussed in **Chapter 2**. Furthermore, some aspects of ultra-high vacuum technology are discussed as well.

A major part of the thesis is dedicated to the design, assembly, and commissioning of a new UHV apparatus with attached high pressure spectroscopic cell to perform in-situ SFG spectroscopy [32]. The new setup, thoroughly described in **Chapter 3**, allows measuring SFG in a broad pressure (from UHV to 1000 mbar) and temperature (100 to 1000 K) range. In this apparatus samples can



be inserted fast via a load lock, prepared and characterized in UHV, and moved under vacuum into a high pressure-compatible spectroscopic cell. There, catalytic activity tests can be performed and simultaneously followed by SFG and mass spectroscopy. Some first results were obtained for adsorption of CO, a useful probe molecule, on Pd and Pt single crystal samples [33]. The setup was further tested by CO oxidation on zirconia supported Pt nanoparticles.

**Chapter 4** describes investigations of the interaction of carbon monoxide (in the mbar pressure range, at RT) with a copper (100) single crystal surface. Both CO and copper are essential ingredients in the industrial synthesis of methanol from synthesis gas. In-situ measurements with PM-IRAS and ex-situ measurements with XPS, LEED, and TPD revealed morphological modifications of the surface ordering upon high pressure CO adsorption. The latter was corroborated by density functional theory (DFT) calculations performed at the KAUST Catalysis Center, Tuwal, Saudi Arabia, and are in line with recent HP-STM results reported by the group of M. Salmeron, Lawrence Berkeley National Laboratory, Berkeley, USA [28-30].

The chance to discuss remarkable differences between SFG and PM-IRAS was given by a project pursued in collaboration with the group of Prof Erik Vesselli from University of Trieste, Italy, with results being presented in **Chapter 5**. The vibrational properties of a carbonylated monolayer of iron phthalocyanines deposited on a graphene sheet on an iridium single crystal were examined both by PM-IRAS (at Technische Universität Wien) and by SFG (at University of Trieste). The experiments demonstrated that during SFG experiments a splitting of the adsorbed CO stretching vibrational mode was induced by the visible laser radiation (low to high spin transition) which could be detected by the infrared probe. In contrast, PM-IRAS detected only a single band due to the absence of an intense visible light excitation. Furthermore, this project enabled to develop in-house a custom built molecular evaporator and to familiarize with self-

## 1. Introduction

assembled monolayers [34] and single-atom catalysts. The latter concepts bring surface science investigations closer to the field of enzymatic catalysis.

The most important conclusions of this work are summarized in **Chapter 6**.

## Bibliography

- [1] G. Ertl, Reactions at surfaces: From atoms to complexity (Nobel lecture), *Angewandte Chemie-International Edition*, 47 (2008) 3524-3535.
- [2] G.A. Somorjai, Modern surface science and surface technologies: An introduction, *Chemical Reviews*, 96 (1996) 1223-1235.
- [3] G.A. Somorjai, G. Rupprechter, The flexible surface, *Journal of Chemical Education*, 75 (1998) 161-161.
- [4] G. Rupprechter, G.A. Somorjai, Adsorbate properties of linear hydrocarbons, in: H.P. Bonzel (Ed.) *Landolt-Börnstein: Physics of Covered Solid Surfaces*, Springer 2006, pp. 243-330.
- [5] G. Rupprechter, Sum Frequency Generation and Polarization-Modulation Infrared Reflection Absorption Spectroscopy of Functioning Model Catalysts from Ultrahigh Vacuum to Ambient Pressure, in: B.C. Gates, H. Knözinger (Eds.) *Advances in Catalysis*, Vol 51, Elsevier Academic Press Inc, San Diego, 2007, pp. 133-263.
- [6] K. Hayek, M. Fuchs, B. Klötzer, W. Reichl, G. Rupprechter, Studies of metal-support interactions with "real" and "inverted" model systems: reactions of CO and small hydrocarbons with hydrogen on noble metals in contact with oxides, *Topics in Catalysis*, 13 (2000) 55-66.
- [7] Special Issue on "In-situ Characterization of Catalysts", 2001.
- [8] Special Issue on "In-situ Characterization of Catalysts", 1999.
- [9] G. Rupprechter, Sum frequency laser spectroscopy during chemical reactions on surfaces, *Mrs Bulletin*, 32 (2007) 1031-1037.

[10] R.W. Joyner, M.W. Roberts, K. Yates, High pressure electron spectrometer for surface studies, *Surface Science*, 87 (1979) 501-509.

[11] V.I. Bukhtiyarov, V.V. Kaichev, I.P. Prosvirin, X-ray photoelectron spectroscopy as a tool for in-situ study of the mechanisms of heterogeneous catalytic reactions, *Topics in Catalysis*, 32 (2005) 3-15.

[12] V.V. Kaichev, I.P. Prosvirin, V.I. Bukhtiyarov, H. Unterhalt, G. Rupprechter, H.J. Freund, High-pressure studies of CO adsorption on Pd(111) by X-ray photoelectron spectroscopy and sum-frequency generation, *Journal of Physical Chemistry B*, 107 (2003) 3522-3527.

[13] M. Morkel, V.V. Kaichev, G. Rupprechter, H.J. Freund, I.P. Prosvirin, V.I. Bukhtiyarov, Methanol dehydrogenation and formation of carbonaceous overlayers on Pd(111) studied by high-pressure SFG and XPS spectroscopy, *Journal of Physical Chemistry B*, 108 (2004) 12955-12961.

[14] B.J. McIntyre, M. Salmeron, G.A. Somorjai, In-situ scanning tunneling microscopy study of platinum (110) in a reactor cell at high pressures and temperatures, *Journal of Vacuum Science & Technology a-Vacuum Surfaces and Films*, 11 (1993) 1964-1968.

[15] P.S. Cremer, B.J. McIntyre, M. Salmeron, Y.R. Shen, G.A. Somorjai, Monitoring surfaces on the molecular level during catalytic reactions at high pressure by sum frequency generation vibrational spectroscopy and scanning tunneling microscopy, *Catalysis Letters*, 34 (1995) 11-18.

[16] G.A. Somorjai, G. Rupprechter, Molecular studies of catalytic reactions on crystal surfaces at high pressures and high temperatures by infrared-visible sum frequency generation (SFG) surface vibrational spectroscopy, *Journal of Physical Chemistry B*, 103 (1999) 1623-1638.

[17] T. Dellwig, G. Rupprechter, H. Unterhalt, H.J. Freund, Bridging the pressure and materials gaps: High pressure sum frequency generation study on supported Pd nanoparticles, *Physical Review Letters*, 85 (2000) 776-779.

## 1. Introduction

[18] G. Rupprechter, A surface science approach to ambient pressure catalytic reactions, *Catalysis Today*, 126 (2007) 3-17.

[19] E. Ozensoy, D.C. Meier, D.W. Goodman, Polarization modulation infrared reflection absorption spectroscopy at elevated pressures: CO adsorption on Pd(111) at atmospheric pressures, *Journal of Physical Chemistry B*, 106 (2002) 9367-9371.

[20] M. Borasio, O.R. de la Fuente, G. Rupprechter, H.J. Freund, In Situ Studies of Methanol Decomposition and Oxidation on Pd(111) by PM-IRAS and XPS Spectroscopy, *Journal of Physical Chemistry B*, 109 (2005) 17791-17794.

[21] J.A. Jensen, K.B. Rider, M. Salmeron, G.A. Somorjai, High pressure adsorbate structures studied by scanning tunneling microscopy: CO on Pt(111) in equilibrium with the gas phase, *Physical Review Letters*, 80 (1998) 1228-1231.

[22] P. Stone, S. Poulston, R.A. Bennett, M. Bowker, Scanning tunnelling microscopy investigation of sintering in a model supported catalyst: nanoscale Pd on TiO<sub>2</sub>(110), *Chemical Communications*, (1998) 1369-1370.

[23] M. Heemeier, S. Stempel, S.K. Shaikhutdinov, J. Libuda, M. Baumer, R.J. Oldman, S.D. Jackson, H.J. Freund, On the thermal stability of metal particles supported on a thin alumina film, *Surface Science*, 523 (2003) 103-110.

[24] S.L. Tait, L.T. Ngo, Q.M. Yu, S.C. Fain, C.T. Campbell, Growth and sintering of Pd clusters on alpha-Al<sub>2</sub>O<sub>3</sub>(0001), *Journal of Chemical Physics*, 122 (2005) 9.

[25] G. Rupprechter, H.J. Freund, Adsorbate-induced restructuring and pressure-dependent adsorption on metal nanoparticles studied by electron microscopy and sum frequency generation spectroscopy, *Topics in Catalysis*, 14 (2001) 3-14.

- [26] T. Schalow, B. Brandt, D.E. Starr, M. Laurin, S. Schauer mann, S.K. Shaikhutdinov, J. Libuda, H.J. Freund, Oxygen-induced restructuring of a Pd/Fe<sub>3</sub>O<sub>4</sub> model catalyst, *Catalysis Letters*, 107 (2006) 189-196.
- [27] C.R. Henry, Surface studies of supported model catalysts, *Surface Science Reports*, 31 (1998) 235-325.
- [28] B. Eren, D. Zherebetsky, L.L. Patera, C.H. Wu, H. Bluhm, C. Africh, L.W. Wang, G.A. Somorjai, M. Salmeron, Activation of Cu(111) Surface by Decomposition into Nanoclusters Driven by CO Adsorption, *Science*, 351 (2016) 475-478.
- [29] B. Eren, Z.Y. Liu, D. Stacchiola, G.A. Somorjai, M. Salmeron, Structural Changes of Cu(110) and Cu(110)-(2 x 1)-O Surfaces under Carbon Monoxide in the Torr Pressure Range Studied with Scanning Tunneling Microscopy and Infrared Reflection Absorption Spectroscopy, *Journal of Physical Chemistry C*, 120 (2016) 8227-8231.
- [30] B. Eren, D. Zherebetsky, Y.B. Hao, L.L. Patera, L.W. Wang, G.A. Somorjai, M. Salmeron, One-dimensional nanoclustering of the Cu(100) surface under CO gas in the mbar pressure range, *Surface Science*, 651 (2016) 210-214.
- [31] F. Tao, S. Dag, L.W. Wang, Z. Liu, D.R. Butcher, H. Bluhm, M. Salmeron, G.A. Somorjai, Break-Up of Stepped Platinum Catalyst Surfaces by High CO Coverage, *Science*, 327 (2010) 850-853.
- [32] M. Roiaz, V. Pramhaas, X. Li, C. Rameshan, G. Rupprechter, Atmospheric Pressure Reaction Cell for Operando Sum Frequency Generation Spectroscopy of Ultrahigh Vacuum Grown Model Catalysts, *Review of Scientific Instruments*, accepted.
- [33] X. Li, M. Roiaz, V. Pramhaas, C. Rameshan, G. Rupprechter, Polarization-Dependent SFG Spectroscopy of Near Ambient Pressure CO Adsorption on Pt(111) and Pd(111) Revisited, *Topics in Catalysis*, accepted.

## 1. Introduction

[34] A. Ulman, Formation and structure of self-assembled monolayers, *Chemical Reviews*, 96 (1996) 1533-1554.

## 2 SPECTROSCOPIC TECHNIQUES AND EXPERIMENTAL SETUP

---

In this chapter the experimental requirements and the techniques which have been mostly used for this thesis work will be described. First, the need for ultra-high vacuum (UHV) for fundamental studies on model catalysts will be shortly discussed. Since a large part of this thesis has been the design and commissioning of a new UHV setup coupled to an atmospheric pressure-compatible spectroscopy and reaction cell (described thoroughly in **Chapter 3**), some technical details about UHV technology will be given. Then the basics and advantages of infrared spectroscopy will be discussed, in particular about polarization-modulation infrared reflection absorption spectroscopy (PM-IRAS) and visible-infrared sum frequency generation vibrational spectroscopy (SFG). Afterwards, other fundamental techniques such as X-ray photoelectron spectroscopy (XPS), low energy electron diffraction (LEED), and temperature programmed desorption (TPD) will be discussed. Their applications can be found in **Chapter 4**, where the interaction of the copper (100) surface with carbon monoxide is discussed.

### 2.1 ULTRA-HIGH VACUUM TECHNOLOGY

For model catalyst studies, an important requirement is to work under controlled conditions. Therefore the ability to precisely control - at least during the time required to perform the experiment - the composition of the surface, the adsorbates, and the gas atmosphere (which is in contact with the sample) is a key premise. In particular, supposing that the sample surface is clean (i.e. of defined atomic composition) at the beginning of the experiment and that the only source of contaminants consists of atoms or molecules adsorbing on it from the gas phase, we would like to estimate for how long the concentration of such contaminants on the surface is negligible. This can be done by defining a quantity known as *rate of arrival*  $r$  of molecules (or

## 2. Spectroscopic Techniques and Experimental Setup

atoms) on the surface. By the kinetic theory of gases it is possible to show [1] that the rate  $r$  is proportional to the gas pressure in the vacuum vessel. It can be expressed, in molecules per unit surface per unit time, as follows:

$$r = \frac{p}{\sqrt{2\pi k_B T m}},$$

where  $p$  is the gas pressure,  $m$  is the particle's mass,  $k_B = 1.381 \times 10^{-23} \text{ J K}^{-1}$  is Boltzmann's constant and  $T$  is the temperature. If we express  $p$  in mbar,  $T$  in K, and  $m$  in molecular weight (remembering the atomic mass unit  $u = 1.661 \times 10^{-27} \text{ kg}$ ), we obtain  $r$  expressed in molecules per  $\text{cm}^2$  per second:

$$r = 2.63 \times 10^{22} \frac{p}{\sqrt{TM}}.$$

If we consider  $\text{N}_2$  molecules ( $M = 28$ ) at room temperature ( $T = 298 \text{ K}$ ), define the surface coverage in terms of monolayer ML (1 ML consists of about  $10^{15}$  molecules per  $\text{cm}^2$ ), and assume that all the molecules impinging on the surface stick and are incorporated into the monolayer, then at atmospheric pressure ( $p = 1013.25 \text{ mbar}$ ) the surface is covered by a monolayer in  $10^{-6}$  s. Conversely, if we want our surface to be adsorbate-free during a typical time needed for an experiment, say 10 hours, then the pressure should be no more than  $10^{-10} \text{ mbar}$ , that is ultra-high vacuum.

Such pressure regimes are obtained by dedicated vacuum pumps. Several designs are available, according to the desired vacuum and other needs (for example type of lubricant for the pump moving parts, or intensity of the pump mechanical vibrations, etc.). It is often necessary to couple in series different pumps working in different ranges. For example a turbomolecular pump providing ultra-high vacuum in the experimental chamber requires a fore-vacuum of no more than  $10^{-2}$  to 1 mbar (medium vacuum), and this can be provided by a rotary vane pump or by a membrane pump. Since these are the pump designs which have been chosen for the new SFG



## 2. Spectroscopic Techniques and Experimental Setup

setup, and they were also present in the PM-IRAS setup, their working principle will be shortly described. All of them are of the gas-displacement type.

In a rotary vane vacuum pump, schematically represented in **Figure 2-1**, an eccentrically installed rotor (2) is equipped with vanes (3) that move radially under centrifugal forces inside the housing (1). The rotor and vanes divide the working chamber (5) into two separate compartments with variable volumes. As the rotor turns, gas flows into the enlarging compartment of the chamber until it is sealed off by the second vane. The enclosed gas is then compressed until the outlet valve opens against atmospheric pressure. Oil is needed to operate the pump, and it accomplishes several tasks: lubricates the moving parts, fills the dead volume under the outlet valve and the narrow gap between the inlet and outlet valve, compresses the gap between the vanes and the working chamber inner surface and ensures optimal temperature balance through heat transfer. Rotary vane pumps allow reaching a pressure in the  $10^{-4}$  to  $10^{-3}$  mbar range (middle vacuum). A drawback consists in the diffusion of oil in the experimental chamber, which can be prevented or at least hindered by installing zeolite traps between the inlet valve and the pipe to the fore-vacuum of the turbomolecular pump.

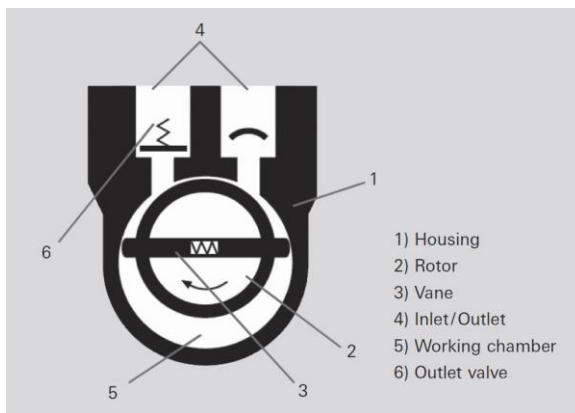


**Figure 2-1:** Schematic section view of a rotary vane pump. Adapted from [2].

A diaphragm vacuum pump, schematically pictured in **Figure 2-2** is a dry (oil-free) positive-displacement pump. A crankshaft drives a connecting rod (4) connected to a diaphragm (1)

## 2. Spectroscopic Techniques and Experimental Setup

tensioned between the head cover (2) and the housing (3), such that the diaphragm moves up-and downwards, and the space between the head cover and the diaphragm forms the working chamber (5). Pressure-controlled shutter valves made of elastomer materials control the gas displacement. The working chamber is sealed off from the drive by the diaphragm, therefore no oil contamination can occur (nor can aggressive media corrode the mechanics). Connecting multiple pumping stages in series makes it possible to attain an ultimate pressure of 0.5 mbar.

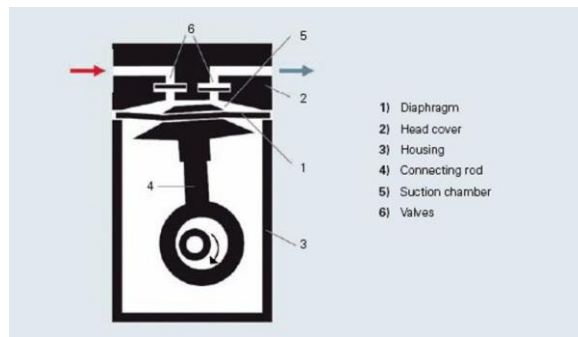


**Figure 2-2:** Schematic section view of a diaphragm vacuum pump. Adapted from [2].

Turbomolecular pumps allow achieving pressures in the ultra-high vacuum range. They belong to the category of kinetic vacuum pumps, and consist of a turbine-like rotor with bladed disks which rotates in a housing. The rotors are driven by DC motors which allow rotational frequencies of up to 1500 Hz. Most turbomolecular pumps require a fore-vacuum of  $10^{-3}$  to  $10^{-2}$  mbar, however the insertion of a Holweck pump (or molecular drag pump) as last stage of the rotor allows a higher fore-vacuum in the 1 to 10 mbar range.

To achieve pressures in the ultra-high vacuum range a major requirement is to remove humidity and residual hydrogen from the UHV system. The reason is that upon exposure to air (venting), water instantly adsorbs on the inner walls of experimental chambers, pipes, and internal instruments components. This adsorbed water is a source of contamination in the UHV system and because of slow desorption it limits the achievable vacuum. On the other hand, it is well known that hydrogen penetrates inside steel during fabrication. Atomic hydrogen

## 2. Spectroscopic Techniques and Experimental Setup

subsequently diffuses from the bulk to the surface, where recombines and desorbs as H<sub>2</sub> causing a roughly constant flux for several years [3]. The solution consists in speeding up the desorption by a process known as bake-out: The complete UHV system is heated to higher temperature for a certain time. For example, a 24-hours bake-out of the preparation chamber of the SFG experimental setup (described in **Chapter 3**) to a temperature of 130-150 °C allowed to reach a background pressure of  $5 \times 10^{-10}$  mbar. Lower pressure ranges may be attained by upgrading the system with a gas-binding pump (e.g. titanium sublimation pump) which would pump the hydrogen further outgassing from the metal components (turbomolecular pumps are not efficient for H<sub>2</sub> pumping because of its low mass).

Concerning vacuum measurement, four different technologies have been applied to the experimental setup developed in the framework of this thesis: hot-cathode and cold-cathode for the high and ultra-high vacuum, Pirani sensor for the middle vacuum, and capacitance gauge for (near-) ambient pressure. A hot-cathode of the Bayard-Alpert design consists of a thermal electron source, a helical grid at positive potential, and a collector wire at negative potential. The emitted electrons are attracted to the grid and fall into the space enclosed by it, causing a fraction of the gas molecules to ionize by collision. The ionized gas molecules are then attracted to the collector, causing an electrical current proportional to the gas density, as well as depending on the gas type. A cold cathode lacks a thermionic electron source, and traps the electrons which are randomly released at the cathode (by an impinging cosmic ray or photon, because of field emission or radioactivity, or due to some other event) in a region of crossed electric and magnetic fields. Either hot- and cold-cathode gauges should not be operated above  $10^{-4}$  mbar, therefore they must be manually switched on/off, or –as it is often the case– they are coupled to a Pirani sensor and an electronic system which allow this task to be performed automatically. A Pirani sensor, by the name of its inventor Marcello Pirani, consists of a heated filament. The latter loses

## 2. Spectroscopic Techniques and Experimental Setup

heat whenever gas molecules collide with it, and a measure of this heat loss is an indirect indication of the gas pressure. The pressure reading strongly depends on the thermal conductivity and heat capacity of the gas, and this effect becomes critical at pressures above  $\sim 1$  mbar. Therefore a gas-type independent gauge, e.g. a capacitive gauge, must be used in the (near-) ambient pressure range. This consists of a diaphragm which is deflected proportionally to the pressure applied to it. A sensor (e.g. a capacitive sensor) measures the deflection and converts it into an electrical signal.

### 2.2 POLARIZATION-MODULATION INFRARED REFLECTION ABSORPTION SPECTROSCOPY

Vibrational spectroscopy can provide a wealth of information on industrial and model catalysts, in particular adsorbed species can be identified and the nature of the adsorption site unraveled. Several probes can be employed to perform vibrational spectroscopy, such as photons (adsorbed or scattered), electrons, or neutrons. We will focus on two techniques based on the absorption of photons, namely polarization-modulation infrared reflection absorption spectroscopy (PM-IRAS) and visible-infrared sum frequency generation vibrational spectroscopy (SFG). Both of them have been applied in the mid-infrared range ( $200$  to  $4000$   $\text{cm}^{-1}$ ), the most interesting for us since it targets the molecular vibrations (especially  $\text{CO}_x$ ,  $\text{CH}_x$ , and  $\text{OH}$ ).

Molecules are characterized by discrete rotational and vibrational energy levels, and transitions between the levels occur upon absorption of photons of matching energy. A commonly employed model to approximate the potential energy function for a non-rotating diatomic molecule is the Morse potential [4]:

$$V(r) = D[1 - e^{-\beta(r-r_e)}]^2,$$

where  $V(r)$  is the interatomic Morse potential,  $r$  is the distance between the vibrating atoms,  $r_e$  is the equilibrium distance between the vibrating atoms,  $D$  is the dissociation energy of the

## 2. Spectroscopic Techniques and Experimental Setup

vibrating atoms, and  $\beta$  is a parameter which controls the steepness of the potential well. In the case of CO, the aforementioned parameters can be spectroscopically estimated as  $r_e = 1.1283 \text{ \AA}$ ,  $D = 88891 \text{ cm}^{-1}$ , and  $\beta = 2.3205 \text{ \AA}^{-1}$ . The Schrödinger equation for the Morse potential can be solved analytically and the eigenvalues are found to be

$$G(v) = \omega_e \left( v + \frac{1}{2} \right) - \omega x_e \left( v + \frac{1}{2} \right)^2 ,$$

with  $\omega_e = 2169.713 \text{ cm}^{-1}$  and  $\omega x_e = 13.23996 \text{ cm}^{-1}$ . From the analytical expression of  $\omega_e$  and  $\omega x_e$  [5] it is possible to see that the vibrational frequencies increase with increasing bond strength and with decreasing reduced mass of the molecule.

Several types of infrared spectroscopy are in use, however we will focus on the (polarization-modulation) reflection absorption spectroscopy. The infrared probe beam impinges on the sample at grazing angle, i.e. almost parallel to the surface. In this geometric configuration, the local electric field induced on a metal surface by *s*-polarized light is vanishing [6], therefore no absorption of *s*-polarized light will occur by adsorbed molecules. Conversely, *p*-polarized light is absorbed. If the technique is applied in polarization modulation (PM-IRAS) – that is, *s*- and *p*-polarized light is alternately shined on the sample – then the subsequent demodulation of the recorded signal provides inherently surface specific information. This makes the technique particularly suitable to be applied at close-to-real pressure conditions.

The main components of the PM-IRAS spectrometer, described below, are the Fourier-transform spectrometer (FT-IR), responsible to generate the broadband IR light and acquire spectra, and the photoelastic modulator which modulates between *s*- and *p*-polarized light. Unlike a dispersive instrument, i.e. a grating monochromator, an FT-IR spectrometer collects all wavelengths simultaneously. Infrared spectra are obtained by first collecting an interferogram of a sample signal using an interferometer, and then performing a Fourier transform (FT) on the interferogram to obtain the spectrum. An FT-IR is typically based on the Michelson

## 2. Spectroscopic Techniques and Experimental Setup

interferometer, schematically represented in **Figure 2-3**. Light from the source *S* falls on the beam splitter *A*, which divides the beam in two parts. These separated beams are reflected back to *A* by a fixed mirror *C* and a second mirror *D* which can move back and forth very precisely. The interference pattern is observed at *E* as an interferogram, that is pairs of values consisting of signal and optical path difference between the two beams. The latter is transformed into a spectrum by a fast Fourier transform algorithm. A single scan of the mirror position should be theoretically sufficient to give an interferogram, but the noise level would be high. In order to decrease it, the mirror is usually scanned *N* times.

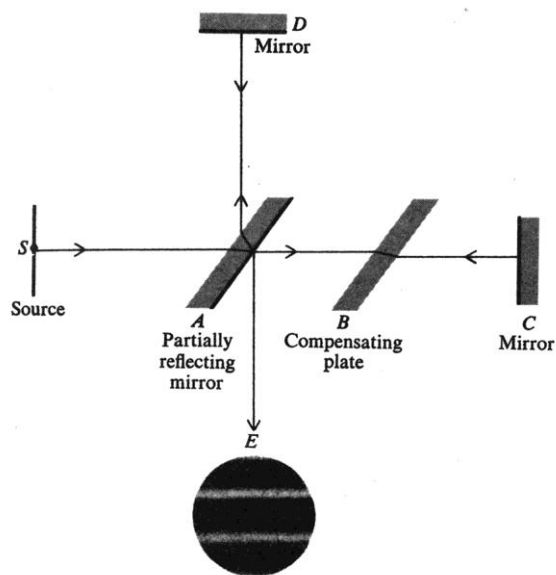


**Figure 2-3:** Optical paths in the Michelson interferometer. Adapted from [7].

The employed Bruker IFS 66v/s FT-IR spectrometer system consists of several different modules: the optical bench (accommodating the interferometer, the optics, the detector, and the vacuum valves), the electronics unit, the source cooling system (by a thermostatically controlled closed loop water circulator), and an external vacuum system (pump, demister, bellows and pipes and valves to pump and backfill the optical bench). The operating vacuum inside the optics bench was less than 3 mbar. “OPUS/IR” software was used to control the spectrometer and acquire the

## 2. Spectroscopic Techniques and Experimental Setup

spectra. An optional exit port was provided to allow the IR radiation routing to the external sample chamber. The detector is a mercury cadmium telluride (MCT) detector, and the source a SiC globar, providing radiation in the  $7500 - 370 \text{ cm}^{-1}$  frequency range. A SiC globar (portmanteau for glow and bar) is a silicon carbide rod which is electrically heated up to  $1000$  to  $1650 \text{ }^\circ\text{C}$  and has a spectral behavior corresponding approximately to that of a black body. The spectrometer can be equipped with other sources, e.g. a mercury lamp (Far-IR), a tungsten lamp (Near-IR), or a deuterium lamp (UV). The spectrometer is also provided with a HeNe laser. This emits light with a wavelength which is known with a very high degree of accuracy ( $633 \text{ nm}$ ,  $1\text{mW}$ ) and which does not significantly change under any circumstances, thus providing an internal reference source for calibration of the interferometer.

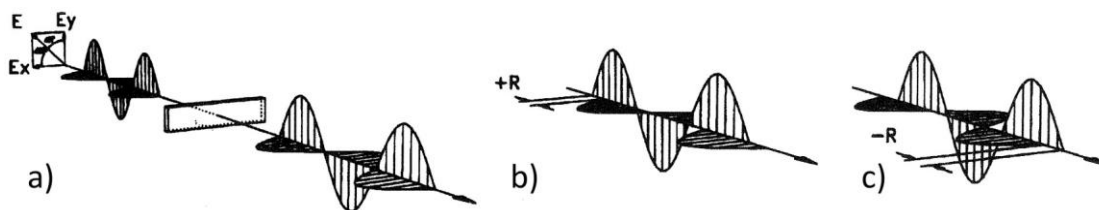


**Figure 2-4:** Retardation effects of compression (b) and extension (c).

The modulation of the IR light polarization is performed by a photoelastic modulator PEM-90. The main component of the PEM-90 consists of a piece of ZnSe bonded to two quartz piezoelectric transducers. The latter are connected to a driver circuit which applies an electrical signal resulting in a modulated mechanical stress on the ZnSe optical element. By the phenomenon known as photoelastic effect, ZnSe exhibits birefringence which is proportional to the strain resulting from the applied stress. By birefringence it is meant that light with different linear polarizations have slightly different speeds when passing through the material. The effect of the modulator on a linear polarized monochromatic light wave is shown in **Figure 2-4**. The plane of polarization is at  $45$  degrees to the modulator axis before passing through the modulator. If the

## 2. Spectroscopic Techniques and Experimental Setup

optical element is relaxed, the light passes through with the polarization unchanged (**Figure 2-4 a**). If the optical element is compressed, the polarization component parallel to the modulator axis travels slightly faster than the vertical component (**Figure 2-4 b**). The horizontal component then “leads” the vertical component after light passes through the modulator. If the optical element is stretched, the horizontal component “lags” behind the vertical component (**Figure 2-4 c**). The phase difference between the components at any instant of time is called the retardation. An important condition occurs when the retardation reaches one-half of the wavelength of the light. When this happens, the PEM acts as a half-wave plate at the instant of maximum retardation and rotates the plane of polarization by 90 degrees.

The intensity of the output light after the polarization can be mathematically described by a time-dependent function as [8]:

$$I(t) = [I_p + I_s + (I_p - I_s) \cos(\varphi_0 \cos(\gamma t))]/2$$

where  $I_{p,s}$  are respectively the  $p$ - and  $s$ -polarized light intensities with respect to the sample surface,  $\cos(\gamma t)$  is set to the modulation frequency of 37 kHz, and the constant  $\varphi_0$  depends linearly on the modulation voltage  $V_m$  and is inversely related to the wavelength  $\lambda$  of the IR light. To obtain the desired differential spectrum, the detector signal is processed by a specialized electronics using a single analog to digital converter, a multiplexing electronics unit, a PEM controller, and a synchronous sampling demodulator (SSD-100, GWC Instruments). This specialized electronics generate the difference and the average interferograms, by digitizing the two signals simultaneously. In the detector signal, in fact, there are two different modulations, the Fourier modulation by the interferometer, and the polarization modulation by the PEM. These two modulations contain different spectral information and they have to be separated in order to retrieve the two spectra. The low frequency signal corresponds to the “normal” interferogram,



## 2. Spectroscopic Techniques and Experimental Setup

containing the Fourier frequencies. The high frequency signal, instead, corresponds to the PEM frequency and carries the differential absorption of *p*- and *s*-polarized light.

The detector signal is processed in the following way. The interferogram is split into two channels. In one channel the signal is passed through a low pass filter to remove the high PEM frequency. This signal, now containing only the low frequencies, is digitized and recorded to produce an interferogram. This interferogram is then transformed in a single beam spectrum of the sample, giving the average of the absorption of *p*- and *s*-polarized light by the sample,  $(I_p + I_s)/2$ . The other channel of the detector signal is processed through a synchronous demodulator, locked onto the PEM frequency. The output from this special lock-in detection is then digitized and recorded by the second digitizer. The spectrum gives the differential absorption of *p*- and *s*-polarized light by the sample,  $I_p - I_s$ .

A PM-IRAS spectrum, also called differential reflectance spectrum  $\Delta R/R$ , is then calculated from the two spectra acquired simultaneously:

$$\frac{\Delta R}{R} \approx \left[ \frac{1 - \cos \varphi_0}{2} - \frac{I_p - I_s}{I_p + I_s} \times \frac{(\sin \varphi_0)^2}{8} \right] \times \frac{I_p - I_s}{\frac{I_p + I_s}{2}} \approx J_2(\varphi_0) \frac{I_p - I_s}{\frac{I_p + I_s}{2}}$$

where  $J_2(\varphi_0)$  is a second order Bessel function [9]. The background can be eliminated by dividing  $\Delta R/R$  either by a fitted polynomial function, or - as has been the case in this work - by a spectrum of the clean sample surface acquired under identical conditions.

### 2.3 SUM FREQUENCY GENERATION SPECTROSCOPY

Another technique which is particularly suitable to investigate vibrational properties of surface adsorbates in-situ under (near-) atmospheric pressure is sum frequency generation spectroscopy (SFG). Although it was originally developed in order to convert the infrared resonant signal to the visible so that it could be more easily detected, and because of its perspective

## 2. Spectroscopic Techniques and Experimental Setup

application to investigate fast surface molecular dynamics [10], it continued to be applied even after IR detector advances. In this optical spectroscopy techniques, two input beams at frequencies  $\omega_1$  (e.g. in the visible) and  $\omega_2$  (e.g. in the mid-IR) overlap in a medium or on a surface and generate a sum frequency output at  $\omega_1 + \omega_2$ .

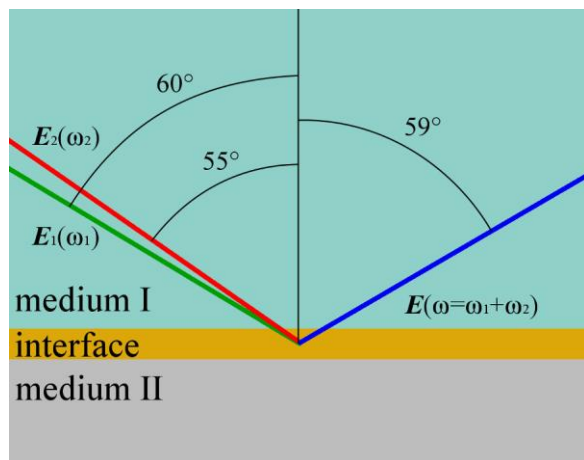


**Figure 2-5:** Schematic representation of an SFG experiment and of the relevant radiation fields.

As a second-order process, SFG is forbidden in a bulk with centrosymmetry in the electric-dipole approximation. Therefore it is inherently surface/interface specific, and the resonances which can be probed by SFG must be both IR and Raman active (which is generally the case for surface modes because of the broken symmetry at the surface). The technique was first demonstrated in 1987 by Y.R. Shen and coworkers [10] by probing the vibrational modes of a monolayer of coumarin 504 molecules (an organic compound of the benzopyrene class) spin-coated on a substrate of fused quartz. The interfacial system subject to an SFG investigation is usually modeled as a three-layer system (see **Figure 2-5**) composed of two centrosymmetric media and an interfacial layer [11]. While under electric-dipole approximation the second-order nonlinear polarization generated under the irradiation of two optical fields  $E_1(\omega_1)$  and  $E_2(\omega_2)$  in the two centrosymmetric media is vanishing, the polarization generated in the interfacial layer is

$$P^{(2)}(\omega = \omega_1 + \omega_2) = \chi^{(2)}(\omega = \omega_1 + \omega_2): E_1(\omega_1)E_2(\omega_2).$$

## 2. Spectroscopic Techniques and Experimental Setup

$\chi^{(2)}$  is the second-order nonlinear susceptibility (a third-rank tensor) of the interface. The sum frequency in the reflected direction, that is in medium 1, can be found to be

$$I(\omega) = \frac{8\pi^3 \omega^2 \sec^2 \beta}{c^3 n_1(\omega) n_1(\omega_1) n_1(\omega_2)} \left| \chi_{\text{eff}}^{(2)} \right|^2 I_1(\omega_1) I_2(\omega_2),$$

where  $n_i(\Omega)$  is the refractive index of medium  $i$  at frequency  $\Omega$ ,  $\beta$  is the reflection angle of the sum-frequency field,  $I_i(\Omega)$  is the intensity of field  $i$  at frequency  $\Omega$ . The effective nonlinear “second-order” susceptibility  $\chi_{\text{eff}}^{(2)}$  is a complex scalar obtained by the contraction of the third-rank tensor  $\chi^{(2)}$  with the impinging and emitted optical field vectors:

$$\chi_{\text{eff}}^{(2)} = [\mathbf{L}(\omega) \cdot \hat{\mathbf{e}}(\omega)]^\dagger \cdot \chi^{(2)} : [\mathbf{L}(\omega_1) \cdot \hat{\mathbf{e}}_1(\omega_1)] [\mathbf{L}(\omega_2) \cdot \hat{\mathbf{e}}_2(\omega_2)],$$

$\hat{\mathbf{e}}_i(\Omega)$  is the polarization vector of the  $i$ -th optical field at frequency  $\Omega$  and  $\mathbf{L}(\Omega)$  the transmission Fresnel coefficient at frequency  $\Omega$ . The Fresnel coefficient relates the field components in medium 1 (where the SFG output is reflected) to the corresponding ones in the polarization interface sheet. The calculation of  $\chi_{\text{eff}}^{(2)}$  in a practical experiment is simplified by (1) the fact that the optical fields are polarized (and some of their components are thus vanishing), and (2) symmetry arguments about  $\chi^{(2)}$ . For example, in the case of an azimuthally isotropic interface, there are only four independent non-vanishing components.

In the case where the interface is composed of molecules,  $\chi^{(2)}$  is related to the molecular hyperpolarizability  $\alpha^{(2)}$  according to

$$\chi_{ijk}^{(2)} = N_s \sum_{\xi, \eta, \zeta} \langle (\hat{i} \cdot \hat{\xi})(\hat{j} \cdot \hat{\eta})(\hat{k} \cdot \hat{\zeta}) \rangle \alpha_{\xi, \eta, \zeta}^{(2)},$$

where  $N_s$  is the surface density of molecules,  $(\hat{i}, \hat{j}, \hat{k})$  and  $(\hat{\xi}, \hat{\eta}, \hat{\zeta})$  are the unit vectors along the laboratory and molecular coordinates, respectively, and the angular brackets denote an average over the molecular orientation distribution. When the IR frequency (i.e.  $\omega_2$ ) is near a vibrational resonance  $\omega_q$ , it is possible to write a microscopic expression for  $\alpha^{(2)}$  according to a four-wave

## 2. Spectroscopic Techniques and Experimental Setup

coupling approach commonly applied to Raman scattering. The four interacting waves are the visible, infrared, SFG, and the molecular excitation  $\rho_{if}$  from an initial state  $i$  to a final  $f$  with resonance frequency  $\omega_{fi}$ . It is found that [12]

$$\alpha^{(2)} = \alpha_{\text{NR}}^{(2)} + \frac{A_{fi}^* M_{fi} (\rho_f - \rho_i)}{\omega_2 - \omega_{fi} + i\Gamma_{fi}},$$

where the subscript NR refers to a non-resonant contribution,  $A_{fi} = \langle f | -e\mathbf{r} \cdot \hat{\mathbf{e}}_2 | i \rangle$  is the transition matrix element for the infrared excitation,  $M_{fi}$  is the Raman matrix element,  $(\rho_f - \rho_i)$  is the difference in population between the final and initial state, and  $\Gamma_{fi}$  denotes the strength of the vibrational modes. When more than one resonance is present, the latter expression can be replaced by a sum over the vibrational modes. Again, from this microscopic expression it is possible to see that a vibrational resonance must be simultaneously infrared and Raman active to be detected by SFG. Further technical details about the experimental setup necessary to perform an SFG experiment are thoroughly discussed in **Chapter 3**.

### 2.4 X-RAY PHOTOELECTRON SPECTROSCOPY

X-ray photoelectron spectroscopy (XPS) is based on the measurement of the kinetic energy of core electrons emitted by photoelectric effect (called photoelectrons) from a sample irradiated with an optical probe in the X-ray region of the electromagnetic spectrum, at characteristic energies depending on the source. When a photon of energy  $h\nu$  shines on the sample, it may provide enough energy to remove an electron bound to the atom nucleus with energy  $E_B$  relative to the Fermi level  $E_F$ , which is then detected by a spectrometer. By conservation of energy, the kinetic energy of the emitted photoelectron measured by the spectrometer is

$$E_K = h\nu - E_B - \phi_{\text{spec}},$$

where  $\phi_{\text{spec}}$  is the spectrometer work function (see **Figure 2-6**). The latter is not a well-defined quantity, therefore spectrometers are generally calibrated with respect to lines of known energy [13].

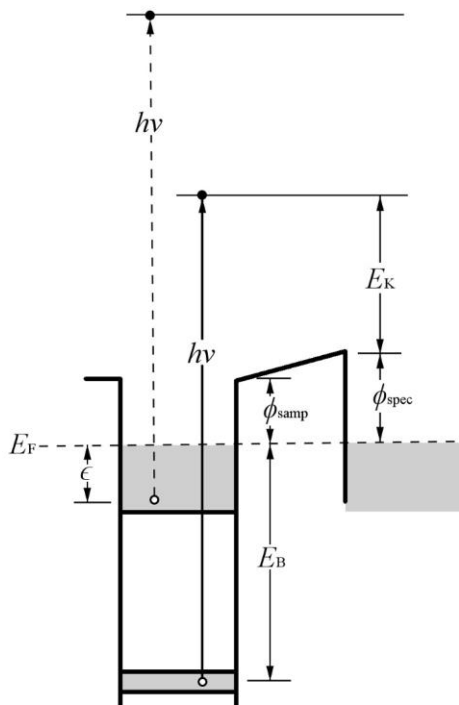


**Figure 2-6:** Energy-level diagram of the X-ray photoelectron experiment. Shaded areas indicate occupied bands/levels.

Therefore, by measuring the  $E_K$  it is possible to obtain  $E_B$ . This quantity is characteristic of the atomic species from which the photoelectron is emitted, the electronic level of origin, and the chemical state of the atomic species. This principle can be employed to analyze sample composition and chemical state, and the technique is indeed also known as electron spectroscopy for chemical analysis (ESCA). A fundamental property of this technique lies in the fact that the emitted photoelectron (with an energy in the 5-2000 eV range) has a high probability to incur in inelastic scattering. As the probability of an energy loss due to scattering increases with path length, electrons emitted deeper in the solid have a lower probability of detection (outside the

## 2. Spectroscopic Techniques and Experimental Setup

surface) than electrons originating from the outermost atomic layers of the surface [1]. Thus, the technique is mainly surface specific. Also other effects play a role in determining the actual depth over which an electron spectroscopy samples the surface and subsurface regions, and this quantity is known as attenuation length. The latter depends on the material, however is of the order of few tens of Å (and typically less than 10 Å in the energy range of 50-200 eV).

The X-ray optical probe in a conventional XPS setup is obtained in an equipment piece known as X-ray source by bombarding a target with a beam of electrons. By collision, the impinging electrons create core holes in the target electron levels. Once these holes are filled by electrons in outer shells, radiation emission occurs at characteristic discrete energies. These are superimposed to a continuum background due to bremsstrahlung, i.e. radiation emission by deceleration of the impinging electrons in the target. The target is chosen according to different parameters. It must have a low bremsstrahlung and the spectrum should be possibly dominated by a single and narrow line. Moreover, since considerable target heating occurs by electron bombardment, a metal target is preferably chosen because it can be cooled by a circulating water loop. Common choices include magnesium and aluminum targets. In both cases the emission spectrum is dominated by the unresolved doublet  $K_{\alpha_{1,2}}$ , associated with the decays  $2p_{1/2} \rightarrow 1s$  and  $2p_{3/2} \rightarrow 1s$ , at energies of 1253.6 eV and 1486.6 eV, respectively. In both cases the full width at half maximum of the  $K_{\alpha_{1,2}}$  line is  $\sim 0.7 - 0.8$  eV, posing a limit to the ability to detect changes in width and position of the photoelectron peaks.

### 2.5 LOW ENERGY ELECTRON DIFFRACTION

In the preceding paragraph we described XPS, a powerful spectroscopy technique to analyze the chemical composition of a surface. Now we will discuss how it is possible to characterize the structure of a surface and adsorbate layers, with large well-ordered areas and

## 2. Spectroscopic Techniques and Experimental Setup

low defect density, by a technique known as low energy electron diffraction (LEED). A typical LEED setup consists of an electron gun and a set of electrostatic lenses, which are needed to focus the electron beam and accelerate it to a desired energy in the 50-200 eV range. The beam impinges on the surface normally, and the scattered electrons then hit a fluorescent screen for visualization of the diffraction spots. An electron of wavevector  $\mathbf{k}$  has energy

$$E = \frac{\hbar^2 k^2}{2m} = 13.6 (ka_0)^2 \text{ eV},$$

with  $a_0 = 0.529 \text{ \AA}$  the Bohr radius. The electron de Broglie wavelength is

$$\lambda = \frac{2\pi}{k} = \frac{12.3}{\sqrt{E}} \text{ \AA}.$$

Therefore we see that if the electron energy is in the 50-200 eV range the corresponding wavelength lies in the  $0.9 - 1.7 \text{ \AA}$  range, it is thus comparable to the interatomic distances in solids and suitable to perform diffraction experiments. In the approximation that only the topmost layer of a sample is involved in scattering, the condition for the occurrence of an elastic Bragg spot is that the component parallel to the surface of the difference of the impinging and scattered vectors ( $\mathbf{K}_{\parallel} = \mathbf{k}'_{\parallel} - \mathbf{k}_{\parallel}$ ) must equal a 2D surface reciprocal lattice vector  $\mathbf{G}_{\parallel}$ .

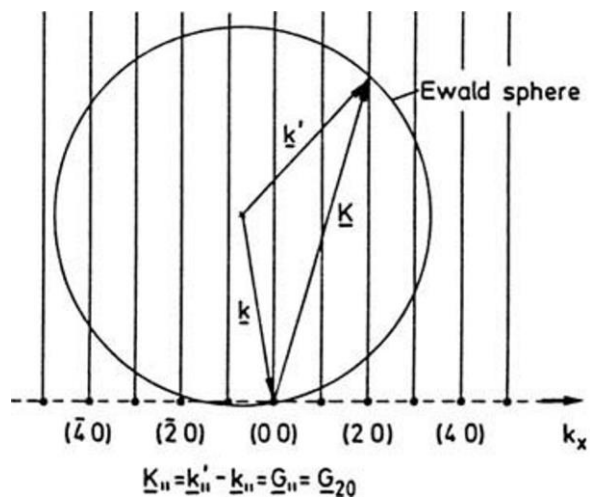


**Figure 2-7:** Ewald construction for elastic scattering on a 2D surface lattice. Adapted from [14].

## 2. Spectroscopic Techniques and Experimental Setup

On the other hand, since in this approximation no periodicity exists in the direction perpendicular to the surface, the restriction on the third Laue equation is relaxed by attributing to every 2D reciprocal lattice point a rod normal to the surface [14]. Accordingly, it is possible to visualize this requirements by the Ewald construction shown in **Figure 2-7**.

In a real experiments, the primary electrons penetrate several atomic layers, and this leads to a modulation of the intensities of the Bragg reflections in comparison with the case of pure 2D scattering.

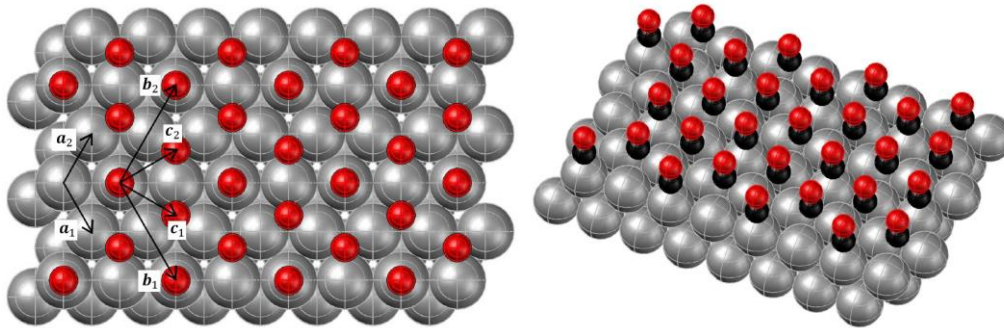


**Figure 2-8:** Ball-model of the  $(2 \times 2) - 3\text{CO}$  superlattice on a Pd(111) substrate, top (left) and perspective (right) view.

To understand how to qualitatively interpret a LEED pattern, let us consider a Pd(111) substrate lattice, and an ordered disposition of adsorbed CO molecules (which we will call superlattice), as shown in **Figure 2-8**. In the chosen disposition of CO molecules, some of them are adsorbed on on-top sites while others in three-fold hollow sites (note that the molecules adsorbed on three-fold hollow sites are actually adsorbed on two *different* sites, i.e. hcp-hollow and fcc-hollow). This disposition corresponds to a CO coverage of 0.75 monolayer. The substrate lattice Pd(111) can be described by the following two 2D translational vectors,

$$\mathbf{a}_1 = a \left( \cos \frac{\pi}{3}, -\sin \frac{\pi}{3} \right), \text{ and } \mathbf{a}_2 = a \left( \cos \frac{\pi}{3}, \sin \frac{\pi}{3} \right),$$

where  $a$  is the lattice parameter. The superlattice can be determined in terms of the substrate net by



$$\mathbf{b}_1 = 2\mathbf{a}_1, \text{ and } \mathbf{b}_2 = 2\mathbf{a}_2.$$

According to Wood notation, the superstructure can be classified as a  $(2 \times 2)$ . However, since two additional CO molecules are present in the superlattice unit cell for a total of three, we may further specify  $(2 \times 2) - 3\text{CO}$ . Moreover, two additional basis vectors are necessary to specify the position in the unit cell of the two additional molecules and fully describe the superlattice:

$$\mathbf{c}_1 = \frac{2\sqrt{3}}{3}a \left( \cos \frac{\pi}{6}, -\sin \frac{\pi}{6} \right), \text{ and } \mathbf{c}_2 = \frac{2\sqrt{3}}{3}a \left( \cos \frac{\pi}{6}, \sin \frac{\pi}{6} \right).$$

As in three-dimensional space, the translational vectors of the 2D reciprocal lattice are defined in terms of the real-space lattice vectors by

$$\mathbf{a}_1^* = 2\pi \frac{\mathbf{a}_2 \times \hat{\mathbf{n}}}{|\mathbf{a}_1 \times \mathbf{a}_2|}, \text{ and } \mathbf{a}_2^* = 2\pi \frac{\hat{\mathbf{n}} \times \mathbf{a}_1}{|\mathbf{a}_1 \times \mathbf{a}_2|},$$

where  $\hat{\mathbf{n}}$  is the unit vector normal to the surface.

With this definition it is possible to construct the reciprocal lattice vectors:

$$\mathbf{a}_1^* = \frac{2\sqrt{3}}{3} \frac{2\pi}{a} \left( \cos \frac{\pi}{6}, -\sin \frac{\pi}{6} \right), \text{ and } \mathbf{a}_2^* = \frac{2\sqrt{3}}{3} \frac{2\pi}{a} \left( \cos \frac{\pi}{6}, \sin \frac{\pi}{6} \right),$$

$$\mathbf{b}_1^* = \frac{1}{2} \mathbf{a}_1^*, \text{ and } \mathbf{b}_2^* = \frac{1}{2} \mathbf{a}_2^*,$$

$$\mathbf{c}_1^* = \frac{2\pi}{a} \left( \cos \frac{\pi}{3}, -\sin \frac{\pi}{3} \right), \text{ and } \mathbf{c}_2^* = \frac{2\pi}{a} \left( \cos \frac{\pi}{3}, \sin \frac{\pi}{3} \right).$$

Finally we can construct the reciprocal lattice, and the corresponding diffraction pattern observable on the phosphorus screen of the LEED, of the Pd(111)/  $(2 \times 2) - 3\text{CO}$  surface/adsorbate system (see **Figure 2-9**). The actual LEED pattern as measured can be seen in **Chapter 3, Figure 3-6**.

## 2. Spectroscopic Techniques and Experimental Setup

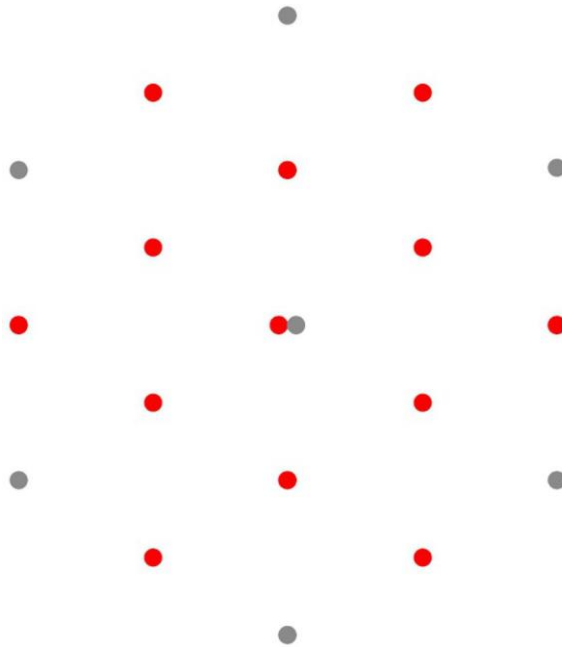


**Figure 2-9:** Reciprocal space of the  $(2 \times 2) - 3\text{CO}$  superlattice (red spots) on a Pd(111) substrate (grey spots).

### 2.6 TEMPERATURE PROGRAMMED DESORPTION

We discussed techniques which allow a chemical characterization of the surface (XPS), of its symmetry properties (LEED), and of vibrational features of adsorbates (PM-IRAS and SFG). Now a technique known as temperature programmed desorption (TPD), or thermal desorption spectroscopy (TDS), will be described. By TPD it is possible to gain information about energies of desorption and interpret desorption in terms of reaction kinetics (desorption order). The experimental setup consists of a sample which can be heated in a controlled fashion while monitoring the temperature, and a mass spectrometer (MS) which detects the desorption products while a programmed temperature ramp is applied to the sample. The typical output of such a measurement is a MS signal vs. temperature graph. If readsorption is neglected, then the rate of desorption, defined as the change in adsorbate coverage per unit of time, is given by [4]:

## 2. Spectroscopic Techniques and Experimental Setup

$$r = -\frac{d\theta}{dt} = k_{\text{des}} \theta^n = \nu(\theta) \theta^n \exp\left(-\frac{E_{\text{des}}(\theta)}{RT}\right),$$

$$\beta = T_0 + \beta t,$$

where  $\theta$  is the coverage in monolayers,  $k_{\text{des}}$  the reaction rate constant for desorption,  $n$  the order of desorption,  $\nu$  the preexponential factor,  $E_{\text{des}}$  the energy of desorption,  $T_0$  the starting temperature, and  $\beta = dT/dt$  is the heating rate. The shape of TPD spectra is characteristic for each order of desorption (zeroth-, first-, and second-order kinetics), therefore even a qualitative analysis provides information about the adsorbate properties. A detailed description of zeroth-, first-, and second-order TPD spectra and their differences can be found in [4] and is not further discussed here.

The quantitative analysis of TPD spectra is however complicated and time-consuming since the parameters in the desorption rate equation depend on coverage. An approximation frequently used to get an estimation of the activation energy of desorption is the one proposed by Redhead [15]:

$$E_{\text{des}} = RT_{\text{max}} \left[ \ln\left(\frac{\nu T_{\text{max}}}{\beta}\right) - 3.46 \right],$$

where  $T_{\text{max}}$  is the peak maximum temperature. In principle this formula should be used only for first-order desorption kinetics and if a reliable value for the prefactor is known, since even small variations in the latter lead to divergence in the calculated desorption energies. A commonly applied choice is  $\nu = 10^{13} \text{ s}^{-1}$ .

### Bibliography

- [1] D.P. Woodruff, T.A. Delchar, Modern Techniques of Surface Science, 2 ed., Cambridge University Press, Cambridge, 1994.
- [2] Pfeiffer Vacuum - The Vacuum Technology Book.

## 2. Spectroscopic Techniques and Experimental Setup

- [3] M. Bernardini, S. Braccini, R. De Salvo, A. Di Virgilio, A. Gaddi, A. Gennai, G. Genuini, A. Giazotto, G. Losurdo, H.B. Pan, A. Pasqualetti, D. Passuello, P. Popolizio, F. Raffaelli, G. Torelli, Z. Zhang, C. Bradaschia, R. Del Fabbro, I. Ferrante, F. Fidecaro, P. La Penna, S. Mancini, R. Poggiani, P. Narducci, A. Solina, R. Valentini, Air bake-out to reduce hydrogen outgassing from stainless steel, *Journal of Vacuum Science & Technology a-Vacuum Surfaces and Films*, 16 (1998) 188-193.
- [4] J.W. Niemantsverdriet, *Spectroscopy in Catalysis - an Introduction*, WILEY-VCH Verlag GmbH & Co. KGaA, Weinheim, 2007.
- [5] K. Lehmann, *The Morse Oscillator*, Princeton University, Princeton, 1997.
- [6] R.G. Greenler, Infrared Study of Adsorbed Molecules on Metal Surfaces by Reflection Techniques, *Journal of Chemical Physics*, 44 (1966) 310-&.
- [7] G.R. Fowles, *Introduction to modern optics*, 2 ed., Dover, New York, 1989.
- [8] B.J. Barner, M.J. Green, E.I. Saez, R.M. Corn, Polarization modulation Fourier transform infrared reflectance measurements of thin films and monolayers at metal surfaces utilizing real-time sampling electronics, *Analytical Chemistry*, 63 (1991) 55-60.
- [9] K.W. Hipps, G.A. Crosby, Application of the photoelastic modulator to polarization spectroscopy, *Journal of Physical Chemistry*, 83 (1979) 555-562.
- [10] X.D. Zhu, H. Suhr, Y.R. Shen, Surface vibrational spectroscopy by infrared-visible sum frequency generation, *Physical Review B*, 35 (1987) 3047-3050.
- [11] Y.R. Shen, Optical second harmonic generation at interfaces, *Annual Review of Physical Chemistry*, 40 (1989) 327-350.
- [12] S. Y.R., *The Principles of Nonlinear Optics*, John Wiley & Sons. Inc., Hoboken, New Jersey, 2003.
- [13] R.L. Park, M.G. Lagally, *Solid State Physics: Surfaces*, Academic Press, Inc., Orlando, Florida, 1985.

## 2. Spectroscopic Techniques and Experimental Setup

- [14] L. Hans, *Solid Surfaces, Interfaces and Thin Films*, 5 ed., Springer-Verlag, Berlin Heidelberg, 2010.
- [15] P.A. Redhead, *Thermal Desorption of Gases*, *Vacuum*, 12 (1962) 203-244.

## 2. Spectroscopic Techniques and Experimental Setup

### 3 ATMOSPHERIC PRESSURE REACTION CELL FOR OPERANDO SUM FREQUENCY GENERATION SPECTROSCOPY OF ULTRAHIGH VACUUM GROWN MODEL CATALYSTS

---

A new custom-designed ultrahigh vacuum (UHV) chamber coupled to a UHV and atmospheric-pressure-compatible spectroscopic and catalytic reaction cell is described, which allows to perform IR-vis sum frequency generation (SFG) vibrational spectroscopy during catalytic (kinetic) measurements. SFG spectroscopy is an exceptional tool to study vibrational properties of surface adsorbates under *operando* conditions, close to those of technical catalysis. This versatile setup allows performing surface science, SFG spectroscopy, catalysis, and electrochemical investigations on model systems, including single crystals, thin films, and deposited metal nanoparticles, under well-controlled conditions of gas composition, pressure, temperature, and potential. The UHV chamber enables to prepare the model catalysts and to analyze their surface structure and composition by low energy electron diffraction (LEED) and Auger electron spectroscopy (AES), respectively. Thereafter, a sample transfer mechanism moves samples under UHV to the spectroscopic cell, avoiding air exposure. In the catalytic cell, SFG spectroscopy and catalytic tests (reactant/product analysis by mass spectrometry or gas chromatography) are performed simultaneously. A dedicated sample manipulation stage allows the model catalysts to be examined from LN<sub>2</sub> temperature to 1273 K, with gaseous reactants in a pressure range from UHV to atmospheric. For post-reaction analysis, the SFG cell is rapidly evacuated and samples are transferred back to the UHV chamber. The capabilities of this versatile setup are demonstrated by benchmark results of CO adsorption on Pt and Pd(111) single crystal surfaces and of CO adsorption and oxidation on a ZrO<sub>2</sub> supported Pt nanoparticle model catalyst grown by atomic layer deposition (ALD).

### 3. Atmospheric Pressure Reaction Cell for Operando SFG Spectroscopy

#### 3.1 INTRODUCTION

The importance of surface science studies for understanding elementary steps of catalytic reactions has been well-established [1-9]. Model catalysts most frequently employed encompass single crystals and thin films, prepared under well-controlled conditions in ultrahigh vacuum (UHV), but also metal nanoparticles grown on planar oxide supports, the latter specifically intended to mimic the properties of industrial-grade catalysts (see [9] and references therein). Single crystalline surfaces and adsorbates on them can be characterized by techniques such as low energy electron diffraction (LEED), Auger electron spectroscopy (AES), electron energy loss spectroscopy (EELS) or photoelectron spectroscopy (PES) [10]. However, because of the required electron mean free path, these methods can typically only be employed in ultrahigh vacuum. Pressures around  $10^{-10}$  to  $10^{-6}$  mbar are, however, far from those of real catalysis and a first attempt to bridge this gap dates back to the pioneering work of G.A. Somorjai and coworkers. They constructed a high-pressure cell inside a UHV chamber, suitable for atmospheric pressure reactions, and single crystals were characterized before and after reaction by surface sensitive methods [6, 11-13]. Afterwards, different variants were built, with high pressure cells attached outside of a UHV chamber, enabling pre- and post-reaction analysis [11, 14, 15].

Nevertheless, most of these early attempts were unable to spectroscopically monitor the sample during the catalytic reaction at high-pressure. This was a drawback, since the active state of a catalyst material under reaction conditions may be different from the state determined by post reaction analysis [6, 9, 16-20].

*In situ* (or now rather called “*operando*” [21]) spectroscopic characterization of catalyst materials during measurements of catalytic performance was achieved by designing high pressure cells compatible with Infrared-Visible Sum Frequency Generation Spectroscopy (IR-vis SFG) [22-24] or Polarization-Modulated Infrared Reflection Absorption Spectroscopy (PM-IRAS) [25-28].



### 3. Atmospheric Pressure Reaction Cell for Operando SFG Spectroscopy

Imaging reactive surfaces was realized by High Pressure Scanning Tunneling Microscopy (HPSTM) [29-31], and surface composition was analyzed by Near Atmospheric Pressure X-ray Photoelectron Spectroscopy (NAP-XPS) [32-37].

Based on the experience in designing UHV systems coupled to high pressure cells enabling simultaneous reactivity and spectroscopic measurements [15, 23, 24, 38, 39], we have recently designed and commissioned a new setup. Although other systems intended for high pressure SFG measurements on UHV-prepared surfaces have recently been constructed [40, 41] and/or upgraded [42, 43], the current setup is able to accomplish all the previously intended goals (UHV sample preparation/characterization, UHV/atmospheric, cryogenic/high temperature, with/without electrical polarization, polarization-dependent SFG, catalytic reactivity measurements) within a single apparatus. In fact, single- or poly-crystalline samples are prepared and analyzed in UHV by standard methods of surface science, whereas SFG and reactivity studies (Mass Spectroscopy (MS) and Gas Chromatography (GC)) are simultaneously performed in a cell of approximately 1.5 liter volume, from UHV to ambient pressure and from LN<sub>2</sub> temperature to 1273 K. The setup and its novelties are thoroughly described, and its capabilities exemplified by first results about CO adsorption on Pt and Pd single crystals and on an ALD (atomic layer deposition)-grown nanoparticle model catalyst, namely ZrO<sub>2</sub>-supported Pt nanoparticles. In the case of the Pt(111) single crystal, polarization-dependent SFG spectra have been acquired as well. For supported Pt nanoparticles, the CO oxidation reaction was monitored, with catalytic testing being performed by MS.

#### 3.2 EQUIPMENT DESIGN

In the following sections, an overview of the general layout of the experimental setup is presented (**3.2.1**). Then, the sample holder (“sample car”) is described (**3.2.2**), together with the

### 3. Atmospheric Pressure Reaction Cell for Operando SFG Spectroscopy

transfer system and the two sample manipulation stages, one in the UHV chamber and the other one in the SFG cell. Afterwards, the UHV chamber (3.2.3), the high-pressure operando spectroscopic SFG cell (3.2.4), and the laser and detection system (3.2.5) are described.

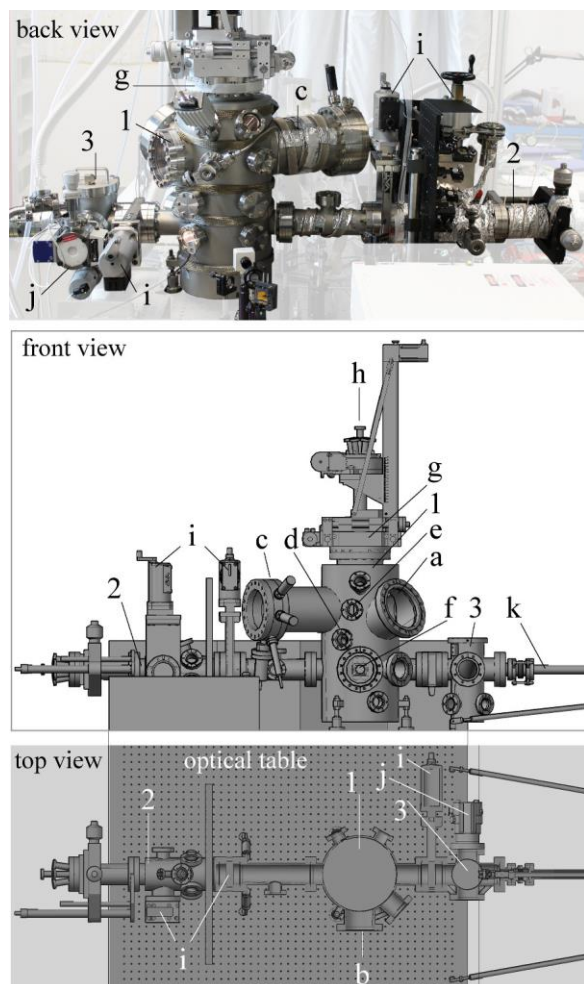


**Figure 3-1:** Overview of the experimental setup, comprising three main sections: the UHV chamber (1), the SFG spectroscopic cell (2), and the load lock (3). The UHV chamber is equipped with viewports (a), turbomolecular drag pump (b), LEED/AES optics (c), ion source (d), mass spectrometer (e), sample manipulation stage (f),  $x,y,z,\phi$ -manipulator (g), and coolant and electrical feedthroughs (h). The UHV chamber is connected to the SFG cell (2) and to the load lock (3) by gate valves (i), and the sample is moved between the three sections by a magnetically coupled transfer arm (k).

### 3. Atmospheric Pressure Reaction Cell for Operando SFG Spectroscopy

#### 3.2.1 General layout

An overview of the experimental setup, consisting of three main parts, is shown in **Figure 3-1**. The UHV chamber (1) allows to prepare and characterize different types of samples (i.e. single crystals, polycrystalline foils, thin films, supported nanoparticles, etc.) by means of standard surface science methods. Samples mounted on the dedicated holder (**Figure 3-2**) can then be transferred, still under UHV, to the SFG cell (2) using a transfer arm. The load lock (3) allows to quickly insert the samples into the system without the need to vent the entire UHV setup. All components are firmly fixed on an optical table that is required for the laser and optics. The UHV chamber, SFG cell and load lock were manufactured by OmniVAC based on our custom design: the manipulation stage and the transfer system are a proprietary design of the company. The laser setup is a commercial EKSPLA SFG system.

#### 3.2.2 Sample holder and xyz $\phi$ manipulator

The sample holder is often the most critical component of a complex UHV apparatus. This especially holds true when the sample should be rapidly transferred back and forth between two manipulation stages. Here we describe an efficient holder, based on the design by OmniVAC, which allows heating the sample to 1273 K, cooling to 95 K, measuring the temperature, and further exhibits additional electrical contacts to apply electrical polarization. All parameters can be accurately adjusted both on the manipulator in the UHV chamber and the one in the SFG cell.

The holder is disc-shaped and equipped with two symmetric side wings. One wing is needed to lock the holder into the manipulation stage, the second allows to grab it with the transfer arm via a retractable ballpoint-pen-like mechanism. The sample holder (**Figure 3-2**) has six electrical connectors on the back side, in the form of screws: two for the heating current (a), two for the thermocouple (b), and two spare ones (c). The latter can e.g. be used to apply polarization to the sample and perform electrochemical measurements [20, 44].

### 3. Atmospheric Pressure Reaction Cell for Operando SFG Spectroscopy

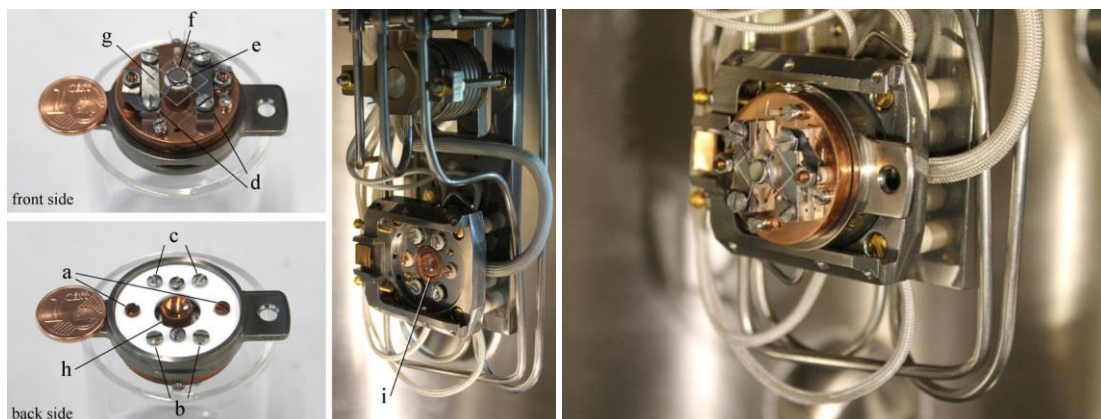


**Figure 3-2:** (left) the sample holder is equipped with six electrical connectors: two for heating (a), two for the thermocouple (b), and two spare ones (c). Two Ta bars (d) hold the sample (e) in place, and the thermocouple (f) is spot-welded on its side. A sapphire piece (g) supports and stabilizes the sample. A further connector (h) provides contact to a sapphire sphere (i) on the sample manipulation stage and guarantees optimal thermal contact for cooling. Further not-labeled screws hold the assembly together. The sample holder receiver on the manipulation stage is shown without (middle) and with (right) sample holder inserted.

The same pin/screw configuration must be apparently mirrored on the sample manipulation stage, so that once the sample holder is slid into the stage and locked in position by a  $N_2$  pneumatic system, an electrical connection is made between each pin on the manipulation stage and the corresponding pin on the back of the sample holder. The front side of the sample holder can be designed in different ways, according to the specific experimental needs. For example, the variant shown in **Figure 3-2** is optimized for electrically conducting samples, which are heated by Joule resistive heating. In this case, the screw-shaped connectors on the back of the holder pass through its body and come out on the front side where the sample is mounted. On the front side, each of the two heating pins (made of copper) are connected to a tantalum bar-shaped piece (d), and these bars are fixed on the holder via extra screws (and with an insulating sapphire piece in between to avoid current shortcut to earth ground). The single crystal sample (e), disk-shaped with 6 mm outer diameter, is fit into a loop made of Ta wire (thickness 0.2 mm)

### 3. Atmospheric Pressure Reaction Cell for Operando SFG Spectroscopy

which has four arms. The arms are fastened on the top of the Ta bars by four stainless steel screws, connecting two arms to each bar. In this way, the heating current flows in via one copper pin to the Ta bar, then through the Ta loop, and similarly out via the second Ta bar and Cu pin. A thermocouple (f) is spot-welded to the side of the sample. With such a setup, a temperature of 1273 K can be reached with a heating current and voltage of 11 A and 2.5 V, respectively. Electrical current for the resistive heating is provided by a power supply (EA-PS 5080-20 A) connected to a PID controller (Eurotherm 3216). A further feature of the holder is a square-shaped quartz piece (g) placed between the back of the sample and the tantalum bars. This prevents the sample from accidentally getting in contact with the bars – causing a current shortcut – and also provides a stable support for the sample and guarantees reproducible alignment for the (optical) spectroscopy measurements.

Apart from the electrical connections, there is an additional contact between the sample holder and the manipulation stage, i.e. between a concave copper piece (h) on the back of the sample holder and a matching sapphire sphere (i) fixed on the manipulator. Sapphire is an electrical insulator, but a fairly good thermal conductor. Therefore, when LN<sub>2</sub> flows through the coils in the manipulation stage, heat is efficiently removed from the sample and a temperature as low as 95 K is reached. The pneumatic system, which locks the sample holder on the manipulating stage, allows choosing whether the sapphire sphere gets in contact with the holder or not. Selecting a pressure of 6 bar ensures electrical and thermal contact, whereas lower pressure (4 bar) prevents the thermal contact while still ensuring electrical connection via the pins/screws. In this way, the sample can be heated to high temperature by minimizing heat loss to the manipulator.

A different sample holder design is used for insulating samples for which Joule heating does not work or for samples with a geometry that does not allow mounting by a wire loop. In this case

### 3. Atmospheric Pressure Reaction Cell for Operando SFG Spectroscopy

heat is provided by conduction, with the top of the holder itself serving as a heating plate (button heater) and the sample directly positioned on top of it. The sample is positioned in the middle of the heating plate while the sample holder is continuously cooled by water, so that during reaction the sample is at higher temperature than the rest of the holder. Moreover, to avoid catalytic side reactions the heating plate is made of ceramics, so that no hot metal parts are exposed to the catalytic reaction environment. Before catalytic studies, blind experiments with inactive samples must be performed, however, to exclude side reactions.

#### 3.2.3 UHV preparation/analysis chamber and load lock

The UHV chamber is a stainless steel vessel of about 40 l volume equipped with various flanges to accommodate instruments, gauges, and connections to the load lock and SFG cell. The setup is schematically presented in **Figure 3-1**. Three large viewports DN 150, 100, and 63 CF (a), and some smaller DN 40 CF viewports enable convenient optical inspection and LED-illumination of the sample in different positions. The vessel is pumped to a routine base pressure of  $<5 \times 10^{-10}$  mbar by a turbomolecular drag pump Pfeiffer TMU 261 (b), monitored by a hot-cathode gauge (Leybold IONIVAC ITR 90, GRAPHIX ONE controller). The chamber is further equipped with a four-grid retractable LEED/AES optics SPECS ErLEED DN 150 CF (c) and 3000D controller with a thoria-coated iridium filament. Photographs of LEED patterns are recorded by a CMOS-sensor camera (The Imaging Source Europe GmbH DFK 72BUC02, lens TCL 1216 5MP). The sample can be sputter-cleaned by an ion source SPECS IQE 11/35 (d), with IQE-11 A controller. A general purpose mass spectrometer with Faraday detector, mks e-Vision<sup>+</sup> (e), allows leak detection and performing temperature programmed desorption (TPD) measurements. In order to use the same MS for gas analysis during high pressure reactions, a thin capillary connects the SFG cell to the MS compartment (which in this case is separated from the main UHV chamber via a DN 40 CF gate valve VAT 01032 and is pumped via the load lock). Gas from the reaction gas line is then admitted

### 3. Atmospheric Pressure Reaction Cell for Operando SFG Spectroscopy

to the MS via a leak valve (Pfeiffer UDV 046). A number of (free) spare flanges allow to equip the chamber with additional instruments, such as an e-beam evaporator and quartz microbalance for thin film or nanoparticle model catalyst preparation. The flanges are arranged such that the system can be upgraded with an X-ray gun and a hemispherical analyzer for XPS.

The sample manipulation stage (f) is positioned inside the chamber by means of an x,y,z, $\phi$ -manipulator (g), installed on the top. The manipulator is differentially pumped by a rotary vane pump (Pfeiffer DUO 5 M). This same pump supplies a pre-vacuum of  $1 \times 10^{-3}$  mbar to the turbomolecular pumps of the UHV chamber and the load lock. The pre-vacuum is monitored by a Pirani gauge (Pfeiffer TPR 280). The manipulator has two feedthroughs for water or LN<sub>2</sub> cooling and six electrical feedthroughs (h). The UHV chamber is connected to, and can be separated from, the SFG cell and the load lock via two DN 63 CF gate valves VAT 10836 (i). The load lock is rapidly evacuated by a turbomolecular pump Pfeiffer TMU 071 P (j) to the base pressure of  $1 \times 10^{-8}$  mbar, as monitored by a compact cold-cathode gauge Pfeiffer IKR 261. The load lock is also connected to the magnetically-coupled transfer arm (k). When the sample has to be transferred and the gate valve between load lock and UHV chamber is opened, the pressure in the latter increases to no more than  $2 \times 10^{-9}$  mbar.

#### 3.2.4 SFG spectroscopy cell and gas supply

The SFG cell, shown in **Figure 3-3**, has a volume of approximately 1.5 l. We emphasize the difficulty to design a cell of significantly smaller volume, given that it requires several components for UHV operation (especially the bulky sample manipulator for cooling and heating) and must also meet the geometry required by the laser beams. The cell can be operated in three different modes described below: in UHV or atmospheric pressure and in recirculating batch reactor mode.

UHV spectroscopic cell: The cell is pumped by a combination of a turbomolecular pump Pfeiffer HiPace 80 (a) and a pre-vacuum diaphragm pump Pfeiffer MVP 015-2 to a routine base

### 3. Atmospheric Pressure Reaction Cell for Operando SFG Spectroscopy

pressure of  $1 \times 10^{-9}$  mbar (the use of a diaphragm pump instead of a rotary vane pump prevents oil back-diffusion, which would cause contamination of the sample and the spectroscopic windows).

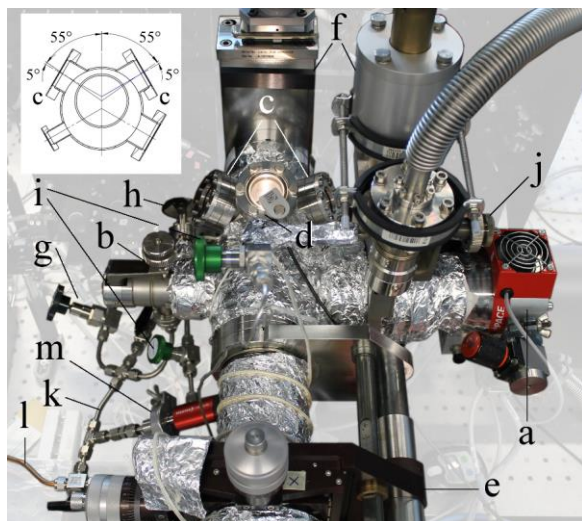


**Figure 3-3:** Photograph of the SFG spectroscopic cell, equipped with a turbomolecular pump (a), gas dosing via leak valve (b),  $\text{CaF}_2$  windows for input of laser radiation and output of SFG (c), viewport for sample positioning (d), sample manipulator (e), gate valves (f), high flow valve (g), capacitance gauge (h), connections to recirculation pump (i), leak valve to MS (j), general-purpose gas line (k), CO-gas line (l), Pirani gauge (m). The inset shows a cross section of the cell at the  $\text{CaF}_2$  windows (c) position to highlight the incident angles of the laser beams and the exit angle of the SFG signal.

Gas from the same manifold serving the preparation chamber can be admitted at “low” pressure by a leak valve Balzers UDV 036 (b), while the pressure is monitored by a full-range combination of a cold-cathode and a Pirani sensor Pfeiffer PKR 261. Low to high-coverage adsorbate structures can be investigated by SFG at temperatures as low as 100 K. Two DN 40 CF  $\text{CaF}_2$  windows (c) allow directing the visible and IR laser radiation into the cell, and the SFG signal to exit the cell. The windows are tilted by  $55^\circ$  with respect to the cell transverse axis, and their surface normal is oriented at  $5^\circ$  with respect to the incident laser beams to avoid back-reflection into the laser optics (see inset of **Figure 3-3**). A third window (d) is placed above the sample stage to control the position when the sample holder is inserted into the sample manipulation stage



### 3. Atmospheric Pressure Reaction Cell for Operando SFG Spectroscopy

using the transfer arm. The  $x,y,z,\phi$ -manipulator (e) allows to place the sample (stage) into the optimal transfer position and to ensure spatial overlap of the vis and IR impinging beams on its surface. A fifth degree of freedom, i.e. the tilt of the sample with respect to the manipulator longitudinal axis is adjusted by tuning the three screws on which the UHV chamber –and therefore the whole setup– is sitting. In any case, this setting has to be rarely –if at all– modified. The manipulator in the SFG cell is designed and operated in the same way as the one in the UHV chamber (see details above).

Atmospheric pressure spectroscopic cell: To study model catalysts at room temperature and above, the pressure can be increased to ensure sufficient adsorbate coverage. Consequently, if a higher (up to 1000 mbar) gas pressure is required, the spectroscopic cell is separated from the UHV chamber and the turbomolecular pump (a) by closing the corresponding gate valves (f). A bellows-sealed valve with PCTFE stem tip Swagelok SS-6BK-MM (g), also connected to the gas manifold, is used for rapid gas dosing, while the pressure can be either monitored by the full-range gauge or by a ceramic capacitance gauge Pfeiffer CMR 361 (h). The capacitance gauge is necessary for more reliable and gas type-independent pressure readings in the (near-) atmospheric regime.

Recirculating batch reactor: A gas mixture at 1000 mbar can recirculate in the spectroscopic cell by means of a bellows pump (Senior Aerospace Metal Bellows MB-41E) whose inlet to and outlet from the cell can be closed by two UHV-compatible shut-off valves (i) (see the schematic representation in **Figure 3-4**). The batch recirculation mode is a typical choice for model catalysis, since the small catalyst surface area (a few  $\text{cm}^2$ ) typically only produces small amounts of products per time. In batch mode, the conversion increases with reaction time and products are easier to detect [9, 45, 46]. A sample of the reaction mixture, extracted from the close vicinity of the catalyst surface by a steel capillary, is leaked via another valve Balzers UDV 040 (j) to the MS

### 3. Atmospheric Pressure Reaction Cell for Operando SFG Spectroscopy

attached to the UHV chamber, as described above. The flow through the capillary to the MS is small compared to the cell volume, thus the overall pressure in the cell and the reaction equilibrium are not modified by performing the MS analysis. Alternatively, the recirculation line can also be connected to a sample loop of a gas chromatograph (GC). After high pressure gas dosing, the cell is evacuated to the background pressure in approximately 20 min (depending on the gas type).

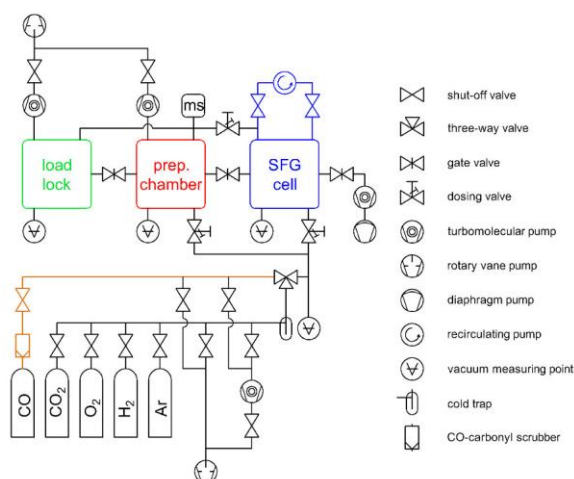


**Figure 3-4:** Schematic overview of the experimental setup, gas supply, connections, and pumping facilities. The part highlighted in blue represents the catalytic cell with the recirculation pump.

Gas Manifold: The gas manifold (k) provides CO<sub>2</sub>, O<sub>2</sub>, H<sub>2</sub>, He, and Ar, and has further spare connections for additional gases and water vapor. CO is dosed via a separate gas line (l) made of medical copper pipe (instead of stainless steel) to prevent the formation of nickel and iron carbonyls. This line is also equipped with a Cu-based carbonyl scrubber to purify the gas from carbonyls which may have formed in the supply bottle. Both gas lines are evacuated by the same rotary vane pump (Pfeiffer DUO 5 M), reaching a base pressure of  $5 \times 10^{-4}$  mbar, as monitored by a Pirani gauge, Pfeiffer TPR 280 (m). Therefore, after purging the lines a couple of times with the desired gas, one can take full advantage of the nominal gas purity (4.7 in the case of CO and 5.0 for all other gases).

#### 3.2.5 Laser and optical detection system

In an SFG experiment, two laser beams, one tunable in the mid-IR from 2.3 to 10  $\mu\text{m}$   $\mathbf{E}_{\text{IR}}(\omega_{\text{IR}})$ , and the other one fixed in the visible at 532 nm  $\mathbf{E}_{\text{vis}}(\omega_{\text{vis}})$ , are superimposed on the sample and an output signal at the sum of the original frequencies  $\mathbf{E}(\omega = \omega_{\text{IR}} + \omega_{\text{vis}})$  is generated according to a second-order nonlinear optical process (see **Figure 3-5**).

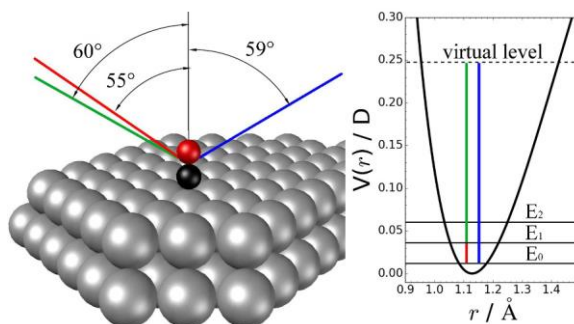


**Figure 3-5:** Representation of an SFG experiment. The infrared radiation excites a molecule from a lower to higher vibrational level (e.g. vibrational eigenvalues  $E_0$  and  $E_1$ , respectively, for a Morse potential of depth  $D=88891 \text{ cm}^{-1}$ ), while the visible radiation excites the system to a virtual electronic level. An anti-Stokes relaxation follows, emitting an SFG signal.

As a second-order process, SFG is forbidden in a bulk with centrosymmetry. Therefore, SFG is highly surface or interface specific because this symmetry is broken at the interface. The SFG signal is enhanced when the impinging infrared is in resonance with a vibrational mode of the sample, e.g. a vibrational mode of an adsorbed molecule such as CO. The signal has an intensity proportional to the square of the effective surface nonlinear polarization [47], which is expressed as

$$I(\omega = \omega_{\text{IR}} + \omega_{\text{vis}}) \propto \left| \chi_S^{(2)}(\omega_{\text{IR}}) \right|^2 I_{\text{IR}}(\omega_{\text{IR}}) I_{\text{vis}}(\omega_{\text{vis}})$$

Close to a resonance, the effective surface nonlinear susceptibility writes

$$\chi_S^{(2)} = \chi_{\text{NR}}^{(2)} + \chi_{\text{R}}^{(2)}, \quad \chi_{\text{R}}^{(2)} = \frac{A_i}{\omega_{\text{IR}} - \omega_i + i\Gamma_i},$$

### 3. Atmospheric Pressure Reaction Cell for Operando SFG Spectroscopy

where  $\chi_{\text{NR}}^{(2)}$  is a non-resonating term depending on the substrate, and  $A_i$ ,  $\omega_i$ , and  $\Gamma_i$  are the amplitude, resonance frequency, and width of the  $i$ -th vibrational mode, respectively.

The laser setup is utilized to generate the visible (532 nm) and tunable mid-infrared (1400-4300  $\text{cm}^{-1}$ ) radiation. The system is commercial from EKSPLA [48], therefore it will be described only briefly. It is comprised of three main parts, the PL2241 laser, the harmonics units, and the parametric generation/ difference frequency generation unit PG501/DFG. The PL2241 is a diode-pumped mode-locked Nd:YAG (neodymium-doped yttrium aluminum garnet  $\text{Y}_3\text{Al}_5\text{O}_{12}$ ) laser and generates the fundamental 35 ps optical pulses at 1064 nm with a repetition rate of 50 Hz. This radiation is converted in a K\*DP (deuterated potassium dihydrogen phosphate  $\text{KD}_2\text{PO}_4$ ) crystal to the second harmonic (532 nm) in the harmonics unit. The second harmonic is split in two parts, directed to the spectroscopic cell (where it serves as vis input for the SFG process) and to the PG501/DFG, respectively. In the PG/DFG it is first fed into BBO ( $\beta$ -phase of barium borate  $\text{BaB}_2\text{O}_4$ ) crystals to generate radiation in the 0.68-2.3  $\mu\text{m}$  range by optical parametric generation, then the latter is mixed with the fundamental pulse at 1064 nm in a AgGaS<sub>2</sub> (silver thiogallate) crystal and provides, by difference frequency generation, the desired mid-IR radiation. The output SFG signal from the spectroscopic cell is finally detected by a monochromator-spectrograph (SOL Instruments MS 2001, photomultiplier tube Hamamatsu R7899). Before performing the SFG experiments, the alignment of the input laser beams and of the output SFG signal can be optimized by measuring the SFG response of a GaAs crystal.

### 3.3 APPLICATIONS OF THE UHV-SETUP AND SFG SPECTROSCOPIC CELL

The purpose of this section is to illustrate the experimental capabilities of the new setup. First results are presented for two different types of samples, namely **(3.3.1)** Pt(111) and Pd(111) single crystal surfaces, a classical benchmark, and **(3.3.2)** a model catalyst of Pt/ZrO<sub>2</sub>, grown by

### 3. Atmospheric Pressure Reaction Cell for Operando SFG Spectroscopy

atomic layer deposition (ALD). In the case of single-crystalline samples the focus is on their preparation and spectroscopic measurements of CO adsorption using different polarization combinations, pressure, and temperature. An example of operando spectroscopy (i.e. simultaneous measurements of spectroscopy and catalytic activity) is provided for CO oxidation on the ALD Pt/ZrO<sub>2</sub> model catalyst.

#### 3.3.1 CO adsorption on single crystalline Pt(111) and Pd(111)

The adsorption of CO on metal surfaces has been extensively investigated in the past, because of the well-known and easy surface preparation procedures, and because of the high absorption coefficient of adsorbed CO, providing a well-established reference for surface spectroscopy [49, 50]. CO on platinum [51-53] and palladium [54, 55] are the most frequently investigated systems, and were thus first revisited for commissioning. This was also an opportunity to further examine the adsorption geometry of CO on Pt(111), a debated topic.

For both Pt and Pd samples the (111) termination was chosen, and the surfaces were prepared in the UHV chamber by Ar<sup>+</sup> ion bombardment ( $3 \times 10^{-6}$  mbar, 1.5 kV) and two minutes annealing to 1200 K (using the sample holder with resistive heating). An additional oxidation was performed for ten minutes ( $1 \times 10^{-7}$  mbar, 1073 K) to remove carbon which may have segregated from the subsurface during the previous annealing steps, finished by flash-annealing to 1200 K in UHV.

The surface ordering was confirmed by LEED, and sharp spots on a low background were observed (see **Figure 3-6**, left panel, for the Pd surface). By cooling the as-prepared Pd(111) sample from 300 to 100 K in  $10^{-7}$  mbar CO (cooling by flowing LN<sub>2</sub> through the sample manipulating stage for approximately 30 min) the well-known (2×2)-3CO structure was obtained [56, 57], in which CO occupies on-top and three-fold hollow sites at an overall coverage of 0.75 ML (**Figure 3-6**, right panel) [34].

### 3. Atmospheric Pressure Reaction Cell for Operando SFG Spectroscopy

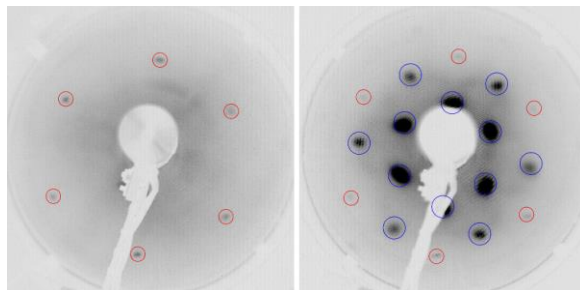


**Figure 3-6:** LEED pictures (94 eV) of the as-prepared Pd surface at 300 K (left) and of the (2×2)-3CO structure at 100 K, the latter corresponding to a CO coverage of 0.75 ML. Diffraction spots originating from Pd surface atoms are highlighted by red circles, additional spots in the presence of adsorbed CO molecules are marked by blue circles.

After the cleaning procedure, the single crystals were transferred into the spectroscopic cell to perform the SFG measurements. In **Figure 3-7** two spectra are shown of Pt(111), exposed to 4 mbar CO and measured in different polarization combinations, *ppp* and *ssp* (the convention is to write the polarization in the following order: SFG, vis, and IR). By choosing different polarization combinations it is possible to selectively probe the components of the  $\chi^{(2)}_R$  tensor. These are in turn related to the components of the molecular hyperpolarizability, thus some insight into the adsorption geometry is obtained. The *ppp* spectrum shows a main peak at 2092  $\text{cm}^{-1}$  due to on-top adsorbed CO [53]. A smaller feature at 2073  $\text{cm}^{-1}$  is due to CO adsorbed on defect sites [53, 58]. The *ssp* spectrum is less intense and only on-top CO is observed at 2092  $\text{cm}^{-1}$ . Although species adsorbed in normal (perpendicular) geometry on metals have often been considered to provide no signal in the *ssp* combination [59], *ssp* spectra of CO/Pt have been measured before [52], which is confirmed by our measurements.

Using a least-square fitting procedure it was possible to obtain the intensity ratio  $I_{ppp}/I_{ssp}=27$  for the on-top CO peak. This value is not sufficient to calculate the adsorption angle because also the molecular hyperpolarizability ratio  $R$  must be known [60]. However, based on the assumption of a zero tilt angle (perpendicularly adsorbed CO), similar to the procedure applied in [55], a hyperpolarizability ratio of 0.5 was deduced.

### 3. Atmospheric Pressure Reaction Cell for Operando SFG Spectroscopy

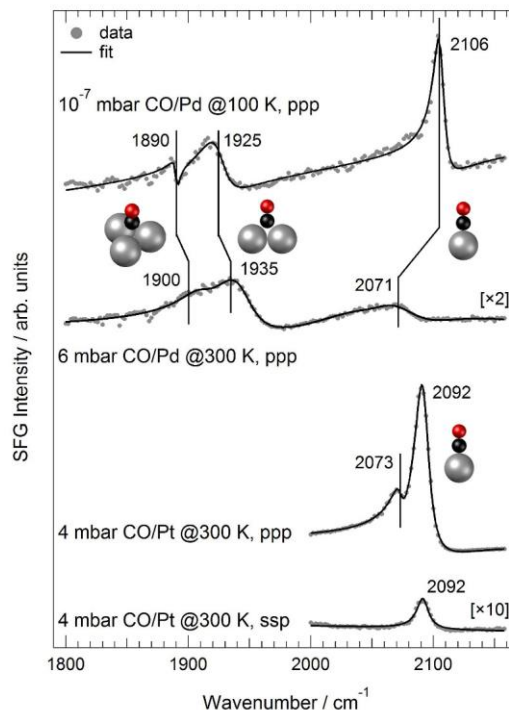


**Figure 3-7:** SFG spectra of the as-prepared clean Pt(111) and Pd(111) surfaces, exposed to CO at the indicated different pressures and temperatures. Spectra of CO on Pt are shown for two different polarization combinations.

**Figure 3-7** also shows two spectra of the Pd(111) surface exposed to 6 mbar CO at 300 K, and to  $10^{-7}$  mbar at 100 K, both measured in the *ppp*-polarization combination. At 6 mbar and 300 K three peaks are observed at  $1900\text{ cm}^{-1}$  (CO at a three-fold hollow site),  $1935\text{ cm}^{-1}$  (CO at a bridge site), and  $2071\text{ cm}^{-1}$  (on-top CO) [54]. A CO overlayer with higher coverage can be obtained by lowering the sample temperature, as demonstrated by the spectrum measured at 100 K in  $10^{-7}$  mbar CO (**Figure 3-7**). In this case the spectrum is dominated by the on-top CO peak, blue-shifted to  $2106\text{ cm}^{-1}$  because of the higher coverage, and also CO in three-fold hollow and bridge sites is observed at  $1890\text{ cm}^{-1}$  and  $1925\text{ cm}^{-1}$ , respectively. For a more detailed description of the SFG spectra of adsorbed CO at different surface coverages we refer to [57].

For a perfect  $(2\times 2)$ -3CO structure (see LEED in **Figure 3-6** right panel), only three-fold hollow and on-top sites should be occupied by CO. However, if the CO adsorbate overlayer is not perfect

### 3. Atmospheric Pressure Reaction Cell for Operando SFG Spectroscopy

and the surface exhibits domains with coverage lower than 0.75 ML, then bridge sites are occupied within these regions sites as well, explaining the appearance of the corresponding spectral feature at  $1925\text{ cm}^{-1}$  [61, 62].

#### 3.3.2 CO oxidation on an ALD-grown Pt-ZrO<sub>2</sub> nanoparticle model catalyst

CO oxidation to CO<sub>2</sub> is an important reaction in heterogeneous catalysis, especially because of its role in pollution control, e.g. for automotive catalysis, and has therefore been repeatedly studied, frequently on platinum single crystals [63-66].

To better mimic the properties of technical catalysts, we have studied Pt-ZrO<sub>2</sub> model catalysts that were prepared by atomic layer deposition (ALD) [67]. ALD allows the preparation of very uniform oxide layers on silicon wafers, creating in this case a well-defined ZrO<sub>2</sub> support surface. The precursors used for growing ZrO<sub>2</sub> at 200 °C were tetrakisdimethylamido-zirconium (Zr(NMe<sub>2</sub>)<sub>4</sub>) and water, in a typical dose/pump/dose/pump cycle [67, 68]. For ZrO<sub>2</sub> 400 cycles were used to grow a thickness of about 40 nm. ALD also allows growing Pt films of varying thickness, ranging from isolated (rough) nanoparticles to continuous (smoother) films with bulk structure – depending on the number of ALD cycles. For Pt, the precursors were methylcyclopentadienyl-trimethyl-platinum (MeCpPtMe<sub>3</sub>) and oxygen, applied at 280 °C.

The structure of a selected model catalyst is shown in **Figure 3-8**, with scanning transmission electron microscopy (STEM) revealing Pt particles of about 7 nm size on a ZrO<sub>2</sub> film of 42 nm thickness. The high resolution TEM image displays lattice fringes of the Pt particles and various facets with different crystallographic orientations.



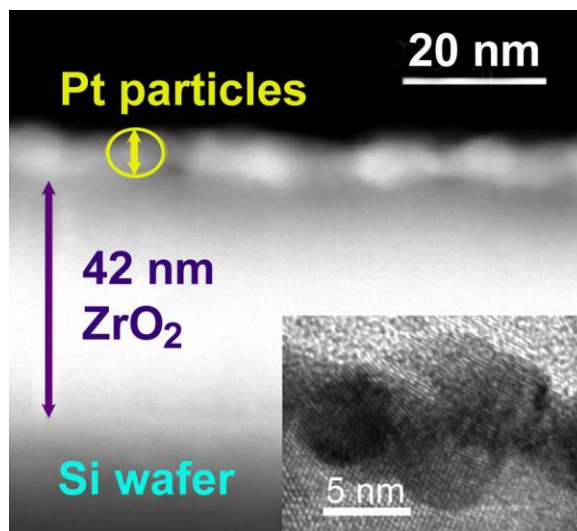


**Figure 3-8:** High angle annular dark-field scanning transmission electron (HAADF-STEM) micrograph of a cross section of the Pt/ZrO<sub>2</sub> model catalyst. An oxide film of ZrO<sub>2</sub> has been grown on a Si wafer by ALD, and has been further covered with Pt particles (50 Pt ALD deposition cycles). The inset shows a high resolution TEM image displaying lattice fringes and surface facets.

Because the samples were prepared in a separate ALD chamber, they had to be chemically cleaned after installation in UHV and transfer to the SFG spectroscopic cell. Since sputtering would destroy the nanoparticle model catalyst, repeated cycles of oxidation by O<sub>2</sub> and reduction by CO were applied, using the sample holder with conductive-type heating. Thereafter, SFG spectra were measured at different temperatures in 30 mbar of a CO/O<sub>2</sub> 1:2 reaction mixture, and simultaneously the signals corresponding to CO, O<sub>2</sub>, and CO<sub>2</sub> were recorded with the mass spectrometer differentially pumped by the load lock. The results for a Pt-ZrO<sub>2</sub> sample are shown in **Figure 3-9**.

The operando SFG measurements allow to correlate the amount/coverage of adsorbed CO with the activity of the surface. At 250 °C an intense on-top CO peak is observed at 2085 cm<sup>-1</sup> (**Figure 3-9a** and **b**). At this temperature only a very small CO<sub>2</sub><sup>+</sup> M/Z=44 signal is observed by MS (**Figure 3-9c**), because the Pt surface is CO covered (CO poisoned). Upon increasing the temperature, an increase in CO<sub>2</sub> is observed, while the SFG spectrum shows a red shift of the peak

### 3. Atmospheric Pressure Reaction Cell for Operando SFG Spectroscopy

position and the peak intensity is reduced. The red shift and lowering of the SFG intensity indicate lower CO coverage [63, 66]. At the highest temperature of 350 °C, the peak position and intensity reach their minimum, as shown in **Figure 3-9a, b**, while the conversion of CO and O<sub>2</sub> are at maximum (**Figure 3-9c**). Nevertheless, the Pt surface still seems mostly covered by CO, which, according to previous studies [69], poisons the surface and makes it inactive. Only when a sufficient number of vacant sites is available for dissociative oxygen adsorption, the reaction can take place [70].

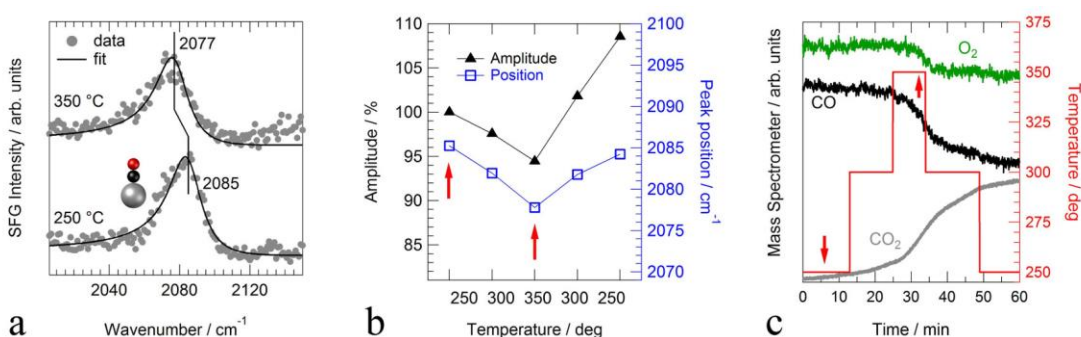


**Figure 3-9:** Operando spectroscopic measurements of CO oxidation (10 mbar CO, 20 mbar O<sub>2</sub>) on Pt-ZrO<sub>2</sub>. Temperature dependent SFG spectra of on-top CO were recorded at 250, 300, 350, 300, 250 °C, while the CO<sub>2</sub>, CO, and O<sub>2</sub> signals were continuously monitored by MS. (a) shows the initial spectrum at 250 °C and the one at 350 °C. (b) shows the fitted values for all spectra, with the amplitude given in % of the initial spectrum. The red arrows correspond to the spectra shown in (a). (c) shows the MS signals and the temperature profile; arrows indicate the times at which the SFG spectra in (a) were measured.

In contrast, the current measurements show CO<sub>2</sub> production when adsorbed CO is detected by the SFG spectra. Apparently, there is partial CO-poisoning, affecting some facets of the Pt nanoparticles while others are unaffected, creating some activity. Related CO oxidation studies on polycrystalline Pt foil [70] indicated a stepwise lifting of the CO poisoning for different facets: (110) ignites at lower T than (100), (100) at lower T than (111). This consequently leads to a stepwise increase in the CO<sub>2</sub> production, as observed here. Upon cooldown, the initial state of the system is reached again, with higher CO coverage (blue shifted peak position and higher intensity) and resulting lower CO and O<sub>2</sub> conversion.

### 3. Atmospheric Pressure Reaction Cell for Operando SFG Spectroscopy

Precise comparison of the MS signal at the temperature steps indicates a delay of 2-3 minutes between increase/decrease of the temperature and a change in the MS CO<sub>2</sub> slope. This is due to the length of the capillary (about 1 m) connecting the spectroscopic cell and the mass spectrometer. Nevertheless, the SFG measurements take about 10 minutes per spectrum, thus the 2-3 minute delay is not relevant. However, the MS measurements do not allow a proper quantification of conversion. Therefore, upgrading the gas analysis by (quantitative) gas chromatography will be a future goal.

#### 3.4 CONCLUSIONS

A new experimental setup to prepare and characterize various model catalysts in UHV and to perform surface-sensitive *operando* SFG spectroscopy, paralleled by reactivity measurements at atmospheric pressure, has been successfully designed and commissioned. Its versatility to study various samples (from single crystals to nanoparticle model catalysts) in a wide range of gas pressure (from UHV to atmospheric) and temperature (from LN<sub>2</sub> to 1273 K) has been demonstrated by presenting (polarization-dependent) SFG spectra of CO adsorption on Pt and Pd(111) single crystals, and CO oxidation on a Pt-ZrO<sub>2</sub> model catalyst.

#### Bibliography

- [1] G.A. Somorjai, The surface science of heterogeneous catalysis, Surf. Sci., 299/300 (1994) 849.
- [2] G. Ertl, Reactions at well-defined surfaces, Surf. Sci., 299/300 (1994) 742.
- [3] R.J. Madix, Through the labyrinth of surface reaction mechanism - a personal account, 1964-1992, Surface Science, 299 (1994) 785-797.
- [4] D.A. King, Chemisorption on metals - a personal review, Surface Science, 299 (1994) 678-689.

### 3. Atmospheric Pressure Reaction Cell for Operando SFG Spectroscopy

[5] D.W. Goodman, Model studies in catalysis using surface science probes, *Chem. Rev.*, 95 (1995) 523.

[6] G.A. Somorjai, Modern surface science and surface technologies: An introduction, *Chemical Reviews*, 96 (1996) 1223-1235.

[7] H.-J. Freund, Adsorption of gases on complex: Solid surfaces, *Angewandte Chemie-International Edition in English*, 36 (1997) 452-475.

[8] G. Ertl, H.-J. Freund, "Catalysis and Surface Science", *Physics Today*, 52 (1999) 32.

[9] G. Rupprechter, Sum Frequency Generation and Polarization-Modulation Infrared Reflection Absorption Spectroscopy of Functioning Model Catalysts from Ultrahigh Vacuum to Ambient Pressure, *Advances in Catalysis*, 51 (2007) 133-263.

[10] D.P. Woodruff, T.A. Delchar, *Modern Techniques of Surface Science*, 2 ed., Cambridge University Press, Cambridge, 1994.

[11] D.W. Blakely, E.I. Kozak, B.A. Sexton, G.A. Somorjai, New Instrumentation and Techniques to Monitor Chemical Surface Reactions on Single Crystals Over a Wide Pressure Range (10<sup>-8</sup>-10<sup>5</sup> Torr) in the Same Apparatus, *Journal of Vacuum Science & Technology*, 13 (1976) 1091-1096.

[12] A.L. Cabrera, N.D. Spencer, E. Kozak, P.W. Davies, G.A. Somorjai, Improved instrumentation to carry out surface analysis and to monitor chemical surface reactions insitu on small area catalysts over a wide pressure range (10<sup>-8</sup>-10<sup>5</sup> Torr), *Review of Scientific Instruments*, 53 (1982) 1888-1893.

[13] D. Godbey, F. Zaera, R. Yeates, G.A. Somorjai, Hydrogenation of chemisorbed ethylene on clean, hydrogen, and ethylidyne covered platinum (111) crystal surfaces, *Surface Science*, 167 (1986) 150-166.

[14] J. Szanyi, D.W. Goodman, Combined Elevated Pressure Reactor and Ultrahigh Vacuum Surface Analysis System, *Review of Scientific Instruments*, 64 (1993) 2350-2352.

### 3. Atmospheric Pressure Reaction Cell for Operando SFG Spectroscopy

- [15] W. Reichl, G. Rosina, G. Rupprechter, C. Zimmermann, K. Hayek, Ultrahigh vacuum compatible all-glass high pressure reaction cell for accurate and reproducible measurement of small reaction rates, *Review of Scientific Instruments*, 71 (2000) 1495-1499.
- [16] Special Issue on "In-situ Characterization of Catalysts", *Topics in Catalysis*, 8 (1999).
- [17] Special Issue on "In-situ Characterization of Catalysts", *Topics in Catalysis*, 15 (2001).
- [18] C. Rameshan, C. Weilach, W. Stadlmayr, S. Penner, H. Lorenz, M. Havecker, R. Blume, T. Rocha, D. Teschner, A. Knop-Gericke, R. Schlögl, D. Zemlyanov, N. Memmel, G. Rupprechter, B. Klötzer, Steam Reforming of Methanol on PdZn Near-Surface Alloys on Pd(111) and Pd Foil Studied by In-Situ XPS, LEIS and PM-IRAS, *Journal of Catalysis*, 276 (2010) 101-113.
- [19] C. Rameshan, W. Stadlmayr, S. Penner, H. Lorenz, N. Memmel, M. Haevecker, R. Blume, D. Teschner, T. Rocha, D. Zemlyanov, A. Knop-Gericke, R. Schloegl, B. Kloetzer, Hydrogen Production by Methanol Steam Reforming on Copper Boosted by Zinc-Assisted Water Activation, *Angew. Chem., Int. Ed.*, 51 (2012) 3002-3006, S3002/3001-S3002/3021.
- [20] A.K. Opitz, A. Nanning, C. Rameshan, R. Rameshan, R. Blume, M. Havecker, A. Knop-Gericke, G. Rupprechter, J. Fleig, B. Klötzer, Enhancing Electrochemical Water-Splitting Kinetics by Polarization-Driven Formation of Near-Surface Iron(0): An In Situ XPS Study on Perovskite-Type Electrodes, *Angewandte Chemie-International Edition*, 54 (2015) 2628-+.
- [21] M.A. Banares, Operando methodology: combination of in situ spectroscopy and simultaneous activity measurements under catalytic reaction conditions, *Catalysis Today*, 100 (2005) 71-77.
- [22] X.D. Zhu, H. Suhr, Y.R. Shen, Surface vibrational spectroscopy by infrared-visible sum frequency generation, *Physical Review B*, 35 (1987) 3047-3050.
- [23] G. Rupprechter, T. Dellwig, H. Unterhalt, H.-J. Freund, CO adsorption on Ni(100) and Pt(111) studied by infrared-visible sum frequency generation spectroscopy: design and application of an SFG-compatible UHV-high-pressure reaction cell, *Topics in Catalysis*, 15 (2001) 19-26.

### 3. Atmospheric Pressure Reaction Cell for Operando SFG Spectroscopy

- [24] K.Y. Kung, P. Chen, F. Wei, G. Rupprechter, Y.R. Shen, G.A. Somorjai, Ultrahigh vacuum high-pressure reaction system for 2-infrared 1-visible sum frequency generation studies, *Review of Scientific Instruments*, 72 (2001) 1806-1809.
- [25] G.A. Beitel, A. Laskov, H. Oosterbeek, E.W. Kuipers, Polarization modulation infrared reflection absorption spectroscopy of CO adsorption on Co(0001) under a high-pressure regime, *Journal of Physical Chemistry*, 100 (1996) 12494-12502.
- [26] Y. Jugnet, F. Aires, C. Deranlot, L. Piccolo, J.C. Bertolini, CO chemisorption on Au(110) investigated under elevated pressures by polarized reflection absorption infrared spectroscopy and scanning tunneling microscopy, *Surface Science*, 521 (2002) L639-L644.
- [27] M. Borasio, O.R. de la Fuente, G. Rupprechter, H.-J. Freund, In Situ Studies of Methanol Decomposition and Oxidation on Pd(111) by PM-IRAS and XPS Spectroscopy, *Journal of Physical Chemistry B*, 109 (2005) 17791-17794.
- [28] G. Rupprechter, C. Weilach, Spectroscopic Studies of Surface-Gas Interactions and Catalyst Restructuring at Ambient Pressure: Mind the Gap!, *Journal of Physics-Condensed Matter*, 20 (2008) 17.
- [29] B.J. McIntyre, M.B. Salmeron, G.A. Somorjai, A Variable Pressure/Temperature Scanning Tunneling Microscope for Surface Science and Catalysis Studies, *Rev. Sci. Instrum.*, 64 (1993) 687.
- [30] J.A. Jensen, K.B. Rider, M. Salmeron, G.A. Somorjai, High P STM, CO on Pt(111), *Phys. Rev. Lett.*, 80 (1998) 1228.
- [31] E. Laegsgaard, L. Osterlund, P. Thostrup, P.B. Rasmussen, I. Stensgaard, F. Besenbacher, A high-pressure scanning tunneling microscope, *Review of Scientific Instruments*, 72 (2001) 3537-3542.
- [32] R.W. Joyner, M.W. Roberts, K. Yates, High pressure electron spectrometer for surface studies, *Surface Science*, 87 (1979) 501-509.

### 3. Atmospheric Pressure Reaction Cell for Operando SFG Spectroscopy

- [33] V.I. Bukhtiyarov, V.V. Kaichev, E.A. Podgornov, I.P. Prosvirin, XPS, UPS, TPD and TPR studies of oxygen species active in silver-catalysed ethylene epoxidation, *Catalysis Letters*, 57 (1999) 233-239.
- [34] V.V. Kaichev, I.P. Prosvirin, V.I. Bukhtiyarov, H. Unterhalt, G. Rupprechter, H.-J. Freund, High-pressure studies of CO adsorption on Pd(111) by X-ray photoelectron spectroscopy and sum-frequency generation, *Journal of Physical Chemistry B*, 107 (2003) 3522-3527.
- [35] M. Morkel, V.V. Kaichev, G. Rupprechter, H.-J. Freund, I.P. Prosvirin, V.I. Bukhtiyarov, Methanol dehydrogenation and formation of carbonaceous overlayers on Pd(111) studied by high-pressure SFG and XPS spectroscopy, *J. Phys. Chem. B.*, 108 (2004) 12955.
- [36] J. Pantförder, S. Pöllmann, J.F. Zhu, D. Borgmann, R. Denecke, H.-P. Steinrück, New setup for in situ x-ray photoelectron spectroscopy from ultrahigh vacuum to 1 mbar, *Rev. Sci. Instrum.*, 76 (2005) 014102
- [37] S. Alayoglu, G.A. Somorjai, Ambient Pressure X-ray Photoelectron Spectroscopy for Probing Monometallic, Bimetallic and Oxide-Metal Catalysts Under Reactive Atmospheres and Catalytic Reaction Conditions, *Topics in Catalysis*, 59 (2016) 420-438.
- [38] J. Silvestre-Albero, M. Borasio, G. Rupprechter, H.-J. Freund, Combined UHV and ambient pressure studies of 1,3-butadiene adsorption and reaction on Pd(111) by GC, IRAS and XPS, *Catalysis Communications*, 8 (2007) 292-298.
- [39] L. Mayr, R. Rameshan, B. Klötzer, S. Penner, C. Rameshan, Combined UHV/high-pressure catalysis setup for depth-resolved near-surface spectroscopic characterization and catalytic testing of model catalysts, *Review of Scientific Instruments*, 85 (2014) 8.
- [40] R.R. Feng, A.A. Liu, S. Liu, J.J. Shi, Y. Liu, Z.F. Ren, Methanol Adsorption on TiO<sub>2</sub> Film Studied by Sum Frequency Generation Vibrational Spectroscopy, *Chinese Journal of Chemical Physics*, 28 (2015) 11-16.

### 3. Atmospheric Pressure Reaction Cell for Operando SFG Spectroscopy

[41] M. Roiaz, E. Monachino, C. Dri, M. Greiner, A. Knop-Gericke, R. Schlögl, G. Comelli, E. Vesselli, Reverse Water-Gas Shift or Sabatier Methanation on Ni(110)? Stable Surface Species at Near-Ambient Pressure, *Journal of the American Chemical Society*, 138 (2016) 4146-4154.

[42] M.C. Yang, D.C. Tang, G.A. Somorjai, Sample mounting and transfer mechanism for in situ IR-visible sum frequency generation vibrational spectroscopy in high-pressure ultrahigh vacuum system, *Review of Scientific Instruments*, 74 (2003) 4554-4557.

[43] S. Liu, A.A. Liu, R.D. Zhang, Z.F. Ren, Compact ultrahigh vacuum/high-pressure system for broadband infrared sum frequency generation vibrational spectroscopy studies, *Review of Scientific Instruments*, 87 (2016) 5.

[44] A.K. Opitz, A. Nenning, C. Rameshan, M. Kubicek, T. Götsch, R. Blume, M. Havecker, A. Knop-Gericke, G. Rupprechter, B. Klötzer, J. Fleig, Surface Chemistry of Perovskite-Type Electrodes During High Temperature CO<sub>2</sub> Electrolysis Investigated by Operando Photoelectron Spectroscopy, *ACS Applied Materials & Interfaces*, 9 (2017) 35847-35860.

[45] G. Rupprechter, H. Unterhalt, M. Morkel, P. Galletto, L.J. Hu, H.-J. Freund, Sum frequency generation vibrational spectroscopy at solid-gas interfaces: CO adsorption on Pd model catalysts at ambient pressure, *Surface Science*, 502 (2002) 109-122.

[46] U. Mann, *Principles of Chemical Reactor Analysis and Design: New Tools for Industrial Chemical Reactor Operations*, 2 ed., John Wiley & Sons, Inc., Hoboken, New Jersey, 2009.

[47] Y.R. Shen, Optical second harmonic generation at interfaces, *Annual Review of Physical Chemistry*, 40 (1989) 327-350.

[48] Ekspla, SFG Spectrometer, in.

[49] P. Hollins, The influence of surface defects on the infrared spectra of adsorbed species, *Surface Science Reports*, 16 (1992) 51-94.



### 3. Atmospheric Pressure Reaction Cell for Operando SFG Spectroscopy

- [50] G. Rupprechter, Sum Frequency Generation and Polarization-Modulation Infrared Reflection Absorption Spectroscopy of Functioning Model Catalysts from Ultrahigh Vacuum to Ambient Pressure, in: B.C. Gates, H. Knözinger (Eds.) *Advances in Catalysis*, Vol 51, Elsevier Academic Press Inc, San Diego, 2007, pp. 133-263.
- [51] C. Klünker, M. Balden, S. Lehwald, W. Daum, CO stretching vibrations on Pt(111) and Pt(110) studied by sum-frequency generation, *Surface Science*, 360 (1996) 104-111.
- [52] S. Baldelli, N. Markovic, P. Ross, Y.R. Shen, G. Somorjai, Sum frequency generation of CO on (111) and polycrystalline platinum electrode surfaces: Evidence for SFG invisible surface CO, *Journal of Physical Chemistry B*, 103 (1999) 8920-8925.
- [53] G. Rupprechter, T. Dellwig, H. Unterhalt, H.-J. Freund, High-pressure carbon monoxide adsorption on Pt(111) revisited: A sum frequency generation study, *Journal of Physical Chemistry B*, 105 (2001) 3797-3802.
- [54] H. Unterhalt, G. Rupprechter, H.-J. Freund, Vibrational sum frequency spectroscopy on Pd(111) and supported Pd nanoparticles: CO adsorption from ultrahigh vacuum to atmospheric pressure, *Journal of Physical Chemistry B*, 106 (2002) 356-367.
- [55] P. Galletto, H. Unterhalt, G. Rupprechter, The molecular orientation of CO on Pd(111): a polarization-dependent SFG study, *Chemical Physics Letters*, 367 (2003) 785-790.
- [56] M. Gierer, A. Barbieri, M.A. VanHove, G.A. Somorjai, Structural reanalysis of the Rb(111)+(root 3x root 3)R30 degrees-CO and Rh(111)+(2x2)-3CO phases using automated tensor LEED, *Surface Science*, 391 (1997) 176-182.
- [57] M. Morkel, G. Rupprechter, H.-J. Freund, Ultrahigh vacuum and high-pressure coadsorption of CO and H-2 on Pd-(111): A combined SFG, TDS, and LEED study, *Journal of Chemical Physics*, 119 (2003) 10853-10866.

### 3. Atmospheric Pressure Reaction Cell for Operando SFG Spectroscopy

[58] V.K. Agrawal, M. Trenary, An Infrared Study of NO Adsorption at Defect Sites on Pt(111), *Surface Science*, 259 (1991) 116-128.

[59] T. Yuzawa, T. Shioda, J. Kubota, K. Onda, A. Wada, K. Domen, C. Hirose, Polarization characteristics from SFG spectra of clean and reguletively oxidized Ni(100) surfaces adsorbed by propionate and formate, *Surface Science*, 416 (1998) L1090-L1094.

[60] H.F. Wang, W. Gan, R. Lu, Y. Rao, B.H. Wu, Quantitative spectral and orientational analysis in surface sum frequency generation vibrational spectroscopy (SFG-VS), *International Reviews in Physical Chemistry*, 24 (2005) 191-256.

[61] G. Rupprechter, H. Unterhalt, M. Morkel, P. Galletto, T. Dellwig, H.-J. Freund, Extending UHV studies to the mbar range: vibrational SFG spectroscopy of high-pressure CO adsorption on Pt(111) and Pd(111), *Vacuum*, 71 (2003) 83-87.

[62] M. Morkel, H. Unterhalt, M. Salmeron, G. Rupprechter, H.-J. Freund, SFG spectroscopy from 10(-8) to 1000 mbar: less-ordered CO structures and coadsorption on Pd(111), *Surface Science*, 532 (2003) 103-107.

[63] H. Härle, K. Mendel, U. Metka, H.R. Volpp, L. Willms, J. Wolfrum, Temperature dependence (90-440 K) of the vibrational spectra of CO adsorbed on platinum(111) studied by sum-frequency generation, *Chemical Physics Letters*, 279 (1997) 275-281.

[64] F. Fournier, W. Zheng, S. Carrez, H. Dubost, B. Bourguignon, Ultrafast laser excitation of CO/Pt(111) probed by sum frequency generation: Coverage dependent desorption efficiency, *Physical Review Letters*, 92 (2004) 4.

[65] E.H.G. Backus, M. Bonn, A quantitative comparison between reflection absorption infrared and sum-frequency generation spectroscopy, *Chemical Physics Letters*, 412 (2005) 152-157.

### 3. Atmospheric Pressure Reaction Cell for Operando SFG Spectroscopy

[66] M. Tüshaus, E. Schweizer, P. Hollins, A.M. Bradshaw, Yet Another Vibrational Study of the Adsorption System Pt(111)-CO, *Journal of Electron Spectroscopy and Related Phenomena*, 44 (1987) 305-316.

[67] S.M. George, Atomic Layer Deposition: An Overview, *Chem. Rev.*, 110 (2010) 111-131.

[68] R.L. Puurunen, Surface chemistry of atomic layer deposition: A case study for the trimethylaluminum/water process

*Journal of Applied Physics*, 97 (2005) 121301

[69] A. Haghofer, P. Sonström, D. Fenske, K. Föttinger, S. Schwarz, J. Bernardi, K. Al-Shamery, M. Bäumer, G. Rupprechter, Colloidally Prepared Pt Nanowires versus Impregnated Pt Nanoparticles: Comparison of Adsorption and Reaction Properties, *Langmuir*, 26 (2010) 16330-16338.

[70] D. Vogel, C. Spiel, Y. Suchorski, A. Trincherro, R. Schlögl, H. Grönbeck, G. Rupprechter, Local Catalytic Ignition during CO Oxidation on Low-Index Pt and Pd Surfaces: A Combined PEEM, MS, and DFT Study, *Angewandte Chemie-International Edition*, 51 (2012) 10041-10044.

### 3. Atmospheric Pressure Reaction Cell for Operando SFG Spectroscopy

## 4 CO-INDUCED SURFACE ROUGHENING OF COPPER (100) AT ELEVATED PRESSURE: CU CLUSTER FORMATION AND CO DISSOCIATION

---

The adsorption of carbon monoxide on the copper (100) single crystal termination at low temperature (120 K) and medium coverage (0.5 ML) was investigated by low energy electron diffraction (LEED), temperature programmed desorption (TPD), X-ray photoelectron spectroscopy (XPS), polarization-modulation infrared reflection absorption spectroscopy (PM-IRAS), and density functional theory (DFT) calculations. Upon dosing in ultra-high vacuum (UHV), the well-known ordered  $c(2\times 2)$ CO overlayer was identified. The interaction of Cu(100) with CO at elevated gas pressure (up to 5 mbar) at 200 and 300 K was examined in situ by PM-IRAS, and ex situ by LEED, TPD, and XPS following exposure. The absorption band of adsorbed CO (2093 to 2082  $\text{cm}^{-1}$ ) was higher than expected for the  $c(2\times 2)$ CO structure (2082  $\text{cm}^{-1}$ ), but was characteristic of CO adsorbed on low-coordinated Cu atoms. The combined PM-IRAS/DFT analysis revealed that mbar exposure to CO induced a morphological modification of the surface forming  $\text{Cu}_1$  and  $\text{Cu}_5$  clusters on terraces. The roughened surface was surprisingly active for CO dissociation.

### 4.1 INTRODUCTION

Both carbon monoxide and copper are key components for the industrial synthesis of methanol. The latter is produced from a mixture of CO,  $\text{CO}_2$ , and  $\text{H}_2$ , typically over a  $\text{Cu}/\text{ZnO}/\text{Al}_2\text{O}_3$  catalyst at reaction conditions of 510 - 530 K and 50 - 100 bar, according to a process developed by ICI in 1996 [1]. It is generally agreed that  $\text{CO}_2$  is the main carbon source of methanol and direct hydrogenation of CO is unlikely [2]. Moreover, there is evidence that Cu is mainly responsible for the observed catalytic activity despite its modification with Zn [3]. Nonetheless, the role of CO is

#### 4. CO-Induced Surface Roughening of Copper (100)

still under debate and especially its interaction with copper at elevated pressure deserves further attention.

The adsorption of carbon monoxide on the (100) single crystal surface of copper in UHV and at cryogenic temperature is considered to be well understood, based on previous studies applying various experimental techniques, such as IRAS [4-7], photoemission spectroscopy (PES) [8-11], LEED [12-14], pump-probe spectroscopy [15-17], and high-resolution electron energy loss spectroscopy (HREELS) [14]. On the other hand, for room (and higher) temperature CO adsorption at higher pressure far less experimental studies were reported. Moreover, there are serious deviations between the obtained results, which may be due to strongly differing experimental conditions. For example, when exposing the Cu(100) sample at 300 K to 0.44 mbar of CO Taylor and Pritchard [18] reported one single IR-absorption band at  $2071\text{ cm}^{-1}$  by IRAS, assigned to on-top CO. Quite differently, using the same technique Truong et al. [19] reported one prominent band at  $2086\text{ cm}^{-1}$  and a shoulder between  $2095$  and  $2110\text{ cm}^{-1}$ , when exposing the sample at 265 K to 0.57 mbar CO. The first was assigned to adsorption on on-top sites whereas the second originated from stepped domains, although the authors did not specify their origin. Furthermore, in these early studies the adsorbate-induced reconstruction of a substrate [20] was not considered.

Examples of this phenomenon include the CO-induced restructuring of supported metal nanoparticles, as investigated by electron microscopy [21], infrared spectroscopy [22], or scanning tunneling microscopy (STM) [23]; and the restructuring of stepped platinum surfaces [24]. Very recent investigations of the Cu(111) [25], Cu(110) [26], and Cu(100) [27] single crystals by Salmeron and coworkers, using high-pressure (HP-) STM and near ambient pressure XPS (NAP-XPS), also revealed surface reconstruction upon exposure to mbar pressure of CO at 300 K: On the (111) and (100) single crystal terminations the formation of Cu clusters with three-, five-, and

#### 4. CO-Induced Surface Roughening of Copper (100)

up to 19-atoms was observed, whereas the (110) termination exhibited single, double or triple missing row reconstructions. In the latter case IRAS experiments were also performed, and an absorption feature of CO adsorbed at low coordinated Cu atoms was detected at 2099  $\text{cm}^{-1}$ . Herein, we extend this picture by presenting a combined LEED/TPD/XPS/PM-IRAS/DFT study of CO/Cu(100), including both *in situ* and *ex situ* studies of the (ongoing) surface roughening of CO at room temperature and near-atmospheric pressure. Apart from Cu cluster formation the modified surface also exhibits activity for CO dissociation which may be relevant for methanol synthesis.

#### 4.2 EXPERIMENTAL DETAILS

All experiments were performed in a custom-built UHV experimental chamber which has been previously described in detail [28, 29]. It has been successfully applied in various investigations such as CO adsorption/hydrogenation and methanol decomposition/oxidation on Pd (111) and supported Pd nanoparticles [30, 31], methanol steam reforming on bimetallic PdZn model catalyst [32-36], and CO adsorption on Ir [37]. In brief, the chamber comprises two parts, a classical UHV chamber and an UHV-compatible high-pressure cell (“Rupprechter-design” [28, 29]). The upper UHV section allows sample preparation and characterization by standard tools of surface science such as ion bombardment and annealing, XPS, LEED and temperature programmed desorption (TPD). Afterwards the sample can be transferred under UHV to the lower section, a gold-coated spectroscopic high pressure cell in which polarization-modulation IRAS (PM-IRAS) experiments can be performed in a pressure range from UHV to  $10^3$  mbar. The disk-shaped (8 mm diameter, 2 mm thickness) 5N-purity copper (100) single crystal (roughness and orientation accuracies better than 30 nm and  $1^\circ$ , respectively) was purchased from MaTeck. It was mounted via a tantalum wire cage on two molybdenum rods which allowed resistive heating

#### 4. CO-Induced Surface Roughening of Copper (100)

and cooling by liquid N<sub>2</sub>. The temperature was monitored through by a chromel-alumel thermocouple spot-welded to the back of the sample. The Cu single crystal was cleaned by repeated cycles of Ar<sup>+</sup> bombardment for 15 min (1×10<sup>-5</sup> mbar, 1.5 kV, 3.6×10<sup>-6</sup> A sputter current) and annealing to 800 K for 5 min. When required, the sample was annealed to 600 K in 1×10<sup>-7</sup> mbar oxygen before sputtering, to remove carbon contamination.

Surface order and cleanliness were confirmed by LEED (SPECS ErLEED 150) and XPS, respectively. X-ray radiation from a non-monochromated dual anode Mg/Al source (SPECS XR 50) was impinging on the sample at an angle of 55° with respect to the surface normal and photoelectrons were detected at normal emission by a hemispherical energy analyzer (SPECS PHOIBOS 150). For the TPD experiments the sample was heated with a linear temperature ramp of 1 K s<sup>-1</sup> (Eurotherm 3216 PID controller). The desorption products were detected by a differentially pumped mass spectrometer (Pfeiffer PrismaPlus 220) through a nozzle closely facing the sample, in order to minimize the detection of species desorbing from the sample mount and to prevent re-adsorption of molecules. Research grade CO (99.997 %) from an aluminum lecture bottle (Messer Austria) was admitted to the experimental chamber only after passing through a carbonyl purifying cartridge (Entegris GateKeeper 300KF) and a cold trap filled with a liquid N<sub>2</sub>/ethanol mixture at 170 K. PM-IRAS (Bruker IFS 66v/S FTIR spectrometer, liquid N<sub>2</sub>-cooled HgCdTe detector, HINDS PEM-90 ZnSe photoelastic modulator) was used to measure the vibrational properties of adsorbed CO species. IRAS is among the most sensitive tools to probe the adsorbate-to-surface coordination and thus the morphological status of the surface itself. When applied in polarization-modulation, it is even more since it can be employed from UHV to atmospheric pressure and allows differentiating between surface adsorbate and gas phase contributions [38-41]. The underlying principle of PM-IRAS is that the local electric field induced by s-polarized light impinging at near-grazing incidence on the metal surface, is vanishing [42].



## 4. CO-Induced Surface Roughening of Copper (100)

Hence no absorption of *s*-polarized light will occur by surface adsorbed and gas phase molecules. In contrast, *p*-polarized light will be absorbed by both surface adsorbed and gas phase molecules. Consequently, the demodulation of the signals obtained from *s*- and *p*-polarized light provides surface specific information. The PM-IRAS spectrum of the clean sample, prior to admitting CO to the spectroscopic cell, was used in all cases to normalize the spectra (not shown). PM-IRAS spectra were fitted with multiple Lorentzian lines and XPS spectra were fitted with the CasaXPS software after linear-background subtraction. The peaks were fitted with mixed Gaussian/Lorentzian line shapes and FWHM and peak positions were left unconstrained.

### 4.3 RESULTS AND DISCUSSION

#### 4.3.1 CO adsorption on Cu(100) under UHV conditions

After cleaning the Cu single crystal prior to each experiment, a LEED pattern characteristic of the (100) surface was observed (**Figure 4-1a**) and no contaminants were detected by XPS (e.g. in the O1s and C1s binding energy regions, **Figure 4-2a**).

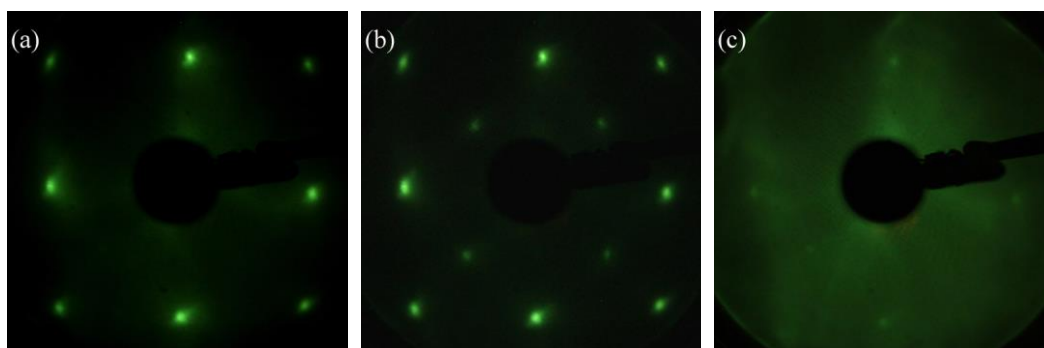


**Figure 4-1:** LEED patterns of (a) the clean and ordered as-prepared Cu(100) surface at room temperature, (b) the  $c(2 \times 2)$ CO overlayer at 120 K after  $\sim 40$  L CO exposure, and (c) the Cu surface after 40 min exposure to 1 mbar CO at room temperature, after which an ordered pattern could not be observed anymore. Energy was 157 eV.

Thereafter, the low temperature adsorption of CO on Cu(100) was addressed, and several benchmark experiments were performed by LEED, XPS, TPD, and IRAS. In all these experiments,

#### 4. CO-Induced Surface Roughening of Copper (100)

the adsorbate layer was prepared by cooling the clean copper single crystal from 300 to 120 K in  $1 \times 10^{-7}$  mbar CO. The cooling takes approximately 9 min, therefore the sample was exposed to  $\sim 40$  L ( $1 \text{ L} = 1 \times 10^{-6}$  Torr s) of carbon monoxide. After evacuation, a sharp  $c(2 \times 2)$  LEED pattern, corresponding to 0.5 ML CO coverage, was observed (**Figure 4-1b**).

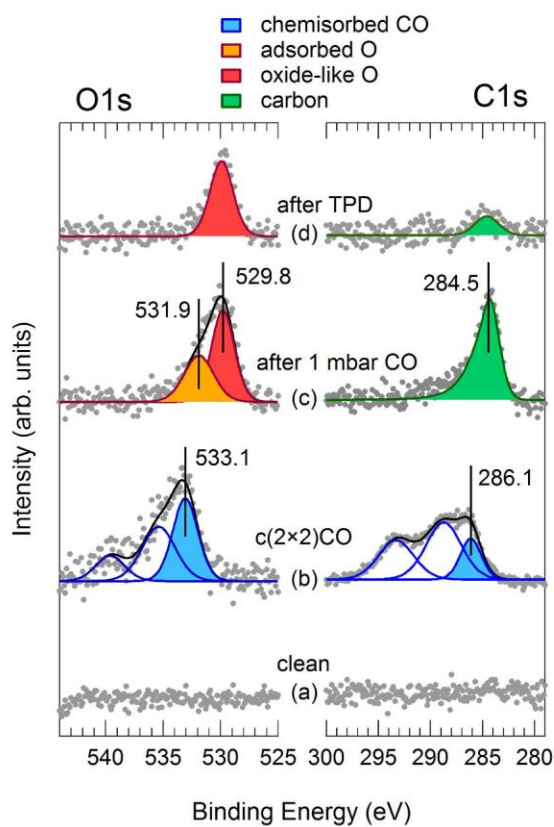


**Figure 4-2:** XPS spectra of the O 1s and C 1s binding energy regions of (a) the clean as-prepared Cu(100) surface, (b) the  $c(2 \times 2)$ CO overlayer at 120 K after  $\sim 40$  L CO exposure, (c) the Cu surface after exposure to 1 mbar CO at 300 K for 40 min and evacuation, and (d) after performing two consecutive TPD experiments after (c).

The  $c(2 \times 2)$ CO overlayer was also examined by XPS and the spectra for O 1s and C 1s binding energy (B.E.) regions are shown in **Figure 4-2b**. In the O 1s B.E. region the spectrum of the clean sample was subtracted from that of the CO overlayer because the spectral features are located on the high kinetic energy tail of the Cu LMM Auger triplet. In both O 1s and C 1s spectra, along with the two main (“adiabatic”) peaks at 533.1 and 286.1 eV, respectively, also satellite features

#### 4. CO-Induced Surface Roughening of Copper (100)

appeared at higher B.E. Such “giant satellites” are characteristic of weakly chemisorbed CO, and it is referred to references [8-11, 43] for an elaborate explanation. Taking advantage of the known CO coverage of 0.5 ML -confirmed by LEED- we have used the XPS peak area for quantitative calibration, enabling to determine the coverage of oxygen and carbon species in subsequent XPS experiments.

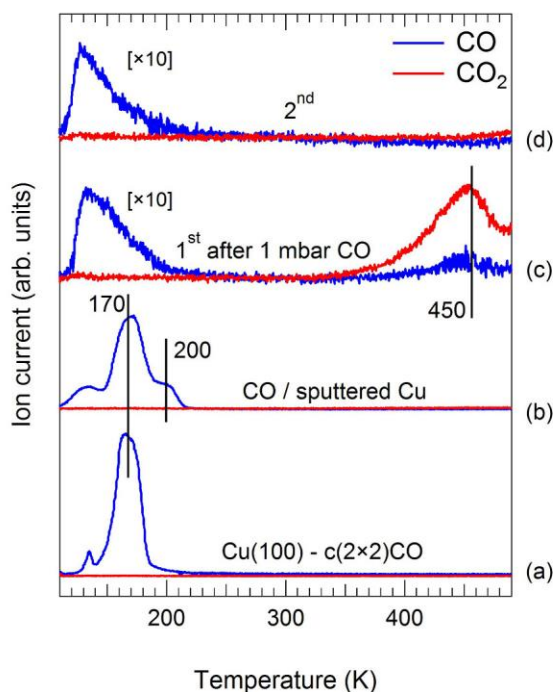


**Figure 4-3:** TPD experiments: (a) CO desorption from the c(2x2)CO overlayer prepared on the well-ordered Cu(100) surface and (b) on the ion-bombarded defective Cu surface. (c) and (d) show two successive TPD experiments performed after exposure to 1 mbar CO at 300 K for 40 min. CO and CO<sub>2</sub> signals in (c) and (d) are scaled by 10.

Before examining the c(2x2)CO overlayer by TPD, we have performed a background TPD experiment in order to determine the amount of potential contaminants originating from the chamber background (base pressure  $2 \times 10^{-10}$  mbar). The contamination level (small quantities of water and CO) turned out to be negligible ( $\sim 0.01$  ML). As shown in **Figure 4-3a**, CO of the c(2x2) overlayer desorbs with maximum rate at 170 K. Desorption below 140 K is due to CO desorbing

#### 4. CO-Induced Surface Roughening of Copper (100)

from the Ta heating wires, as already observed previously using the same experimental setup [44]. Based on the Redhead approximation [45] and assuming a desorption rate prefactor of  $1 \times 10^{13} \text{ s}^{-1}$ , the activation energy of desorption is estimated to be 0.46 eV per molecule ( $44 \text{ kJ mol}^{-1}$ ), in good agreement with the reported value [46]. We further observed that the adsorption was fully reversible, so that the TPD spectrum of the  $c(2 \times 2)\text{CO}$  structure could be repeated several times. We also performed a TPD experiment after preparing a CO adsorbate layer on the sputtered, defect-rich, Cu(100) surface. As shown in **Figure 4-3b**, an additional desorption feature appeared at 200 K, due to CO desorbing from defect sites created by ion bombardment. An activation energy of desorption of 0.55 eV per molecule ( $53 \text{ kJ mol}^{-1}$ ) was calculated for the defect sites.

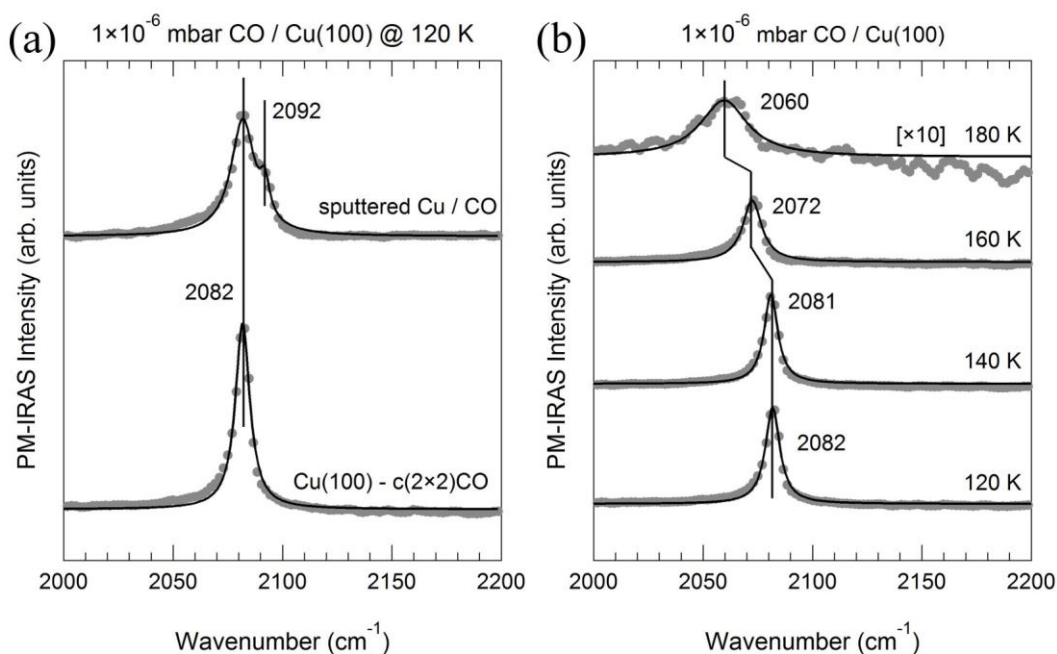


**Figure 4-4:** PM-IRAS results of (a) the as-prepared Cu(100) surface and the sputtered Cu surface cooled from 300 to 120 K under  $1 \times 10^{-6}$  mbar CO. (b) shows the redshift of the CO stretching band on well-ordered Cu(100) as a function of the sample temperature.

The low temperature CO adsorption on Cu(100) at  $1 \times 10^{-6}$  mbar CO pressure was also investigated by PM-IRAS, with results summarized in **Figure 4-4**. A vibrational feature attributed to the  $c(2 \times 2)\text{CO}$  overlayer at 120 K was observed at  $2082 \text{ cm}^{-1}$ . When the sample was heated to

#### 4. CO-Induced Surface Roughening of Copper (100)

>140 K, the CO coverage decreased and the combined effect of reduced dipole-dipole interaction and chemical shift led to a redshift of the band position, as previously discussed [6, 7, 47], (see **Figure 4-4b**). At 160 K, the band was observed at  $\sim 2072\text{ cm}^{-1}$ , with the redshift well reproducing data by Ryberg [7]. Heating to higher temperature (180 K) led to a further redshift to  $2060\text{ cm}^{-1}$ . It should be noted that above 170 K (the TPD desorption maximum in **Figure 4-3a**) the peak is very small. Similar as for TPD, we also performed PM-IRAS measurements for CO adsorbed at low temperature on the sputtered Cu(100) surface. As shown in **Figure 4-4a**, apart from the (weaker) band at  $2082\text{ cm}^{-1}$  assigned to CO adsorbed on well-ordered terraces, a shoulder appeared at  $2092\text{ cm}^{-1}$ , which may be due to CO adsorbed on defect sites such as steps, kinks or adatoms generated by ion bombardment (an assignment based on DFT will be discussed below).

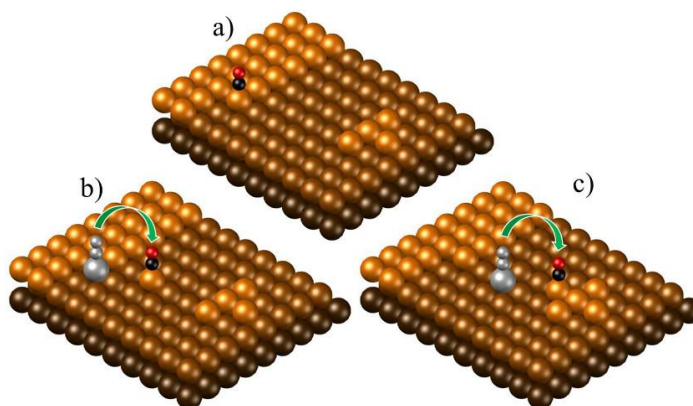


**Figure 4-5:** Model of adsorbed CO molecules on different Cu sites: on a kink atom with CN=6 (a), on an adatom  $\text{Cu}_1$  with CN=4 (b), and on-top of a  $\text{Cu}_5$  cluster atom with CN=5 (c). According to the proposed mechanisms for cluster formation, a CO molecule adsorbed on a kink (a) lowers its binding energy and forms a  $\text{Cu}_1\text{CO}$  complex mobile on the terrace (b). The latter can then coalesce with other adatoms forming clusters (c).

These sites, sketched in **Figure 4-5**, have a lower coordination number than a Cu atom within a terrace. For CO adsorbed on low coordinated sites, a shift to higher wavenumber was reported for polycrystalline copper films, to  $\sim 2105\text{ cm}^{-1}$  [18, 48-51] or to  $2090\text{--}2093\text{ cm}^{-1}$  [52].

#### 4. CO-Induced Surface Roughening of Copper (100)

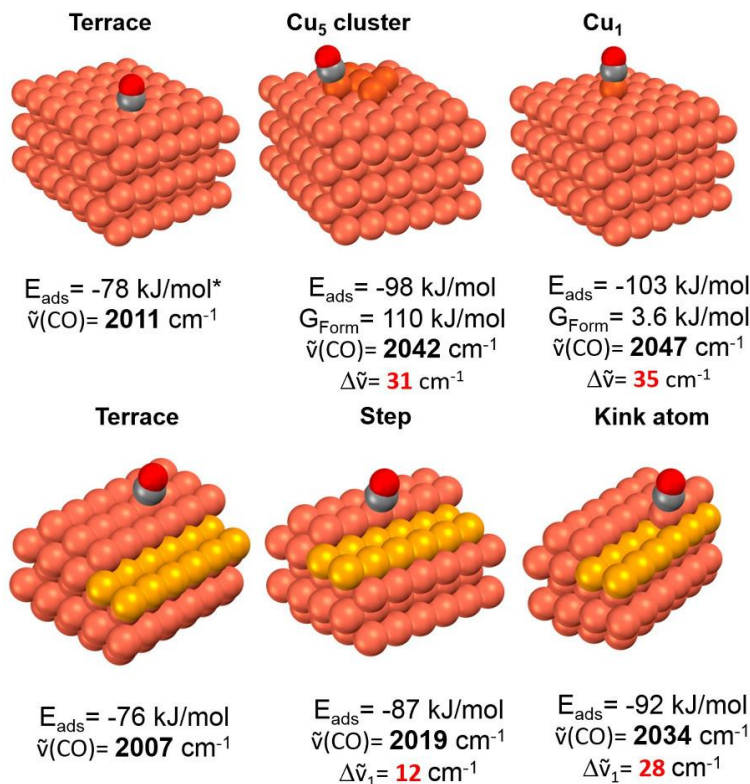


**Figure 4-6:** Results of DFT calculations of CO adsorption on Cu(100) terraces, steps, and kinks, as well as on Cu<sub>1</sub> and Cu<sub>5</sub> clusters (on Cu(100)).

To identify the vibrational frequencies expected for CO adsorbed on different sites of smooth and roughened Cu(100) DFT calculations were performed (**Figure 4-6**). For an isolated CO molecule on a Cu(100) terrace the calculated vibrational frequency is  $2007 \text{ cm}^{-1}$ , and for a low coverage of CO on Cu(100), a vibrational band at  $2060 \text{ cm}^{-1}$  was observed (**Figure 4-4b**, 180 K). The deviation between calculated and experimental vibrational signatures is a well-known effect, due to the potential used. However, based on the accurate measurements/calculations, a reasonable corrector factor of  $2060/2007=1.026$  can be obtained and the calculated shifts can be compared to the measured ones. The second band at  $2092 \text{ cm}^{-1}$ , experimentally observed after sputtering (frequency shift of  $+10 \text{ cm}^{-1}$  with respect to CO on terrace at 0.5 ML coverage) and shown in **Figure 4-4a** can thus be explained based on the DFT calculations as being due to CO adsorbed on low-coordinated Cu sites. Indeed for CO on step edges a shift of  $12 \text{ cm}^{-1}$  was

determined. A good agreement is found in the activation energies of desorption as well: an experimental value of 44 kJ mol<sup>-1</sup> for CO/terrace (53 kJ mol<sup>-1</sup> for CO/step) scales well with the theoretical one of 76 kJ mol<sup>-1</sup> (87 kJ mol<sup>-1</sup>).

##### 4.3.2 CO adsorption on Cu(100) at mbar pressure

After collecting UHV benchmark data at low temperature, CO adsorption at elevated temperature and at near atmospheric pressure was addressed. Because of the well-known issue of nickel or iron contamination when working with CO in this pressure regime, special cleaning precautions were made (see the “Experimental” section). Signatures of a Ni-poisoned Cu surface would include unusual low wavenumbers for adsorbed CO in IRAS (from 2020 to 2060 cm<sup>-1</sup> [53]), CO desorption features at about 360 K in TPD, and detection of the Ni 2p doublet in post reaction XPS analysis [2, 18]. **Figure 4-7a** shows a PM-IRAS experiment performed in 0.1 mbar CO at 200 K. In this case two bands were observed at 2082 cm<sup>-1</sup> and 2112 cm<sup>-1</sup>. It is well known [54] that at room temperature Cu single crystalline surfaces exhibit ordered terraces but also defect sites such as step edges, kink atoms, or adatoms. On the (100) terraces the c(2×2)CO overlayer formed, and was responsible for the band observed at 2082 cm<sup>-1</sup>. Furthermore, a second peak at 2112 cm<sup>-1</sup> developed (blue-shift of 30 cm<sup>-1</sup>).

Upon CO exposure, the binding energy of a Cu adatom may be lowered by an adsorbed CO molecule [25] and may thus detach from a step and form a mobile Cu<sub>1</sub>CO complex. Accordingly, we assign the band at 2112 cm<sup>-1</sup> to such a complex, namely CO on a single Cu adatom on a terrace. This is in line with the DFT calculations, since a shift of 35 cm<sup>-1</sup> was calculated for Cu<sub>1</sub> clusters with respect to CO adsorbed on a terrace at 0.5 ML coverage. The detachment of the adatoms from the step edges is favored by the high CO pressure (explaining why the band at 2112 cm<sup>-1</sup> was absent in **Figures 4-4**) and by the higher temperature. Correspondingly, the formation of Cu<sub>1</sub>CO complexes was found by DFT calculations to be slightly endothermic ( $G_{\text{form}}=110$  kJ mol<sup>-1</sup>). Indeed,

#### 4. CO-Induced Surface Roughening of Copper (100)

when the temperature was increased to 225 K further Cu adatoms were apparently formed and the corresponding band increased in intensity (**Figure 4-7a**).

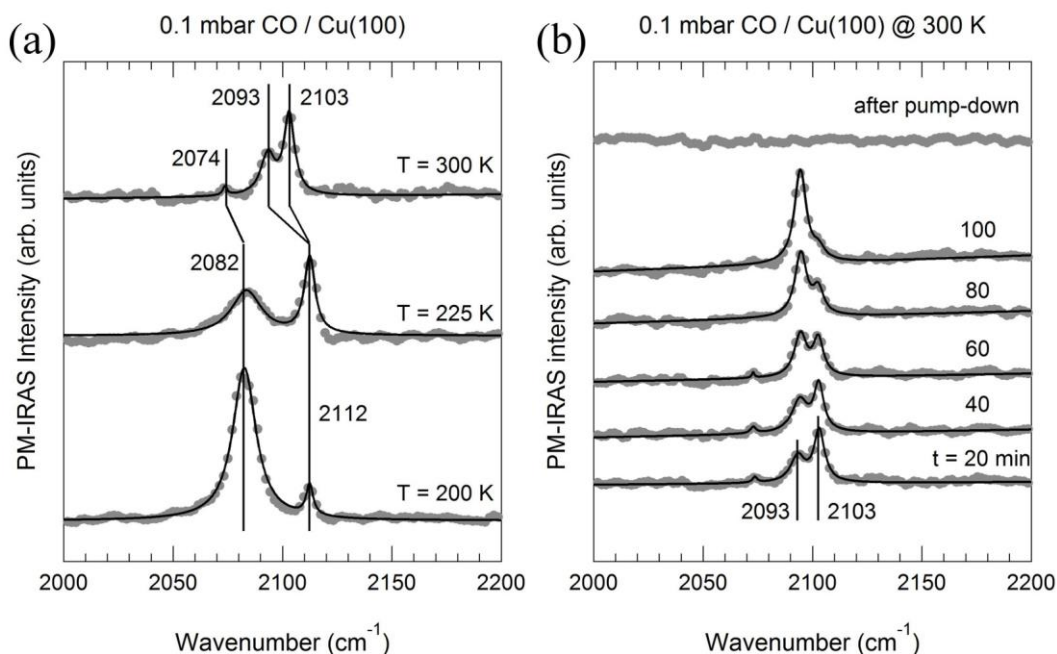


**Figure 4-7** (a) PM-IRAS spectra recorded in 0.1 mbar CO at 200 K, 225 K, and 300 K. The features at 2082 and 2112 cm<sup>-1</sup> are assigned to CO adsorbed on terraces and Cu<sub>1</sub>CO complexes, respectively. (b) Time evolution of PM-IRAS spectra recorded in 0.1 mbar CO at 300 K. The features at 2093 and 2103 cm<sup>-1</sup> are assigned to CO adsorbed at Cu<sub>5</sub>CO clusters and Cu<sub>1</sub>CO complexes, respectively.

Both the spectral features at 2082 cm<sup>-1</sup> and 2112 cm<sup>-1</sup> (now assigned to CO adsorption on terraces and defects, respectively) and changes of their relative intensities upon increasing the CO pressure from 1×10<sup>-5</sup> to 0.43 Torr at 265 K, have already been reported [19], although no explanation was provided. If the temperature is raised, not only more Cu<sub>1</sub>CO complexes can detach from the steps, but also their diffusion rate is expected to increase and they may coalesce into larger Cu clusters, according to Ostwald ripening [23]). When the temperature was increased to 300 K (a temperature higher than the CO desorption temperature), the CO coverage on the Cu(100) terraces decreased and was barely noticeable, and redshifted to 2074 cm<sup>-1</sup> (**Figure 4-7a**). The peak characteristic of Cu<sub>1</sub>CO was still present at 300 K but due to the reduced coverage (and



#### 4. CO-Induced Surface Roughening of Copper (100)

the reduced CO coupling), it shifted from  $2112\text{ cm}^{-1}$  to  $2103\text{ cm}^{-1}$ . This is again in good agreement with DFT, since the calculated shift of  $35\text{ cm}^{-1}$  for  $\text{Cu}_1\text{CO}$  with respect to CO/terrace, if applied to the observed value of  $2074\text{ cm}^{-1}$ , would predict a feature at  $2109\text{ cm}^{-1}$  for  $\text{Cu}_1\text{CO}$  (only  $6\text{ cm}^{-1}$  different from the experimental value).

In addition, a new species appeared at  $2093\text{ cm}^{-1}$ . This is clearly not CO on (100) terraces but indicates the formation of  $\text{Cu}_5\text{CO}$  clusters. This agrees with the observation of such clusters on Cu(100) with HP-STM by Salmeron and coworkers [27] in 0.25 mbar CO pressure, although in that work no IRAS experiments were performed. Further confirmation of this assignment is found by the DFT calculations: CO adsorbed on  $\text{Cu}_5$  would provide a vibrational feature  $31\text{ cm}^{-1}$  blue-shifted with respect to CO/terrace, that is  $4\text{ cm}^{-1}$  lower than  $\text{Cu}_1\text{CO}$ . A similar absorption feature at  $2099\text{ cm}^{-1}$  was observed before when exposing a Cu(110) surface to 0.02 Torr CO at room temperature [26], however this was assigned to CO adsorbed on CN=6 Cu atoms in a missing-row reconstruction.

The formation of  $\text{Cu}_5$  clusters from  $\text{Cu}_1$  was followed by a time-dependent PM-IRAS experiment under 0.1 mbar CO at 300 K (**Figure 4-7b**). The peak at  $2093\text{ cm}^{-1}$  ( $\text{Cu}_5\text{CO}$ ) increased, whereas the  $2103\text{ cm}^{-1}$  peak ( $\text{Cu}_1\text{CO}$ ) decreased in intensity. This indicates that  $\text{Cu}_5$  is formed by coalescence of  $\text{Cu}_1$ .

The surface restructuring of Cu(100) was further confirmed by two PM-IRAS experiments at 1 and 5 mbar CO pressure, shown in **Figure 4-8**. In 1 mbar, a main band was observed at  $2095\text{ cm}^{-1}$  and was assigned to CO adsorption on  $\text{Cu}_5$  clusters. The shoulder at  $2102\text{ cm}^{-1}$  was again due to  $\text{Cu}_1\text{CO}$  complexes. At this higher pressure the  $\text{Cu}_1$  clusters disappeared faster and the  $\text{Cu}_5$  clusters formed in a shorter time. A dynamical equilibrium between detachment of  $\text{Cu}_1$  adatoms from steps and  $\text{Cu}_5$  cluster formation explains why no strong time-dependent changes were observed. In 5 mbar, only the band due to CO adsorbed on  $\text{Cu}_5$  clusters could be detected because

#### 4. CO-Induced Surface Roughening of Copper (100)

of faster coalescence of  $\text{Cu}_1$  clusters. Finally, at this elevated pressure, an equilibrium state was reached, and the detachment of  $\text{Cu}_1$  atoms from step edges and their coalescence to  $\text{Cu}_5$  clusters led to the formation of a highly-stepped Cu surface, in agreement with the observation by HP-STM of the formation of 3-atom wide one-dimensional elongated structures covering the surface.

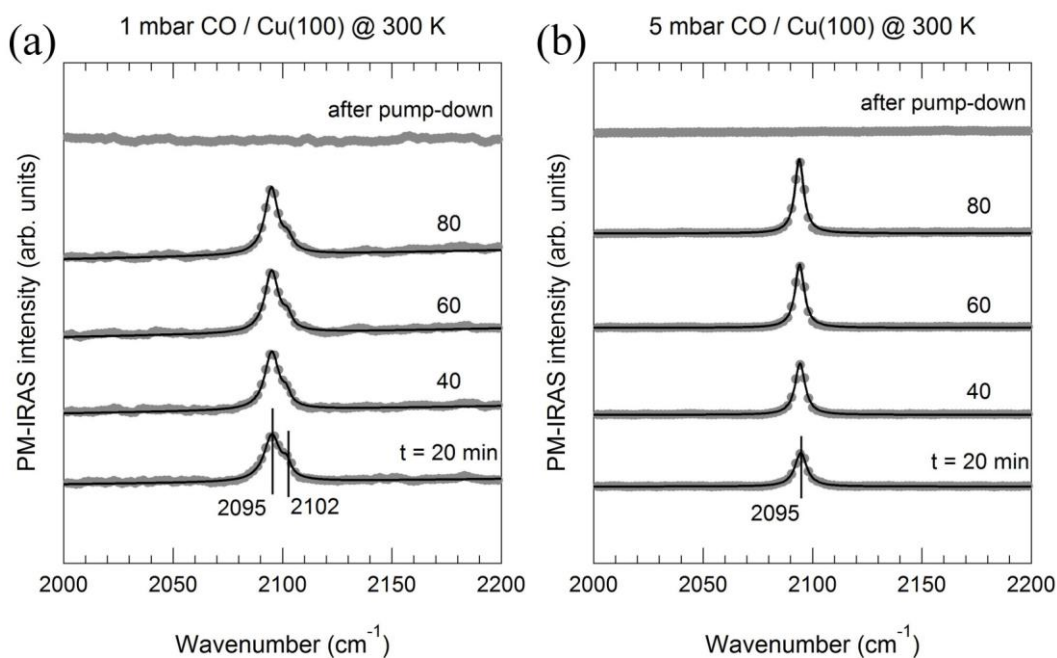


**Figure 4-8** (a) Time evolution of PM-IRAS spectra recorded in 1 mbar CO at 300 K. (b) Time evolution of PM-IRAS spectra recorded in 5 mbar CO at 300 K.

After the room temperature experiment at 1 mbar and evacuation, a thorough post reaction analysis has been carried out by LEED, XPS, and TPD. Using LEED (**Figure 4-1c**), an ordered pattern could not be observed but the background was brighter (the LEED and camera settings were the same as those of **Figure 4-1a and b**), also suggesting surface restructuring (roughening). Using XPS (**Figure 4-2c**), two different oxygen species at 531.9 and 529.8 eV (coverage of 0.15 and 0.23 ML, respectively) and one carbon species at 284.5 eV (0.27 ML) were detected after exposure and evacuation (these species were not detected after exposing the sample to 1 mbar Ar for 40 min instead of CO). The presence of carbon and oxygen suggests CO dissociation,  $\text{CO}^* \rightarrow \text{C}^* + \text{O}^*$ ,

#### 4. CO-Induced Surface Roughening of Copper (100)

or maybe a Boudouard process,  $2\text{CO}^* \rightarrow \text{CO}_2^{(\text{g})} + \text{C}^*$  [55]. Since such reactions are not favorable on the “smooth” single crystalline surface, as shown above by the reversible adsorption of CO in UHV, this once more indicates that the surface was roughened by high pressure CO. This is supported by recent studies of copper nanoclusters on alumina [56] and of the stepped Cu(211) surface [57], indicating that both are active for the two above mentioned reactions. Interestingly, for Cu(211) the carbon resulting from a first dissociation and located at the step edge turned out to be an active site for further CO adsorption and dissociation, leading to the formation of carbide and graphene islands and thus justifying the presence of carbon.

After exposure to 1 mbar CO at 300 K and evacuation, a TPD experiment was performed, cooling the sample from 300 to 120 K in  $1 \times 10^{-7}$  mbar CO ( $\sim 40$  L). As seen in **Figure 4-3c**, CO adsorption on the roughened copper surface was strongly suppressed. Although spectra were scaled by a factor of 10, the amount of CO desorbing from the roughened Cu surface was negligible ( $\sim 5\%$ ), when compared to that desorbing from the as-prepared clean sample (**Figure 4-3a**). The reason is that oxygen and carbon species were passivating the surface, as detected by XPS and shown in **Figure 4-2c**. Furthermore, even the “adsorbate-free” Cu sites ( $\sim 0.35$  ML) seemed not energetically favorable for CO adsorption because of neighboring O adatoms. To exclude any other effects of high pressure dosing, a TPD was also performed after 40 min exposure to 1 mbar Ar, however this had no influence on subsequent CO adsorption properties. Returning to the CO exposed sample, both CO *and* CO<sub>2</sub> were detected at 450 K during the first TPD. However, when the TPD was repeated immediately after the first TPD (**Figure 4-3d**) CO<sub>2</sub> was no longer observed. XPS analysis performed after this second TPD (**Figure 4-2d**) revealed that the O species at higher B.E. had completely disappeared and that the C species were diminished (0.05 ML). We propose to assign the former species (531.9 eV) to adsorbed oxygen which during the first TPD reacts with carbon via recombination to CO ( $\text{C}^* + \text{O}^* \rightarrow \text{CO}^{(\text{g})}$ ) or CO<sub>2</sub> ( $\text{CO}^{(\text{g})} + \text{O}^* \rightarrow \text{CO}_2^{(\text{g})}$ ),

#### 4. CO-Induced Surface Roughening of Copper (100)

thus leaving the surface. In contrast, the O species at lower B.E. (529.8 eV) must be assigned to a more strongly bound oxide-like oxygen species (that also originate from CO dissociation). This species was nonetheless present only in small amounts, so that no changes in the copper oxidation state (metallic) could be observed.

**Table:** Summary of binding and vibrational energies of the detected species. Species in grey are satellites.

<i>Species</i>	XPS O1s B.E. / eV	XPS C1s B.E. / eV	PM-IRAS / $\text{cm}^{-1}$
CO/defect Cu sites	-	-	2092-2112
Cu(100)-c(2×2)CO	539.6, 535.4, 533.1	293.3, 290.3, 286.1	2084
Carbon	-	284.5	-
Oxide-like oxygen	529.8	-	-
Adsorbed oxygen	531.9	-	-

#### 4.4 CONCLUSIONS

The interaction of CO with Cu(100), from UHV to mbar gas pressure, was studied in-situ and ex-situ by LEED, XPS, TPD, PM-IRAS, and DFT. The main findings can be summarized as follows:

CO adsorption on Cu(100) under UHV: When cooling the sample from 300 to 120 K in  $1 \times 10^{-7}$  mbar CO a well-ordered c(2×2)CO overlayer was obtained, as demonstrated by LEED. Such a structure, in which the CO molecules are located on-top of Cu atoms in terraces, was characterized by a vibrational absorption band at  $2082 \text{ cm}^{-1}$ . The vibrational energy was calculated by DFT to be  $2007 \text{ cm}^{-1}$ , thus providing a correction factor of 1.026. The c(2×2)CO was also characterized by XPS peaks at B.E. 533.1 (O1s) and 286.1 (C1s) eV. These two adiabatic peaks were accompanied by characteristic satellites at higher binding energy. The CO molecules of the c(2×2)

#### 4. CO-Induced Surface Roughening of Copper (100)

structure desorbed with a maximum at 170 K. An activation energy of desorption was estimated to be  $44 \text{ kJ mol}^{-1}$  (DFT:  $76 \text{ kJ mol}^{-1}$ ). PM-IRAS and TPD experiments of CO on the ion-bombarded Cu surface showed that both the vibrational energy and the activation energy of desorption were higher ( $2092 \text{ cm}^{-1}$  and  $53 \text{ kJ mol}^{-1}$ , respectively) on low-coordinated Cu atoms of steps. DFT calculations provided a  $12 \text{ cm}^{-1}$  blue-shift for the vibrational feature of ontop CO on Cu step edges, in good agreement with the experimentally observed shift ( $10 \text{ cm}^{-1}$ ), and a  $87 \text{ kJ mol}^{-1}$  activation energy of desorption.

CO adsorption on Cu(100) at mbar pressure: The interaction of Cu(100) with CO from 0.1 to 5 mbar pressure and at 200 and 300 K was investigated by PM-IRAS, and two absorption bands were detected: one at  $2093 \text{ cm}^{-1}$  and a second between  $2103 \text{ cm}^{-1}$  and  $2112 \text{ cm}^{-1}$  (shifting according to coverage). The latter was assigned to CO adsorbed on Cu adatoms detaching from step edges and getting mobile on the terraces as  $\text{Cu}_1\text{CO}$  complexes, whereas the band at  $2093 \text{ cm}^{-1}$  was assigned to CO adsorbed on  $\text{Cu}_5$  clusters formed by coalescence of the adatoms. These assignments were validated by DFT calculations predicting a blue-shift of  $31 \text{ cm}^{-1}$  and  $35 \text{ cm}^{-1}$  for  $\text{Cu}_5\text{CO}$  and  $\text{Cu}_1\text{CO}$  species, respectively, with respect to CO adsorbed on terraces. Both the detachment of the Cu adatoms from the step edges and their coalescence into clusters, which lead to an overall surface roughening, were induced by the presence of high pressure CO and were favored by higher temperature (with the formation of  $\text{Cu}_1\text{CO}$  predicted by DFT to be endothermic). In an experiment at 200 K, because of the higher CO coverage and a slower surface roughening (lower adatom mobility), along with the band at  $2112 \text{ cm}^{-1}$  ( $\text{Cu}_1\text{CO}$ ), also a band assigned to CO adsorbed on terraces could be detected at  $2083 \text{ cm}^{-1}$  ( $c(2\times 2)\text{CO}$  overlayer). Combining XPS and TPD studies after 1 mbar CO exposure at 300 K (and evacuation) it was demonstrated that the rough Cu surface was active for CO dissociation. XPS revealed the presence of carbon, at B.E.  $284.5 \text{ eV}$ , and of two different oxygen species, at B.E.  $531.9 \text{ eV}$  and  $529.8 \text{ eV}$ . The  $531.9 \text{ eV}$  species was active and

#### 4. CO-Induced Surface Roughening of Copper (100)

desorbed at 450 K as CO or CO<sub>2</sub> via recombination, whereas the 529.8 eV species was rather part of a less reactive surface Cu-oxide.

#### Bibliography

- [1] K. Weissermel, H.-J. Arpe, *Industrial Organic Chemistry*, 3 ed., Wiley-VCH, Weinheim, 1997.
- [2] J. Nerlov, S. Sckerl, J. Wambach, I. Chorkendorff, Methanol Synthesis from CO<sub>2</sub>, CO and H<sub>2</sub> over Cu(100) and Cu(100) Modified by Ni and Co, *Applied Catalysis a-General*, 191 (2000) 97-109.
- [3] L.C. Grabow, M. Mavrikakis, Mechanism of Methanol Synthesis on Cu through CO<sub>2</sub> and CO Hydrogenation, *Acs Catalysis*, 1 (2011) 365-384.
- [4] M.A. Chesters, Pritchard, J., M.L. Sims, Infrared Spectrum and Surface Potential of Carbon Monoxide Chemisorbed on a Copper (100) Single-Crystal Surface, *Journal of the Chemical Society D-Chemical Communications*, (1970) 1454-&.
- [5] K. Horn, J. Pritchard, Infrared Spectrum of CO Chemisorbed on Cu(100), *Surface Science*, 55 (1976) 701-704.
- [6] B.N.J. Persson, R. Ryberg, Vibrational Interaction Between Molecules Adsorbed on a Metal Surface - The Dipole-Dipole Interaction, *Physical Review B*, 24 (1981) 6954-6970.
- [7] R. Ryberg, Carbon Monoxide Adsorbed on Cu(100) Studied by Infrared Spectroscopy, *Surface Science*, 114 (1982) 627-641.
- [8] J.C. Fuggle, E. Umbach, D. Menzel, K. Wandelt, C.R. Brundle, Adsorbate Line-Shapes and Multiple Lines in XPS - Comparison of Theory and Experiment, *Solid State Communications*, 27 (1978) 65-69.
- [9] P.R. Norton, R.L. Tapping, J.W. Goodale, High-Resolution Photoemission Study of Physisorption and Chemisorption of CO on Copper and Gold, *Surface Science*, 72 (1978) 33-44.

#### 4. CO-Induced Surface Roughening of Copper (100)

- [10] W. Wurth, D. Coulman, A. Puschmann, D. Menzel, E. Umbach, Relation Between X-Ray Photoemission Binding Energies and Absorption Resonance Energies for CO Adsorbates, *Physical Review B*, 41 (1990) 12933-12936.
- [11] H. Antonsson, A. Nilsson, N. Martensson, I. Panas, P.E.M. Siegbahn, Vibrational Motion and Geometrical Structure in Adsorbed CO Studied by Core Level Photoelectron Spectroscopy, *Journal of Electron Spectroscopy and Related Phenomena*, 54 (1990) 601-613.
- [12] J. Pritchard, Structure of CO Adlayers on Cu(100) and Cu(111), *Surface Science*, 79 (1979) 231-244.
- [13] S. Andersson, J.B. Pendry, Structure of CO Adsorbed on Cu(100) and Ni(100), *Physical Review Letters*, 43 (1979) 363-366.
- [14] P. Uvdal, P.A. Karlsson, C. Nyberg, S. Andersson, N.V. Richardson, On the Structure of Dense CO Overlayers, *Surface Science*, 202 (1988) 167-182.
- [15] A.L. Harris, N.J. Levinos, L. Rothberg, L.H. Dubois, L. Dhar, S.F. Shane, M. Morin, Vibrational-Energy Transfer to Metal Surfaces Probed by Sum Generation - CO/Cu(100) and CH<sub>3</sub>S/Ag(111), *Journal of Electron Spectroscopy and Related Phenomena*, 54 (1990) 5-16.
- [16] M. Morin, N.J. Levinos, A.L. Harris, Vibrational-Energy Transfer of CO/Cu(100) - Nonadiabatic Vibration Electron Coupling, *Journal of Chemical Physics*, 96 (1992) 3950-3956.
- [17] T.A. Germer, J.C. Stephenson, E.J. Heilweil, R.R. Cavanagh, Picosecond Time-Resolved Adsorbate Response to Substrate Heating - Spectroscopy and Dynamics of CO/Cu(100), *Journal of Chemical Physics*, 101 (1994) 1704-1716.
- [18] A.O. Taylor, J. Pritchard, CO Adsorbed on Cu(100) - RAIRS at Ultrahigh Vacuum and Higher Pressures, *Journal of the Chemical Society-Faraday Transactions*, 86 (1990) 2743-2748.

#### 4. CO-Induced Surface Roughening of Copper (100)

- [19] C.M. Truong, J.A. Rodriguez, D.W. Goodman, CO Adsorption-Isotherms on Cu(100) at Elevated Pressures and Temperatures Using Infrared Reflection Absorption-Spectroscopy, *Surface Science*, 271 (1992) L385-L391.
- [20] G.A. Somorjai, *Modern surface science and surface technologies: An introduction*, *Chemical Reviews*, 96 (1996) 1223-1235.
- [21] G. Rupprechter, H.J. Freund, Adsorbate-induced restructuring and pressure-dependent adsorption on metal nanoparticles studied by electron microscopy and sum frequency generation spectroscopy, *Topics in Catalysis*, 14 (2001) 3-14.
- [22] A. Haghofer, P. Sonstrom, D. Fenske, K. Föttinger, S. Schwarz, J. Bernardi, K. Al-Shamery, M. Baumer, G. Rupprechter, Colloidally Prepared Pt Nanowires versus Impregnated Pt Nanoparticles: Comparison of Adsorption and Reaction Properties, *Langmuir*, 26 (2010) 16330-16338.
- [23] F. Yang, M.S. Chen, D.W. Goodman, Sintering of Au Particles Supported on TiO<sub>2</sub>(110) during CO Oxidation, *Journal of Physical Chemistry C*, 113 (2009) 254-260.
- [24] F. Tao, S. Dag, L.W. Wang, Z. Liu, D.R. Butcher, H. Bluhm, M. Salmeron, G.A. Somorjai, Break-Up of Stepped Platinum Catalyst Surfaces by High CO Coverage, *Science*, 327 (2010) 850-853.
- [25] B. Eren, D. Zhrebetsky, L.L. Patera, C.H. Wu, H. Bluhm, C. Africh, L.W. Wang, G.A. Somorjai, M. Salmeron, Activation of Cu(111) Surface by Decomposition into Nanoclusters Driven by CO Adsorption, *Science*, 351 (2016) 475-478.
- [26] B. Eren, Z.Y. Liu, D. Stacchiola, G.A. Somorjai, M. Salmeron, Structural Changes of Cu(110) and Cu(110)-(2 × 1)-O Surfaces under Carbon Monoxide in the Torr Pressure Range Studied with Scanning Tunneling Microscopy and Infrared Reflection Absorption Spectroscopy, *Journal of Physical Chemistry C*, 120 (2016) 8227-8231.



#### 4. CO-Induced Surface Roughening of Copper (100)

- [27] B. Eren, D. Zhrebetsky, Y.B. Hao, L.L. Patera, L.W. Wang, G.A. Somorjai, M. Salmeron, One-dimensional nanoclustering of the Cu(100) surface under CO gas in the mbar pressure range, *Surface Science*, 651 (2016) 210-214.
- [28] G. Rupprechter, T. Dellwig, H. Unterhalt, H.J. Freund, CO adsorption on Ni(100) and Pt(111) studied by infrared-visible sum frequency generation spectroscopy: design and application of an SFG-compatible UHV-high-pressure reaction cell, *Topics in Catalysis*, 15 (2001) 19-26.
- [29] G. Rupprechter, Surface vibrational spectroscopy from ultrahigh vacuum to atmospheric pressure: adsorption and reactions on single crystals and nanoparticle model catalysts monitored by sum frequency generation spectroscopy, *Physical Chemistry Chemical Physics*, 3 (2001) 4621-4632.
- [30] O.R. de la Fuente, M. Borasio, P. Galletto, G. Rupprechter, H.J. Freund, The Influence of Surface Defects on Methanol Decomposition on Pd(111) Studied by XPS and PM-IRAS, *Surface Science*, 566 (2004) 740-745.
- [31] M. Borasio, O.R. de la Fuente, G. Rupprechter, H.J. Freund, In Situ Studies of Methanol Decomposition and Oxidation on Pd(111) by PM-IRAS and XPS Spectroscopy, *Journal of Physical Chemistry B*, 109 (2005) 17791-17794.
- [32] C. Rameshan, C. Weilach, W. Stadlmayr, S. Penner, H. Lorenz, M. Havecker, R. Blume, T. Rocha, D. Teschner, A. Knop-Gericke, R. Schlogl, D. Zemlyanov, N. Memmel, G. Rupprechter, B. Klotzer, Steam Reforming of Methanol on PdZn Near-Surface Alloys on Pd(111) and Pd Foil Studied by In-Situ XPS, LEIS and PM-IRAS, *Journal of Catalysis*, 276 (2010) 101-113.
- [33] C. Rameshan, W. Stadlmayr, C. Weilach, S. Penner, H. Lorenz, M. Havecker, R. Blume, T. Rocha, D. Teschner, A. Knop-Gericke, R. Schlogl, N. Memmel, D. Zemlyanov, G. Rupprechter, B. Klotzer, Subsurface-Controlled CO<sub>2</sub> Selectivity of PdZn Near-Surface Alloys in H<sub>2</sub> Generation by Methanol Steam Reforming, *Angewandte Chemie-International Edition*, 49 (2010) 3224-3227.

#### 4. CO-Induced Surface Roughening of Copper (100)

[34] W. Stadlmayr, C. Rameshan, C. Weilach, H. Lorenz, M. Havecker, R. Blume, T. Rocha, D. Teschner, A. Knop-Gericke, D. Zemlyanov, S. Penner, R. Schlogl, G. Rupprechter, B. Klotzer, N. Memmel, Temperature-Induced Modifications of PdZn Layers on Pd(111), *Journal of Physical Chemistry C*, 114 (2010) 10850-10856.

[35] C. Weilach, S.M. Kozlov, H.H. Holzapfel, K. Föttinger, K.M. Neyman, G. Rupprechter, Geometric Arrangement of Components in Bimetallic PdZn/Pd(111) Surfaces Modified by CO Adsorption: A Combined Study by Density Functional Calculations, Polarization-Modulated Infrared Reflection Absorption Spectroscopy, and Temperature-Programmed Desorption, *Journal of Physical Chemistry C*, 116 (2012) 18768-18778.

[36] H.H. Holzapfel, A. Wolfbeisser, C. Rameshan, C. Weilach, G. Rupprechter, PdZn Surface Alloys as Models of Methanol Steam Reforming Catalysts: Molecular Studies by LEED, XPS, TPD and PM-IRAS, *Topics in Catalysis*, 57 (2014) 1218-1228.

[37] K. Anic, A.V. Bulchtiyarov, H. Li, C. Rameshan, G. Rupprechter, CO Adsorption on Reconstructed Ir(100) Surfaces from UHV to mbar Pressure: A LEED, TPD, and PM-IRAS Study, *Journal of Physical Chemistry C*, 120 (2016) 10838-10848.

[38] G. Rupprechter, Surface Vibrational Spectroscopy on Noble Metal Catalysts from Ultrahigh Vacuum to Atmospheric Pressure, *Annual Reports on the Progress of Chemistry, Section C, Physical Chemistry*, Vol 100, 100 (2004) 237-311.

[39] G. Rupprechter, Sum Frequency Generation and Polarization-Modulation Infrared Reflection Absorption Spectroscopy of Functioning Model Catalysts from Ultrahigh Vacuum to Ambient Pressure, in: B.C. Gates, H. Knozinger (Eds.) *Advances in Catalysis*, Vol 51, Elsevier Academic Press Inc, San Diego, 2007, pp. 133-263.

- [40] G. Rupprechter, C. Weilach, Spectroscopic Studies of Surface-Gas Interactions and Catalyst Restructuring at Ambient Pressure: Mind the Gap!, *Journal of Physics-Condensed Matter*, 20 (2008) 17.
- [41] K. Föttinger, C. Weilach, G. Rupprechter, Sum Frequency Generation and Infrared Reflection Absorption Spectroscopy, in: M. Che, J. Védrine (Eds.) *Characterization of Solid Materials and Heterogeneous Catalysis: from Structure to Surface Reactivity*, Wiley-VCH, Weinheim, 2012, pp. 211-252.
- [42] R.G. Greenler, Infrared Study of Adsorbed Molecules on Metal Surfaces by Reflection Techniques, *Journal of Chemical Physics*, 44 (1966) 310-&.
- [43] H. Tillborg, A. Nilsson, N. Martensson, Shake-Up and Shake-Off Structures in Core-Level Photoemission Spectra from Adsorbates, *Journal of Electron Spectroscopy and Related Phenomena*, 62 (1993) 73-93.
- [44] H. Li, J.I.J. Choi, W. Mayr-Schmolzer, C. Weilach, C. Rameshan, F. Mittendorfer, J. Redinger, M. Schmid, G. Rupprechter, Growth of an Ultrathin Zirconia Film on Pt<sub>3</sub>Zr Examined by High-Resolution X-ray Photoelectron Spectroscopy, Temperature-Programmed Desorption, Scanning Tunneling Microscopy, and Density Functional Theory, *Journal of Physical Chemistry C*, 119 (2015) 2462-2470.
- [45] P.A. Redhead, Thermal Desorption of Gases, *Vacuum*, 12 (1962) 203-244.
- [46] S. Vollmer, G. Witte, C. Woll, Determination of Site Specific Adsorption Energies of CO on Copper, *Catalysis Letters*, 77 (2001) 97-101.
- [47] D.P. Woodruff, B.E. Hayden, K. Prince, A.M. Bradshaw, Dipole Coupling and Chemical Shifts in IRAS of CO Adsorbed on Cu(110), *Surface Science*, 123 (1982) 397-412.
- [48] A.M. Bradshaw, Pritchard, J., M.L. Sims, Reflection Spectroscopy of Chemisorbed Carbon Monoxide Under Ultrahigh Vacuum Conditions, *Chemical Communications*, (1968) 1519-&.

#### 4. CO-Induced Surface Roughening of Copper (100)

- [49] H.G. Tompkins, R.G. Greenler, Experimental Development of Reflection-Absorption Spectroscopy - Infrared Spectrum of Carbon Monoxide Adsorbed on Copper and Copper Oxide, *Surface Science*, 28 (1971) 194-&.
- [50] J. Pritchard, T. Catterick, R.K. Gupta, Infrared Spectroscopy of Chemisorbed Carbon Monoxide on Copper, *Surface Science*, 53 (1975) 1-20.
- [51] R.W. Stobie, B. Rao, M.J. Dignam, Infrared Ellipsometry of Adsorbed Molecules - CO on Evaporated Cu Films, *Surface Science*, 56 (1976) 334-353.
- [52] H. Seki, M. Takada, T. Tanabe, T. Wadayama, A. Hatta, Infrared Absorption Study of CO Chemisorption on Copper Island Films, *Surface Science*, 506 (2002) 23-32.
- [53] M. Roiaz, E. Monachino, C. Dri, M. Greiner, A. Knop-Gericke, R. Schlogl, G. Comelli, E. Vesselli, Reverse Water-Gas Shift or Sabatier Methanation on Ni(110)? Stable Surface Species at Near-Ambient Pressure, *Journal of the American Chemical Society*, 138 (2016) 4146-4154.
- [54] M. Poensgen, J.F. Wolf, J. Frohn, M. Giesen, H. Ibach, Step Dynamics on Ag(111) and Cu(100) Surfaces, *Surface Science*, 274 (1992) 430-440.
- [55] A.F. Holleman, E. Wiberg, *Inorganic Chemistry*, 1 ed., Academic Press, San Diego, 2001.
- [56] J.A. Olmos-Asar, E. Monachino, C. Dri, A. Peronio, C. Africh, P. Lacovig, G. Comelli, A. Baldereschi, M. Peressi, E. Vesselli, CO on Supported Cu Nanoclusters: Coverage and Finite Size Contributions to the Formation of Carbide via the Boudouard Process, *Acs Catalysis*, 5 (2015) 2719-2726.
- [57] M.L. Ng, F. Abild-Pedersen, S. Kaya, F. Mbuga, H. Ogasawara, A. Nilsson, Low Barrier Carbon Induced CO Dissociation on Stepped Cu, *Physical Review Letters*, 114 (2015) 5.

## 5 VIBRONIC PROPERTIES OF CARBOXYLATED IRON PHTHALOCYANINES

---

This chapter highlights a joint research project with Prof. Erik Vesselli (Department of Physic, University of Trieste, Italy) and his PhD student Manuel Corva. For this I performed PM-IRAS measurements together with Manuel who has been for a couple of months visiting student at the Institute of Materials Chemistry, Technische Universität Wien, while SFG and STM measurements were performed at the University of Trieste.

### 5.1 INTRODUCTION

There were several reasons which encouraged me to include in my thesis work a summary of the results obtained in the framework of this joint project, namely on the interaction of a 2D layer of Fe phthalocyanines supported on a graphene on Ir(111) with CO at near-ambient pressure:

- Working on this system gave me the opportunity to broaden my scientific expertise by acquiring the know-how necessary to prepare a graphene sheet and metalorganic layers on a single crystal support. For this task I also had to build myself an evaporator for the deposition of metalorganic molecules (powder).
- The investigated system gives the occasion to discuss some remarkable differences between sum frequency generation spectroscopy (SFG) and infrared spectroscopy (specifically PM-IRAS), the two main techniques employed in my doctoral work.
- The monolayer of iron phthalocyanines supported on graphene represent a unique option, in perspective, to push the limits of model catalysts to that of single-atom catalysts. Therefore it is a topic intimately connected to the scientific purpose of this thesis.

## 5. Vibronic Properties of Carbonylated Iron Phthalocyanines

In the following, I will discuss how such a system can be prepared and characterized experimentally. Thereafter some results on near-ambient pressure CO adsorption, investigated by PM-IRAS and SFG, will be shown.

### 5.2 EXPERIMENTAL DETAILS

The system of choice was a metalorganic 2D film obtained by self-assembly on graphene, a weakly interacting support [1]. The metalorganic film consisted of Fe-phthalocyanines (FePc) which were adsorbed under ultra-high vacuum conditions on a single, closed graphene (GR) sheet. The graphene sheet was grown prior the deposition of the molecules on the Ir(111) single crystal.

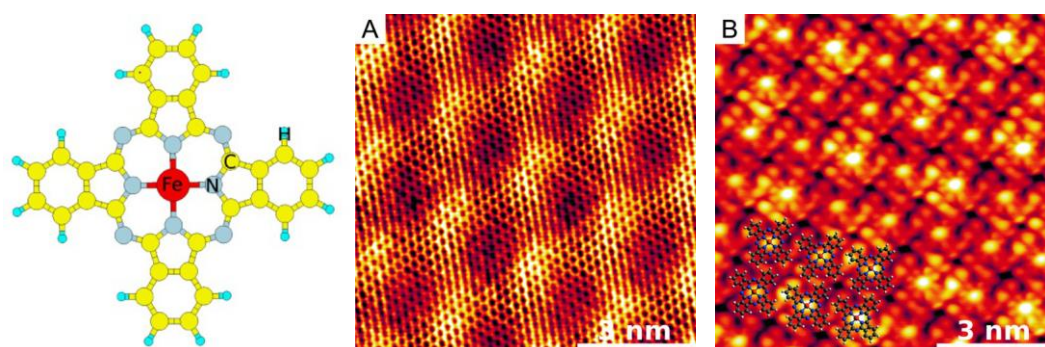


**Figure 5-1:** Drawing of a FePc molecule (left) and two STM pictures showing (A) the bare graphene on Ir(111) with the characteristic Moiré pattern and (B) the well-ordered monolayer of FePc on graphene on Ir(111), both prepared according to the procedure described below. Adapted from [2].

The Ir(111) single crystal was cleaned by repeated cycles of Ar<sup>+</sup> ion bombardment and thermal annealing to 1300 K. The surface cleanliness was checked by XPS. The graphene sheet was grown on the iridium substrate by thermal decomposition of ethylene according to an established recipe [3], which for the sake of completeness will be described in steps:

- Expose the clean Ir(111) crystal to 6 Langmuir of ethylene at 350 K (e.g.  $5 \times 10^{-8}$  mbar for 120 s).

## 5. Vibronic Properties of Carbonylated Iron Phthalocyanines

- Heat the sample with a linear temperature ramp. At  $\sim 1070$  K start opening the ethylene leak valve while continuing to heat, so that a background pressure of  $5 \times 10^{-8}$  mbar is established at 1125 K.
- While maintaining the ethylene background, heat further to the maximum temperature of 1275 K and keep the sample at that temperature for two minutes.
- Cool the sample down to 525 K, and then heat it up again (always in the ethylene environment). At  $\sim 1070$  K open the leak valve further, so that the ethylene background pressure increases to  $3 \times 10^{-7}$  mbar at 1125 K.
- While maintaining the  $3 \times 10^{-7}$  mbar ethylene background, heat further to the maximum temperature of 1275 K and keep the sample at that temperature for two minutes.
- Cool down the sample. At 1125 K shut the ethylene valve and let cool to RT under UHV.

As a word of caution, the preparation parameters given in detail here should be taken as a general guideline: Slight modifications could be necessary according to the experimental setup (different chamber, different sample holder, etc.). The quality of the graphene sheet was checked by STM (**Figure 5-1**) and by ensuring that no CO-intercalation of the sheet was occurring upon CO near-ambient pressure exposure: CO does not adsorb on defect-free graphene at room temperature [4, 5], however a strong CO vibrational feature is observed for CO/Ir in the 2075-2094  $\text{cm}^{-1}$  range. Therefore, the absence of such vibrational feature during CO exposure provides indirect evidence of the graphene sheet integrity. The graphene sheet is stable and, if it needs to be utilized several hours after preparation, it can be cleaned from weakly-adsorbed contaminants by flash thermal annealing to 485 K.

## 5. Vibronic Properties of Carbonylated Iron Phthalocyanines

The 2D metalorganic film consisted of Fe phthalocyanines, planar organic molecules containing the  $\text{FeN}_4$  species which adsorb on the graphene sheet with almost square symmetry (see **Figure 5-1**), similarly to the case of Co phthalocyanines [6]. This system and its stability properties are known from previous investigations [7-10]. The molecules (TCI Europe, I0783-1G, 132-16-1, purity 98%) were evaporated from a resistively-heated boron nitride crucible loaded with the respective powder. Boron nitride was chosen as crucible material because of its excellent thermal and chemical stabilities.

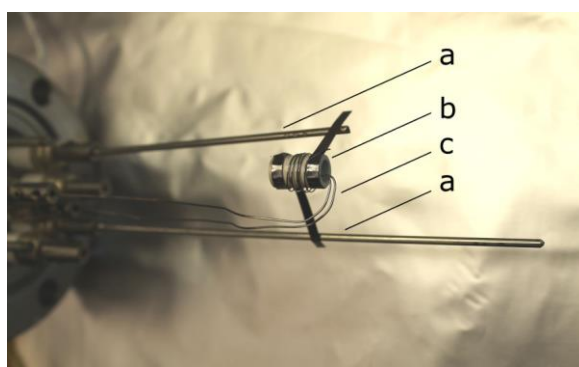


**Figure 5-2:** Photograph of the home-built evaporator for the preparation of the FePc film. It is comprised of tantalum rods (a) to mechanically support and lead the current to the cage for heating of the boron nitride crucible (b). The temperature inside the crucible was monitored by type-K thermocouple (c).

The home-built evaporator is shown in **Figure 5-2** and described in the following: A DN 40 CF flange provided with four electrical feedthroughs was equipped on the vacuum side with two tantalum rods (a). These were used as electrical contact for the heating cage wrapping the crucible (b), and were thick enough to guarantee mechanical support for the crucible/cage assembly. The cage for the crucible was fixed at the top and bottom by rolled tantalum foil. In the middle the coil-shaped heating cage was built by tantalum wire. These pieces were assembled together by spot-welding and constituted the electrical wiring responsible for joule heating of the crucible. The other two available electrical feedthroughs on the flange accommodated the wiring for a type-K thermocouple, whose tip was inserted inside the crucible to monitor the evaporation



## 5. Vibronic Properties of Carbonylated Iron Phthalocyanines

temperature. With a standard power supply it was easy to achieve an evaporation temperature of 650 K inside the crucible with a current and voltage of 2.3 A and 3.7 V, respectively. Before being loaded with the powder, the evaporator was degassed in vacuum to remove major contaminants (mainly water from the atmosphere). Afterwards, during a typical evaporation cycle, the background pressure increased to no more than  $2 \times 10^{-9}$  mbar. By temperature programmed XPS measurements [9] it was possible to identify the ideal temperature for the evaporation of FePc from the crucible. With this information the procedure was tuned in order to either prepare the multilayer (ML) or single layer (SL) of molecules on the sample. Accordingly, the molecules start to desorb at 570 K and are chemically stable up to 900 K. Therefore an evaporation temperature of 650 K was chosen, to guarantee a stable and reproducible flow of molecules. The evaporator was pre-heated for 5 minutes (i.e. for a stable evaporation rate), and in the next 5 minutes the sample surface, at room temperature, was normally exposed to the crucible aperture at a distance of approximately 5 cm. Monitoring of the N 1s and Fe 2p core electron signals by XPS allowed to determine the amount of the molecules adsorbed on the sample. Such an evaporation cycle corresponded to a multilayer. Indeed, a flash annealing of the sample to 640 K allowed the multilayer to desorb and left the graphene sheet covered by a single layer of FePc. The latter is more strongly bound to graphene, and would require a temperature of 820 K or higher to desorb/decompose.

### 5.3 RESULTS AND DISCUSSION

As a benchmark experiment, the vibrational properties of CO adsorbed on iridium were addressed first, by PM-IRAS. CO adsorbs on the Ir(111) readily at room temperature, as shown in **Figure 5-3 a**, after exposing the sample to 10 L.

## 5. Vibronic Properties of Carbonylated Iron Phthalocyanines

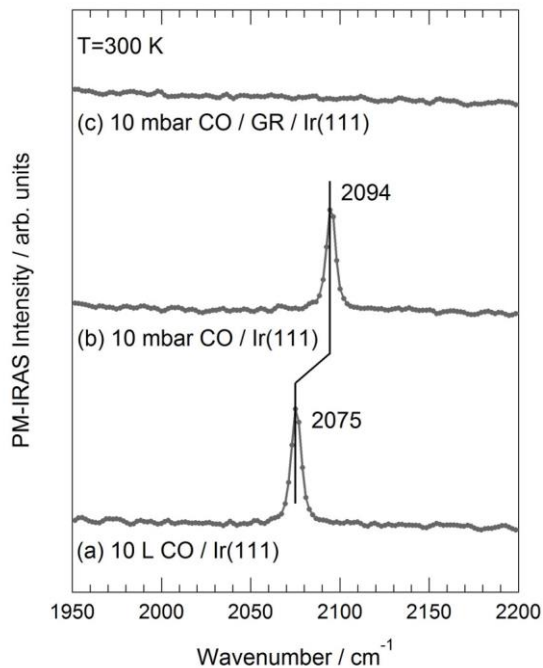


**Figure 5-3:** PM-IRAS spectra of the clean Ir(111) after exposure to 10 L CO (a), in-situ in 10 mbar CO, and 10 mbar CO in-situ PM-IRAS spectrum of the Ir(111) passivated by the graphene sheet (c). All spectra are measured at room temperature.

A single vibrational feature is observed at 2075 cm<sup>-1</sup>, corresponding to on top CO. The latter shifts to 2094 cm<sup>-1</sup> when the CO coverage is increased by exposing the sample in-situ to 10 mbar CO, all spectra are recorded at 300 K (**Figure 5-3 b**). **Figure 5-3 c** shows that no vibrational feature could be observed, again in 10 mbar CO, when the Ir(111) was passivated prior to CO exposure by the graphene sheet prepared as discussed above. This was an indirect proof of the quality of the sheet, which was defect-free.

After these benchmark infrared measurements, the Ir(111) covered by the graphene sheet was ready to proceed with the deposition of Fe phthalocyanines. The process in its different phases was monitored by XPS measurements (with non-monochromated Mg K $\alpha$  radiation), as summarized in **Figure 5-4**. As reference, the spectra in the Fe 2p and N 1s binding energy regions of the clean GR/Ir(111) sample were measured, and are shown in **Figure 5-4 a**.

## 5. Vibronic Properties of Carbonylated Iron Phthalocyanines

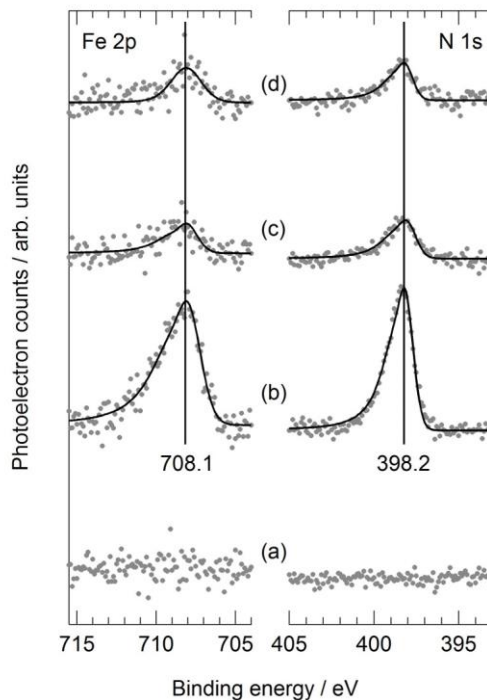


**Figure 5-4:** XPS spectra measured in the Fe 2p and N 1s binding energy regions to monitor the Fe phthalocyanines deposition procedure on GR/Ir(111). (a) shows the clean background. (b) is the spectrum corresponding to the multilayer immediately after evaporation, while (c) shows the single FePc layer after the flash annealing to 640 K. (d) is the spectrum measured after the PM-IRAS experiment in-situ in 10 mbar CO.

The spectrum in **Figure 5-4 b** was measured after the 5-minutes evaporation of FePc. The characteristic Fe  $2p_{3/2}$  and N 1s photoelectron peaks can be observed at 708.1 and 398.2 eV, respectively, as determined by fitting after background subtraction and in agreement with the results reported in [9].

After a flash annealing to 640 K, the multilayer desorbed and left the GR/Ir(111) substrate covered by one single FePc layer. The corresponding XPS spectrum is shown in **Figure 5-4 b**. The Fe  $2p_{3/2}$  and N 1s photoelectron peaks were observed with no shifts. Since the area ratios between spectra **b** and **c** of the components in the regions of Fe 2p and N 1s are 3.9 and 3.6, respectively, and assuming that **c** corresponds to a single layer, we conclude that our evaporation procedure

## 5. Vibronic Properties of Carbonylated Iron Phthalocyanines

covered the substrate with 3 to 4 layers of FePc. **Figure 5-4 d** shows the XPS spectra measured after exposure of the FePc single layer to 10 mbar CO. No changes in the Fe  $2p_{3/2}$  and N 1s components could be observed.

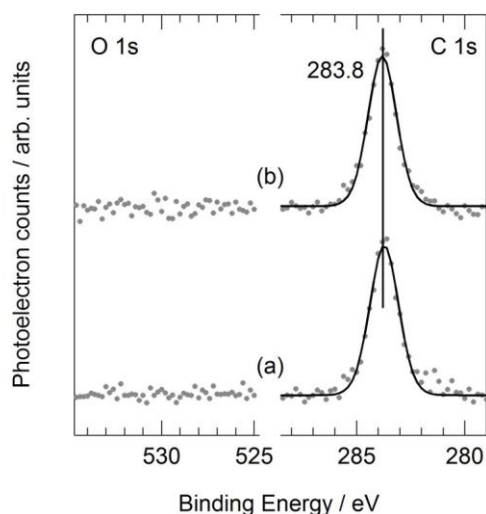


**Figure 5-5:** XPS spectra measured in the O 1s and C 1s binding energy regions of the FePc single layer on GR/Ir(111) immediately after preparation (a) and after exposure to 10 mbar of CO (b).

Similarly, no changes in the O 1s and C 1s binding energy regions could be observed after exposure of the FePc single layer on GR/Ir(111) to 10 mbar of CO, as shown in **Figure 5-5**. The O 1s shows no component, as expected, while in the C 1s a single non-resolved peak could be observed at 283.8 eV and is due to both the graphene sheet and the carbon atoms in the phthalocyanine layer. A difference in binding energy between these two non-equivalent chemical species could not be appreciated with laboratory XPS.

In **Figure 5-6** are shown PM-IRAS measurements of CO adsorption on a single layer of FePc supported by a graphene sheet on Ir(111). During in-situ exposure to 10 mbar CO a single spectral fingerprint could be observed at  $2008\text{ cm}^{-1}$ , and was assigned to a single CO molecule adsorbed on the Fe centers in the phthalocyanines. The adsorption was reversible, and no modification on

## 5. Vibronic Properties of Carbonylated Iron Phthalocyanines

the molecular layer could be detected by XPS after CO exposure and pump down, as discussed above and shown in **Figure 5-4** and **Figure 5-5**.

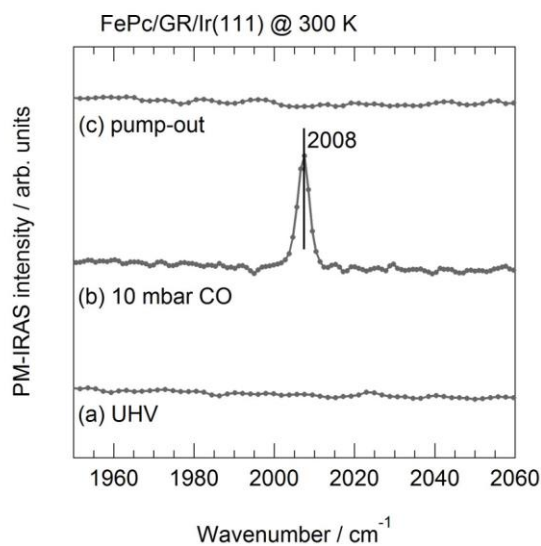


**Figure 5-6:** PM-IRAS measurements of the single layer of FePc supported by GR/Ir(111), as prepared in UHV (a), in situ in 10 mbar CO (b), and after pump-out (c).

The same preparation and characterization of the single FePc layer supported on GR/Ir(111) was carried out at the SFG vibronic spectroscopy laboratory - Department of Physics, University of Trieste, Italy. Spectroscopy investigations of adsorbed CO molecules on the Fe centers of the phthalocyanines were performed under the same conditions by means of SFG. Quite differently from the PM-IRAS results, in the case of SFG four distinct contributions could be resolved at 1986, 1992, 2005, and 2011 cm<sup>-1</sup> (**Figure 5-7**).

## 5. Vibronic Properties of Carbonylated Iron Phthalocyanines

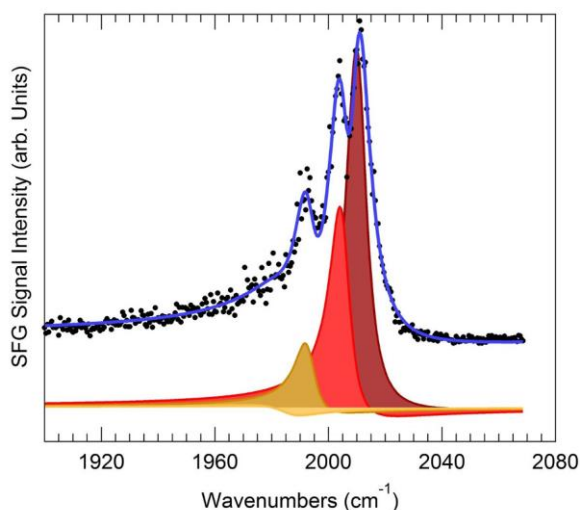


**Figure 5-7:** IR-vis SFG intensity spectra of the C-O stretching region collected in situ at room temperature in 10 mbar CO on the FePc monolayer on graphene. Experimental data are represented (black dots), together with the results of best fits (blue lines) and the interference of each resonance with the non-resonant background according to the effective susceptibility. Adapted from [2].

The reason for this difference is currently under investigation and may lie in an effect induced in the 2D metalorganic layer by the visible laser beam employed in the SFG technique. According to one suggestive interpretation, the observed splitting could be of the vibronic type and would be associated with contributions from excited triplet electronic molecular states that are populated upon exposure to the visible light beam (indeed the vis input matches a typical singlet excitation energy [11]). This effect, known as light-induced excited spin-state trapping (LIESST), consists in the change of the electronic spin state of a compound caused by irradiation with light. The corresponding change in distribution of the 3d valence electrons in the iron atom can then be observed indirectly as a vibrational splitting in the stretching mode of the CO ligand.

Other effects which commonly induce vibrational splitting, such as dipole-dipole interaction or molecular adsorption on non-equivalent sites have been ruled out. In the first case because of the large distance between Fe centers and in the second because *Ab initio*

calculations show that further CO adsorption beyond mono-coordination is strongly endothermic [2].

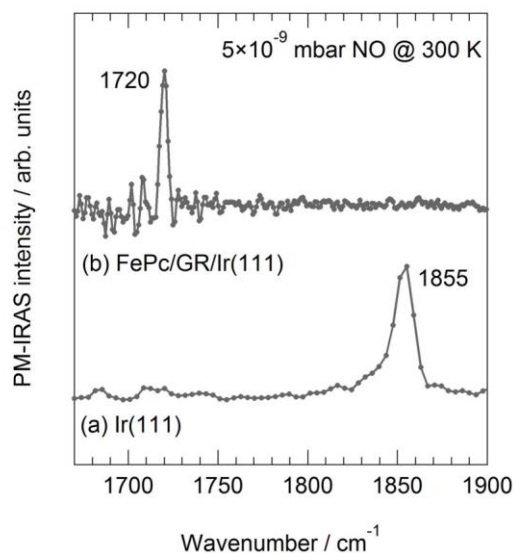


**Figure 5-8:** PM-IRAS measurements of NO adsorption at 300 K on clean Ir(111) (a) and on a single FePc layer supported on GR/Ir(111) (b).

The investigation has been carried further by choosing other ligands for the Fe atom in the phthalocyanines. In **Figure 5-8** two PM-IRAS spectra for NO adsorption are shown. On the bare Ir(111) a single vibrational fingerprint is observed at 1855 cm<sup>-1</sup>, consistently with previous EELS measurements [12]. The NO adsorbed on the Fe atoms in the FePc single layer could be observed at 1720 cm<sup>-1</sup>, even though much weaker.

Concerning another ligand which was tested, ammonia, which would have been particularly interesting because of its different symmetry properties, no chemisorbed NH<sub>3</sub> could be detected. Only by cooling the sample to 90 K it was possible to observe the characteristic vibrational fingerprints of physisorbed ammonia, i.e. at 1076 (N-H wagging, or “umbrella motion”), 3286 (N-H symmetric stretch), and 3379 (asymmetric stretch) cm<sup>-1</sup>. In the case of physisorption at 90 K, no differences were apparent between adsorption on the bare Ir(111), on the GR/Ir(111), or on the

## 5. Vibronic Properties of Carbonylated Iron Phthalocyanines

FePc layer on GR/Ir(111), as shown in the spectra in **Figure 5-9**. The investigation of this other ligands, NO and NH<sub>3</sub>, by SFG is currently under progress.

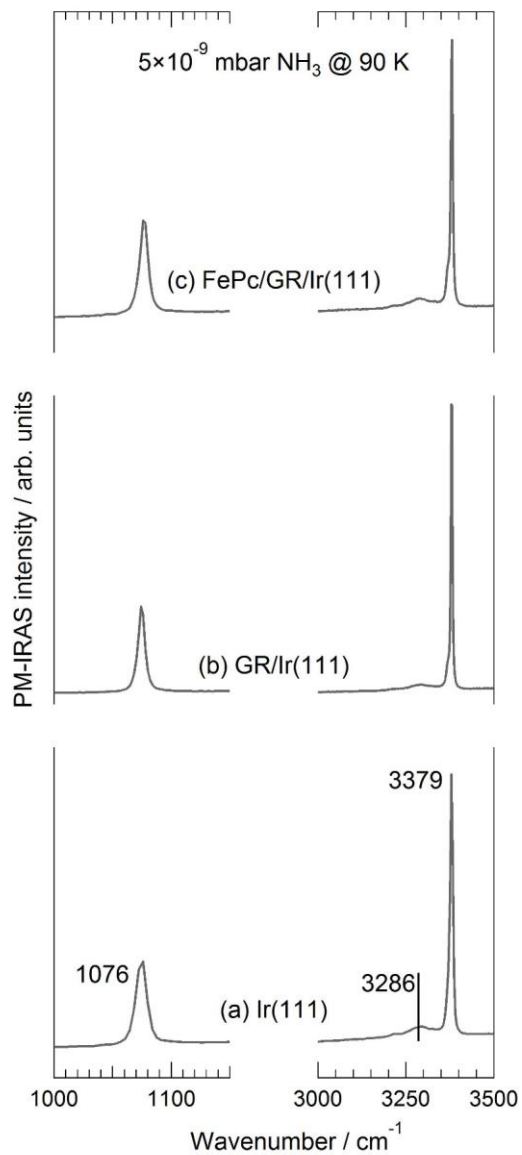


**Figure 5-9:** PM-IRAS measurements of NH<sub>3</sub> physisorbed on Ir(111) (a), on GR/Ir(111) (b), and on a single layer of FePc on GR/Ir(111) (c).



### 5.4 CONCLUSIONS

An evaporator for Fe phthalocyanines (powder) was built, and it allowed the preparation of a single FePc monolayer supported on a graphene sheet on a Ir(111) single crystal. The evaporation procedure was monitored by XPS, and afterwards the interaction of the Fe center in the organic molecules with different ligands (CO, NO, and NH<sub>3</sub>) was investigated by PM-IRAS. Adsorbed CO was observed at 300 K in-situ in 10 mbar of CO, by the identification of a vibrational fingerprint at 2008 cm<sup>-1</sup>. The latter was observed to experience a four-fold vibronic splitting when measured by SFG, probably as an effect of the impinging visible radiation employed in the SFG technique (in contrast PM-IRAS has no excitation in the visible region). NO adsorbed on the Fe centers of the phthalocyanines could be observed at 300 K at much lower pressure, namely 5×10<sup>-9</sup> mbar, by the identification of a vibrational fingerprint at 1720 cm<sup>-1</sup>. Conversely, in the case of NH<sub>3</sub>, only physisorption could be observed by cooling the sample to 90 K, and no vibrational differences were detected by physisorption on bare Ir(111), on GR/Ir(111), or on the FePc single layer supported on Gr/Ir(111).

### Bibliography

- [1] C. Wackerlin, J. Nowakowski, S.X. Liu, M. Jaggi, D. Siewert, J. Girovsky, A. Shchyrba, T. Hahlen, A. Kleibert, P.M. Oppeneer, F. Nolting, S. Decurtins, T.A. Jung, N. Ballav, Two-Dimensional Supramolecular Electron Spin Arrays, *Advanced Materials*, 25 (2013) 2404-2408.
- [2] M. Corva, M. Ferrari, M. Rinaldi, Z. Feng, M. Roiaz, C. Rameshan, G. Rupprechter, G. Pastore, G. Comelli, N. Seriani, E. Vesselli, Vibrational fingerprints of localized spin excitons in a 2D metalorganic crystal at room temperature, submitted.

## 5. Vibronic Properties of Carbonylated Iron Phthalocyanines

[3] H. Hattab, A.T. N'Diaye, D. Wall, G. Jnawali, J. Coraux, C. Busse, R. van Gastel, B. Poelsema, T. Michely, F. Heringdorf, M. Horn-von Hoegen, Growth temperature dependent graphene alignment on Ir(111), *Applied Physics Letters*, 98 (2011) 3.

[4] E. Granas, M. Andersen, M.A. Arman, T. Gerber, B. Hammer, J. Schnadt, J.N. Andersen, T. Michely, J. Knudsen, CO Intercalation of Graphene on Ir(111) in the Millibar Regime, *Journal of Physical Chemistry C*, 117 (2013) 16438-16447.

[5] N. Podda, M. Corva, F. Mohamed, Z. Feng, C. Dri, F. Dvorak, V. Matolin, G. Comelli, M. Peressi, E. Vesselli, Experimental and Theoretical Investigation of the Restructuring Process Induced by CO at Near Ambient Pressure: Pt Nanoclusters on Graphene/Ir(111), *Acs Nano*, 11 (2017) 1041-1053.

[6] S.K. Hämäläinen, M. Stepanova, R. Drost, P. Liljeroth, J. Lahtinen, J. Sainio, Self-Assembly of Cobalt-Phthalocyanine Molecules on Epitaxial Graphene on Ir(111), *Journal of Physical Chemistry C*, 116 (2012) 20433-20437.

[7] M. Scardamaglia, G. Forte, S. Lizzit, A. Baraldi, P. Lacovig, R. Larciprete, C. Mariani, M.G. Betti, Metal-phthalocyanine array on the moiré pattern of a graphene sheet, *Journal of Nanoparticle Research*, 13 (2011) 6013-6020.

[8] M. Scardamaglia, S. Lisi, S. Lizzit, A. Baraldi, R. Larciprete, C. Mariani, M.G. Betti, Graphene-Induced Substrate Decoupling and Ideal Doping of a Self-Assembled Iron-phthalocyanine Single Layer, *Journal of Physical Chemistry C*, 117 (2013) 3019-3027.

[9] M. Scardamaglia, C. Struzzi, S. Lizzit, M. Dalmiglio, P. Lacovig, A. Baraldi, C. Mariani, M.G. Betti, Energetics and Hierarchical Interactions of Metal Phthalocyanines Adsorbed on Graphene/Ir(111), *Langmuir*, 29 (2013) 10440-10447.

[10] M. Endlich, S. Gozdzik, N. Neel, A.L. da Rosa, T. Frauenheim, T.O. Wehling, J. Kroger, Phthalocyanine adsorption to graphene on Ir(111): Evidence for decoupling from vibrational spectroscopy, *Journal of Chemical Physics*, 141 (2014) 6.

## 5. Vibronic Properties of Carbonylated Iron Phthalocyanines

[11] M.B. Smith, J. Michl, Singlet Fission, *Chemical Reviews*, 110 (2010) 6891-6936.

[12] J.C.L. Cornish, N.R. Avery, Adsorption of N<sub>2</sub>, O<sub>2</sub>, N<sub>2</sub>O and NO on Ir(111) by EELS and TPD, *Surface Science*, 235 (1990) 209-216.

## 5. Vibronic Properties of Carbonylated Iron Phthalocyanines

## 6 CONCLUSIONS

---

The aim of this thesis was to study heterogeneous catalytic model systems with techniques allowing to bridge the pressure gap encountered between standard surface science investigations and the conditions found in real catalysis. Model catalysts are tailored to mimic one (or more) of the properties responsible for the performances of industrial catalysts: Different samples are examined in order of increasing complexity under controlled conditions of pressure, temperature, and chemical compositions, the rationale behind this being the ability to understand the reaction mechanism at the nanoscale. To bridge the pressure gap between real catalysis and standard surface science studies, the focus of this work was on sum frequency generation spectroscopy (SFG) and polarization-modulation infrared reflection absorption spectroscopy (PM-IRAS), since these photon-based spectroscopies can be employed in a wide pressure range, from UHV to ambient. Additionally, UHV techniques such as X-ray photoelectron spectroscopy (XPS), low energy electron diffraction (LEED), and temperature programmed desorption (TPD), have been employed to characterize model catalyst surfaces in UHV before and after exposure to reactive gas atmospheres, using respective spectroscopic cells (in the SFG- and PM-IRAS-setup).

A major part of the thesis was dedicated to the planning, design, assembly, and commissioning of a new UHV chamber coupled to an SFG high-pressure compatible spectroscopic cell to simultaneously perform SFG and catalytic activity measurements. The new setup enables fast sample insertion via a load lock, is equipped with standard tools of UHV sample preparation such as cooling by LN<sub>2</sub>, heating (to 1273 K), ion bombardment (sputtering), evaporation via physical vapor deposition (PVD), and characterization by LEED or Auger. Afterwards the model catalyst samples can be transferred in UHV to the spectroscopic cell. There, SFG spectra can be recorded in wide pressure and temperature ranges, from UHV to ambient pressure and from 100

## 6. Conclusions

to 1000 K, respectively. The setup has been tested by benchmark experiments of CO adsorption on Pt(111) and Pd(111) single crystals and by investigating the CO oxidation reaction on a Pt-ZrO<sub>2</sub> model catalyst.

Both on Pt(111) and Pd(111) well-ordered CO overlayers were observed by LEED, and spectroscopic evidence of CO adsorbed at different sites was obtained by SFG. On-top CO was observed on Pt(111) at 300 K and 5 mbar equilibrium pressure, with a major signal at 2092 cm<sup>-1</sup>. A weaker spectral feature due to adsorption on defect sites was detected at 2073 cm<sup>-1</sup>. On Pd(111), at 300 K and 5 mbar equilibrium pressure, CO adsorbed on three-fold hollow (1900 cm<sup>-1</sup>), bridge (1935 cm<sup>-1</sup>), and on-top (2071 cm<sup>-1</sup>) sites was observed. These spectra were recorded in *ppp* polarization combination, however in the case of platinum a detailed polarization-dependent investigation was carried out. In brief, assuming a zero tilt angle of the adsorbed CO molecule it was possible to deduce the molecular hyperpolarizability ratio. After this commissioning phase was accomplished by revisiting well-known systems, the more complex Pt-ZrO<sub>2</sub> model catalyst was addressed. The sample consisted of a topmost layer of platinum nanoparticles deposited by atomic layer deposition (ALD) on a zirconia thin film supported by a silicon wafer. The activity of this system towards CO oxidation was investigated simultaneously by SFG and mass spectrometry in a CO/O<sub>2</sub> 1:2 reaction mixture (30 mbar equilibrium pressure) at different temperatures. At the highest temperature examined (350 °C) both adsorbed CO (on the Pt-nanoparticles) and CO<sub>2</sub> (in the gas phase) could be detected, suggesting that some facets of the particles were CO-poisoned while others active.

The second part of the thesis focused on investigating the interaction of CO with a Cu(100) single crystal surface by PM-IRAS. By TPD it was found that CO absorbs on Cu(100) only weakly, with 0.46 eV desorption energy. The weak adsorption was also seen in the XPS spectra by detecting strong satellites in the C 1s and O 1s regions. After cooling the sample to 120 K in 1×10<sup>-</sup>

<sup>6</sup> mbar CO, a characteristic vibrational feature was detected by IR spectroscopy at 2082 cm<sup>-1</sup>. This was originating from the c(2×2)CO overlayer, as observed by LEED measurements performed in identical conditions. The spectral feature originating from CO adsorbed on low-coordinated Cu atoms, obtained by ion-bombardment of the surface, was blue-shifted to 2092 cm<sup>-1</sup> (at 120 K in 1×10<sup>-6</sup> mbar CO). This shift was in good agreement with the one calculated by density functional theory (DFT) by L. Falivene, S.M. Kozlov, and L. Cavallo at the KAUST Catalysis Center, Thuwal, Saudi Arabia. In the case of the Cu(100) surface exposed to CO at 300 K in the 0.1 to 5 mbar pressure range, it was found by PM-IRAS that CO adsorbs only on the under-coordinated Cu atoms, and that the surface density of such sites increased with exposure time of CO. Moreover, the higher the CO pressure was, the more this roughening effect induced by the CO itself was pronounced. By comparing the IR measurements and the DFT calculations with a recent high-pressure scanning tunneling microscopy investigation by M. Salmeron and coworkers, a mechanism was proposed: Accordingly, CO molecules adsorb on Cu atoms at the steps, which subsequently detach as Cu<sub>1</sub>CO complexes. These complexes are mobile on the (100) terraces, and they further coalesce forming Cu<sub>5</sub> clusters. This process eventually leads to a roughening of the Cu surface.

The last part of the thesis describes an interesting difference between the SFG and PM-IRAS techniques. The opportunity to discuss the latter was given by a collaboration with the group of E. Vesselli at University of Trieste, Italy. By studying the vibrational properties of a monolayer of carbonylated Fe phthalocyanines supported on a graphene sheet on Ir(111), it was found that the input visible laser radiation of an SFG experiment induced a vibronic splitting of the coordinated CO stretching mode (low spin to high spin transition), and this splitting could be detected by the IR probe. Conversely, in a PM-IRAS experiment in which infrared radiation was the only input and visible light excitation was absent, such splitting did not occur and only a single

## 6. Conclusions

vibrational feature was observe. This project was also used to develop and build in-house a molecular evaporator for powders, allowing to deposit the Fe-phthalocyanines monolayer.



## PUBLICATION LIST

---

### JOURNAL ARTICLES

M. Roiaz, V. Pramhaas, X. Li, C. Rameshan, G. Rupprechter: "Atmospheric Pressure Reaction Cell for Operando Sum Frequency Generation Spectroscopy of Ultrahigh Vacuum Grown Model Catalysts"; Review of Scientific Instruments (2018), published.

X. Li, M. Roiaz, V. Pramhaas, C. Rameshan, G. Rupprechter: "Polarization-Dependent SFG Spectroscopy of Near Ambient Pressure CO Adsorption on Pt(111) and Pd(111) Revisited"; Topics in Catalysis (2018), in press.

C. Rameshan, H. Li, K. Anic, M. Roiaz, V. Pramhaas, R. Rameshan, R. Blume, M. Hävecker, J. Knudsen, A. Knop-Gericke, G. Rupprechter: "In situ NAP-XPS Spectroscopy during Methane Dry Reforming on ZrO<sub>2</sub>/Pt(111) Inverse Model Catalyst"; Journal of Physics: Condensed Matter, submitted.

M. Roiaz, E. Monachino, C. Dri, M. Greiner, A. Knop-Gericke, R. Schlögl, G. Comelli, E. Vesselli: "Reverse Water-Gas Shift or Sabatier Methanation on Ni(110)? Stable Surface Species at Near-Ambient Pressure"; Journal of the American Chemical Society, 138:12 (2016) 4146.

### ORAL AND POSTER PRESENTATIONS AS FIRST AUTHOR

M. Roiaz, V. Pramhaas, X. Li, C. Rameshan, G. Rupprechter: "A New Experimental Setup For UHV And Ambient Pressure SFG", Oral presentation; 17. Österreichische Chemietage 2017, Salzburg; 25.09.2017 - 28.09.2017; in: "17. Österreichische Chemietage 2017", (2017), 1 S.

M. Roiaz, C. Rameshan, G. Rupprechter: "A New UHV System Including a High Pressure Cell for In-Situ Sum Frequency Generation Spectroscopy", Poster; EUROPACAT 13th European

## Publication List

Congress on Catalysis, Florence; 27.08.2017 - 31.08.2017; in: "EUROPACAT Catalysis - A Bridge to the Future", (2017), S. 133.

M. Roiaz, V. Pramhaas, X. Li, C. Rameshan, G. Rupprechter: "*A New Ultra-High Vacuum System Including a High Pressure Cell for In-Situ Sum Frequency Generation Spectroscopy*", Oral presentation; Solids4Fun Summerschool 2017, Waidhofen a.d.Ybbs; 03.07.2017 - 07.07.2017.

M. Roiaz, C. Rameshan, G. Rupprechter: "*A New UHV System Including a High Pressure Catalysis Cell for In-Situ SFG Spectroscopy*", Poster; 6th SFB-F45 "FOXSI" Annual PhD Workshop, Haus im Ennstal; 01.02.2017 - 04.02.2017.

M. Roiaz, C. Rameshan, G. Rupprechter: "*Surface Roughening of Copper (100) by High Pressure Carbon Monoxide Exposure*", Poster; The 16th International Congress on Catalysis, Beijing; 03.07.2016 - 08.07.2016; in: "The 16th International Congress on Catalysis - Poster Presentations", (2016), S. 7.

M. Roiaz, C. Rameshan, G. Rupprechter: "*Roughening of Copper (100) by High Pressure Carbon Monoxide Exposure*", Poster; 5th SFB-F45 "FOXSI" Annual PhD Workshop 2016, Haus im Ennstal; 30.03.2016 - 02.04.2016.

M. Roiaz, C. Rameshan, G. Rupprechter: "*Roughening of Copper (100) by High Pressure Carbon Monoxide Exposure*", Poster; 31. Workshop on Novel Materials and Superconductivity, Obertraun; 07.02.2016 - 13.02.2016.

M. Roiaz, V. Pramhaas, D. Demir, C. Rameshan, G. Rupprechter: "*Sum Frequency Spectroscopy for Investigations in Heterogeneous Catalysis*", Oral presentation; 16. Österreichische Chemietage, Innsbruck; 21.09.2015 - 24.09.2015; in: "16. Österreichische Chemietage", Book-of-Abstracts.com, Gumpoldskirchen (2015), 1 S.

M. Roiaz, C. Rameshan, G. Rupprechter: *"Towards an Investigation in Catalysis: CO Adsorption on Cu(100)"*, Oral presentation; Invitation at CNR-IOM Istituto Officina dei Materiali, University of Trieste, Trieste; 22.07.2015.

M. Roiaz, G. Rupprechter: *"Towards a Catalytic Investigation: CO Adsorption on Cu(100)"*, Oral presentation; Solids4Fun Summer School 2015, Schloss Hernstein; 29.06.2015 - 03.07.2015.

M. Roiaz, V. Pramhaas, D. Demir, C. Rameshan, G. Rupprechter: *"SFG Spectroscopy in Catalytic Reactions from UHV to Ambient Pressure: Setup and Principle Investigations"*, Poster; International Workshop: Sum Frequency Spectroscopy, Wilhelm-Kempff-Haus, Wiesbaden Naurod, Germany; 30.03.2015 - 01.04.2015; in: "International Workshop: Sum Frequency Spectroscopy", (2015), S. 1.

## Publication List

## CURRICULUM VITAE

---

### PERSONAL DATA

Name and surname: Matteo Roiaz

Date and place of birth: 02/10/1990, Trieste, Italy

Citizenship: Italian

✉ Via Donato Bramante 4, 34143 Trieste, Italy

☎ +39 393 9010250

💻 m.roiaz@gmail.com

📺 Matteo Roiaz (live:m.roiaz)



### WORKING EXPERIENCE

11/2014–10/2017 Project Assistant at *Institute of Materials Chemistry, Technische Universität Wien, Vienna, Austria.*

2015 and 2016 Teaching activity: assistant in Laboratory Course of Physical Chemistry, at *Technische Universität Wien, Vienna, Austria.*

### EDUCATION

5/2018 (planned) Dr.rer.nat Technical Chemistry at *Technische Universität Wien, Vienna, Austria.* Title: "Operando PM-IRAS and SFG Spectroscopy of Cu, Pt and Pd Model Catalysts Prepared in Ultra-High Vacuum". Supervisors: Prof. Günther Rupprechter and Dr. Christoph Rameshan.

10/2014 Master of Science in materials physics at *Università degli Studi di Trieste, Trieste, Italy.* Title: "Catalytic reduction of CO<sub>2</sub>: SFG vibrational spectroscopy at near-ambient pressure and in liquid." Supervisor: Prof. Erik Vesselli, grade: 110/110 *con lode.*

## Curriculum Vitae

- 11/2012 Bachelor of Science in physics at *Università degli Studi di Trieste*, Trieste, Italy. Supervisor: Prof. Fabio Benatti, grade: 102/110.
- 06/2012 Conservatory graduation in accordion at *Conservatorio Statale di Musica G. Tartini*, Trieste, Italy. Supervisor: M. Corrado Rojac, grade: 9.5/10.
- 07/2009 High school graduation at *Liceo Scientifico Statale G. Galilei*, Trieste, Italy. Grade: 85/100.

### LANGUAGE AND DIGITAL SKILLS

- Italian, mother tongue
- German, intermediate (B2)
- English, TOEFL iBT 108/120 (C1)
- Slovenian, basic (A1)
- Operating systems: MS Windows, Linux, macOS.
- Programming languages: fortran90, C, SciPy, LabVIEW.
- Software: Igor Pro, AutoCAD 3D, mathematica, gnuplot, MS Office.

### FURTHER INFORMATION

- Driving licence category B.
- First-aider licence obtained at Arbeiter-Samariter-Bund.

Trieste, May 2018

Matteo Roiaz

